Role of substrates morphology and chemistry in ALD HfO_2 on Si(111)-H terminated surfaces as model

Von der Fakultät für MINT - Mathematik, Informatik, Physik,

Elektro- und Informationstechnik

der Brandenburgischen Technischen Universität Cottbus–Senftenberg

zur Erlangung des akademischen Grades eines

Doktor der Naturwissenschaften

(Dr. rer. nat.)

genehmigte Dissertation

vorgelegt von

Master of Science

Zied Rouissi

geboren am 11. April 1986 in Sidi Bourouis (Tunisia)

Gutachter: Prof. Dr. rer. nat. habil. Dieter Schmeißer

Gutachter: Prof. Dr. rer. nat. habil. Ehrenfried Zschech

Gutachter: Prof. Dr. Christian Pettenkofer

Tag der mündlichen Prüfung: 30. Mai 2017

Dedicated for the soul of my father

For first and last love of my life *Makia* and *Mejda*

For my brother and sister and all my friends

Kurzfassung

Diese Arbeit beschäftigt sich mit einer Methode, die fundamentalen Aspekte des anfänglichen Schichtwachstums auf gestuften Oberflächen während des Prozesses der Atomlagenabscheidung (ALD) zu untersuchen. Die initiale Wechselwirkung zwischen den Präkursoren und der Oberfläche ist entscheidend für das ALD-Wachstum, wobei diese Wechselwirkung noch nicht komplett verstanden ist.

Zu diesem Zweck wurden einige ALD-Zyklen mit Tetrakis(dimethylamido)hafnium (TDMAH) und Trimethylaluminium (TMA) als metallische Präkursoren und Wasser (H_2O) als Oxidant durchgeführt, um das initiale Filmwachstum von Metalloxiden auf gestuften Oberflächen zu untersuchen. Als Oberflächen kamen dabei Wasserstoff-terminiertes Silizium(111), HOPG (HOPG: ‚*highly oriented pyrolytic graphite*') und mit Silber beschichtetes HOPG (Ag-HOPG) zum Einsatz. Diese Untersuchungen wurden an Schichten, die mit verschiedenen Substrattemperaturen gewachsen wurden, durchgeführt, wobei die Methode der Rastertunnelmikroskopie (RTM, englisch STM für ‚*scanning tunneling microscopy*') systematisch angewendet wurde, um die ALD spezifischen Besonderheiten zu erforschen. Diese Technik liefert einzigartige Erkenntnisse über die örtliche Verteilung von Wachstumskeimen und deren Dichte auf verschiedenen Substraten. Die gemessenen Daten wurden anschließend mit einem mathematischen Modell korreliert, um das Wachstum zu verstehen und den Einfluss der Oberflächenmorphologie und –chemie auf das Keimbildungsverhalten zu bestimmen.

Die Zyklus für Zyklus durchgeführten in-situ STM-Untersuchungen der ersten 4 ALD-Zyklen von TDMAH und H_2O auf Wasserstoff-terminierten Si(111) bei Raumtemperatur (RT) und 280°C (Substrattemperatur) liefern zwei Wachstumsregimes: Im ersten Regime (I, erster und zweiter ALD-Zyklus) erhöht sich die Oberflächenrauigkeit im ersten Zyklus auf 0,2nm (RT) bzw. 0,34nm (280°C) mit einer partiellen Oberflächenbedeckung von 71% (RT) bzw. 54% (280°C). Nach dem zweiten Zyklus erhöht sich die Oberflächenbedeckung auf 98% (RT) bzw. 94% (280°C), wobei die gleiche Filmdicke wie im ersten Zyklus beibehalten wird. In diesem Regime wird eine komplette Schicht gebildet. Die Ergebnisse wurden auf Basis des Puurunen-Modells [R.L. Puurunen, Chem.Vap. Deposition, 5, 9, 2003] diskutiert. Dabei wurde bei der Untersuchung der Reaktionsmechanismen in Abhängigkeit der auf der Oberfläche haftenden Hafnium-Atome (pro nm^2) festgestellt, dass im ersten Regime zwei Liganden-Austauschprozesse bei RT und ein Liganden-Austauschprozess bei 280°C stattfinden. Zusätzlich wurde gefunden, dass die Reaktionssättigung durch sterische Behinderung

determiniert ist. Die Analyse der universellen dynamischen Rauigkeitsexponenten (α, β, 1/z) der Filme führt zum Schluss, dass in diesem ersten Regime das Wachstum durch eine willkürliche Beschichtung gefolgt von der Mullins-Diffusion bestimmt wird. Im zweiten Wachstumsregime (II, dritter und vierter Zyklus) wurden starke Oberflächenveränderungen speziell für das Wachstum bei RT beobachtet. Hier wurde basierend auf STM-Messungen und der Skalierungstheorie der Einfluss von Stufen auf das Wachstum demonstriert, wobei die Oberflächendiffusion zur Bildung von streifenförmigen Strukturen führte. Jedoch wird bei der Substrattemperatur von 280°C in diesem Regime (dritter und vierter Zyklus) das Wachstum weiterhin von der willkürlichen Beschichtung bestimmt.

Bei der ALD-Abscheidung von Al_2O_3 auf HOPG und Ag-HOPG wurden starke Einflüsse der Stufenkanten auf das Wachstumsverhalten registriert. Auf HOPG diffundieren die Moleküle zu den Stufenregionen und bilden Keime an willkürlichen Positionen, dieser Prozess wird von der Bildung von 2D- und 3D-Inseln begleitet. Dieser Wachstumsmodus erfüllt nicht die typische ALD-Charakteristik einer homogenen Beschichtung. Auf der mit Silber beschichteten HOPG-Oberfläche (Ag-HOPG) diffundieren die Präkursoren entlang der Stufenkanten und bilden Wachstumskeime mit definierten Strukturen. Danach findet das Wachstum in Richtung der Stufen statt. Dieses Verhalten stimmt gut mit theoretischen Voraussagen des ALD-Wachstums auf Oberflächen mit eingeschränkter Reaktivität überein.

Abstract

This work presents an approach to investigate fundamental aspects concerning the early stage of the atomic layer deposition (ALD) growth process on stepped surfaces. The first interaction between precursors and surface is strongly important for the ALD growth that it is still far away from the status to be completely understood.

For this purpose, a few ALD-cycles with tetrakis(dimethylamido)hafnium (TDMAH) and trimethylaluminum (TMA) as metallic precursors and water (H_2O) as oxidant has been performed in order to study the initial metal oxide film growth on stepped surfaces such as silicon Si(111)-H terminated, highly oriented pyrolytic graphite (HOPG) and silver deposited HOPG (Ag-HOPG). These investigations have been carried out at various substrate temperatures, where scanning tunneling microscopy (STM) has been used systematically to probe the ALD features. This technique is delivering unique knowledge about the locality and the density of nucleation's sites on the different substrates. The data collected are then subjected to a mathematical model to understand the growth and to determine the effect of the surface morphology and chemistry on the behavior of the nucleation.

The in-situ cycle-by-cycle STM investigation of 4 initial ALD cycles of TDMAH and H_2O on Si(111)-H terminated at room temperature (RT) and at 280°C displays two regimes of growth: In Regime I (1^{st} - 2^{nd} cycle) an increase in roughness in the first cycle to 0.2nm and 0.34nm respectively for RT and 280°C with a partial surface coverage of 71% and 54% is observed. In the 2^{nd} cycle, the coverage increased to ~98% and 94% maintaining the same film height of the 1^{st} cycle. A complete layer is formed in this regime. The results are discussed in reference to the Puurunen model [R.L. Puurunen. Chem.Vap. Deposition, No.5, 9, 2003]. Following this model, the determination of the reaction mechanism in relation to the number of Hf atoms/nm^2 attached to the surface reveals that two ligands exchanges occur at RT and one ligand exchange at 280°C in the first regime. In addition, the origin of the reaction saturation was determined to be caused by the steric hindrance effect. In this first regime, the growth model is governed by random deposition followed by Mullins diffusion as determined from the universal values found for the roughness dynamic exponents (α, β, $1/z$) of the film. The second regime of the growth (3^{rd}-4^{th} cycles) displays strong changes on the surface especially for the film grown at RT. Here, based on STM measurements and the scaling theory the effect of steps is demonstrated where surface diffusion leads to the formation of stripes. However, at 280°C in this growth regime (3^{rd}-4^{th}) , the growth is dominated by random deposition mode.

The Al_2O_3 growth on HOPG and Ag-HOPG shows the strong effect of the steps edges on the growth behavior. On HOPG, the molecules diffuse to the steps region and nucleate in random positions accompanied by the formation of 2D and 3D islands. This growth mode does not fulfill the typical ALD characteristic of homogeneous deposition. On Ag-HOPG, the precursors diffuse and nucleate along the steps edges in defined structures; afterward the molecules start to grow toward the steps. This growth behavior fits well with the theoretical prediction of ALD on inhibited substrates.

Table of Contents

Introduction

In the 1970's, Tuomo Suntola [1] and his co-workers developed a new deposition technique "Atomic Layer Epitaxy" which developed towards Atomic Layer Deposition (ALD) in the following years. Within the last two decades ALD has gained world-wide attention and became an intensive research field as an important technique for depositing thin films for a wide variety of applications [2-6]. The ALD process allows the deposition and the growth of conformal and homogeneous thin-film layers with atomic precession enabling fine control of the film thickness. This technique is widely used to grow thin films of metal oxides and binary materials, where it works through adsorption reaction steps of alternated precursors in cycle by cycle procedures. In every cycle the deposited precursors nucleate on the surface with constant amount of material. As a consequence, the grown thin film is homogeneous and conformal and stacked in a layer-by-layer mode. The ALD process, performed cycle-by-cycle, enhances the control of the film thickness in the sub-nanometers scale. This control of the thickness is based on the adsorption mechanism of the metallic precursors (e.g. Al, Hf, Ti ...) which occur on the surface, where ligand exchanges, dissociation or association with the surfaces species are taking place.

Important achievements of ALD coatings on large structures have been reached, such as the coverage of narrow holes trenches done by Roy G.Gordon, Junghun Chae et al. [7]. In microelectronics, ALD is used as a potential technique to deposit high-k (high permittivity) gate oxides [8-10], high-k memory capacitor dielectrics [11] and metals and nitrides for electrodes and interconnects [12]. The coating of nanostructures was a main target of the researchers since the nanostructure materials has multiple applications starting from microelectronics to catalysis. For these nanostructures, the ALD technique is a perfect tool for growing ultra-thin films, for example Fe_3O_4, ZrO_2, and FeO_x, which enhance the efficiency of nano-particles (NPs) in catalytic activity [13]. It was shown, that solar cells made of coreshell ZnO-NWs coated with Al_2O_3 and TiO_2 have significantly higher efficiency compared to the cells using un-coated ZnO NWs [14]. The ALD is highly used in photocatalytic water splitting applications to protect the photoelectrode against photo-electrochemical degradation [15-16]. As the general awareness of ALD has increased, the interest in its usage in other potential application areas has also increased.

Despite the achievements made over recent years, many challenges still remain for the future development of ALD in microelectronics applications. The integration of the ALD processes and materials to the overall process flow focuses to another important area of the research, and this should

be properly addressed during the early stages of the process development [17]. It was reported that few cycles of ALD deliver unexpected particular features that increase the functionality of many materials. Examples of these features are the removal of native oxide in semiconductors [18-20] and the tailoring of physical and chemical properties of ALD oxides by the substrate [21]. These ALD features have the potential to emerge novel material functionalities if a conformal growth with high surface coverage rate can be obtained in the first ALD cycles. However, the nucleation of precursors in the beginning of the ALD process is still far away from being understood Different nucleation and growth behaviors of precursors were observed on different substrates. There is no common universal model which explains the way of growth within the ALD process.

However, certain models such as layer-by-layer or islands growth have been accepted in the ALD community as growth models for the early ALD stage. The growth-per-cycle (GPC) is the amount of materials deposited for every cycle. This parameter is used for defining the different growth models of ALD. The first model is based on two-dimensional (2D) growth of layer-by-layer (LBL) (Frank–van der Merwe growth) [22-29], where the deposited precursor nucleates in the lowest unfilled layers of the surface (vacancies on the film) leading to the closure of the film with total surface coverage after *n* numbers of ALD cycles. As a result, a complete layer is formed. This model presents the ideal version of the ALD growth mode. Even so it was valid just for few systems [30-31]; it cannot describe the real ALD growth which is more complicate. The second model of the growth is based on islands-growth (Volmer–Weber growth) [32-34], where the deposited material nucleate in different sites in the first cycle leading to a partial growth. Afterwards, in the following ALD cycles the precursors arriving to the surface nucleate only on the ALD materials formed previously. This model favors the growth in the height direction of the film (i.e. usually indexed as z-direction) producing islands and as a result non conformal layers coverage is obtained [35-42]. A statistical model has been developed to describe the growth of islands known as random deposition where statistically an equal probability of deposition over the surface exists [43-45]. All these models of growth are based on the assumption that the growth rate per cycle GPC is affected by the number n of reactive sites. This number is varying with the number of ALD cycles or with different substrate temperatures. The reduction or increasing of this number leads to different chemisorptions reactions and surface relaxation, because the extra amount of precursors on the surface (which didn't react) still can diffuse to nucleate on surface defects (steps, kinks, grain boundaries...). This means that in the case of an inhibited substrate (very low number of nucleation sites) the precursors diffuse to the defects and agglomerate; then they become nucleation sites for the following deposition cycles. This diffusion is an important parameter for the homogeneity of the growth, which depends on the substrate temperature, substrate morphology and precursor adsorption mechanism.

The aim of this work is to study the early growth within the ALD process on well defined stepped surfaces in order to investigate how the presence of steps, e.g. defects, and the surfaces chemistry influence the nucleation behavior of ALD films. For this purpose, the approach is based on microscopy (basically scanning tunneling microscopy (STM)) of the ALD features. The recorded data are then subjected to different statistic models where the surfaces statistics are used to evaluate which theoretical growth model is most valid for the investigated ALD film growth on the selected stepped surface. The results are further related to the physical/chemical properties of the surfaces.

In the present investigation tow standard ALD processes, i.e. widely investigated, have been used applying tetrakis-dimethylamido-Hafnium (TDMAH) and trimethylaluminum (TMA) as metallic precursors and H_2O as oxygen precursor. The first four ALD cycles of HfO_2 have been investigated on the stepped surface of Si(111)-H terminated at room temperature (RT) and at 280°C. On HOPG and Ag-HOPG the first five ALD cycles of Al_2O_3 deposited at RT have been examined. In literature it has been already demonstrated that Al_2O_3 can be successfully deposited by ALD at RT using TMA and H_2O; hence only the growth at RT has been investigated in these cases. An in-situ STM experiment was performed for the cycle-by-cycle measurement of the surface morphology evolution during the ALD. As STM is known for its high spatial resolution [46], it is used to determine the ALD-film characteristics such as thickness, roughness and surface coverage. Also, the distribution density of the nucleation sites of precursors at various distances from the steps edges is resolved.

In the first chapter of this thesis, the methods used in these studies are described in detail. The basics of the ALD process including generalities, surface reactions and growth models are overviewed. Subsequently, a detailed description of the Riikka L. Puurunen model [45] is given which relates the GPC to the precursor's adsorption reaction mechanism with the surface species. In the second part the scaling theory of the surface is introduced by the definition of the statistical components of surfaces and the different dynamics of growth that can occur. The application of these two methods (for the film grown on Si(111)-H) needs the determination of the surfaces heights profiles which is delivered by STM. Therefore, STM theory is introduced. Finally, a short introduction into basics of X-ray photoelectron spectroscopy (XPS) is given, which is used (besides STM) to characterize the Al_2O_3 growth on HOPG and on Ag-HOPG.

Chapter 2 deals with the experimental-setup of the ALD in-situ STM technique as the basic tool used in this investigation. The calibration of the STM was done through the measurement of a graphene sheet. In the second part of this chapter, the sample preparation and the materials used are presented in detail.

In chapter 3, the results of the ALD growth, are respectively presented for the growth on Si(111)-H at RT and 280°C and the growth on HOPG and Ag-HOPG. The data consist of the films parameters such as RMS roughness, thickness, coverage, and islands heights. The application of the scaling theory method leads to the calculation of the height-height correlation function (HHCF), resulting in the determination of the statistics components of the HfO_2 film in every cycle of ALD on Si(111)-H surfaces. For HOPG and Ag-HOPG, the results consist of STM measurements of the nucleation sites regarding the steps edges and the terraces widths of the grown Al_2O_3 films.

In the 4th chapter, first major part dictated to the ALD on the Si(111)-H terminated. The Puurunen model is used to study the different reactions mechanisms of precursors adsorbed on the substrate, the nucleation sites and the surface chemistry of the Si(111)-H surface. Further, the interpretation of the statistical components evolution with the number of cycles reveals the effect of the surface morphology on the growth mode. In terms of the surface chemistry, these results are compared to the same statistical analysis done by Kolanek et al. [46] for HfO_2 deposited on Si-OH at 280°C. In the second part the growth of Al_2O_3 on HOPG and Ag-HOPG would be discussed. Describe a model, in correlation with experimental results, for the effect of the terraces widths and presence of barrier on the steps edges on the film nucleation in the way to correlate the ALD growth to the effect of the terraces width and steps decoration.

Finally, a summary of the findings and the conclusion about the growth model in relation to all methods used are presented in the final chapter.

Chapter 1: Methods

In this first chapter, the general basics of ALD principle are introduced. The process of the cycle by cycle, window temperature, ALD reactants are non-arbitrary chosen, where some characteristics should be fulfilled to be adapted for ALD process, in correlation some ALD precursors are introduced. The reactions of the reactants on the surface of the ALD process are then introduced for different reactions possible to take place on the surface. The growth model models on the surface are described especially Puurunen model which is used in this work to identify the different reaction on the surfaces. The ALD film is characterized by surface microscopy of scanning tunneling microscopy (STM), that why the STM theory are then introduced in this chapter. For the statistics investigation, scaling theory of surface is used so an overview of this theory and statistics component would be introduced.

The last part of this chapter is dedicated to the main precursors used, TDMAH and TMA, then the preparation of the stepped surfaces silicon by NH_4F 40% wet chemical etching and the thermal growth of silver (Ag) nano-islands on the steps of the HOPG surfaces.

1.1. Atomic layer deposition (ALD)

1. 1. 1. ALD principles

The ALD process belongs to the family of vapor to solid deposition techniques used for deposition of thin films. ALD is distinct from others techniques as such as chemical vapor depiction (CVD), physical vapor deposition (PVD) and molecular beam epitaxy (MBE) by the high ratio film thickness control. Thus, depositing a film with a high coating of complex structures polymers, NWs, NPs, control over the thickness of atomic scale and pinhole-free thin film. Films grown by ALD grow based upon sequential self-terminating gas-solid reactions, involving ligand-exchange of alternately reactants pulses. The sequence of reactants pulses is known as one cycle of deposition (Figure 1.1), which contains two steps:

- First half cycle: Pulse step of reactant A and subsequent self-terminating gas-solid reaction.
- Second half cycle: Pulse step of reactant B and subsequent self-terminating gas-solid reaction.

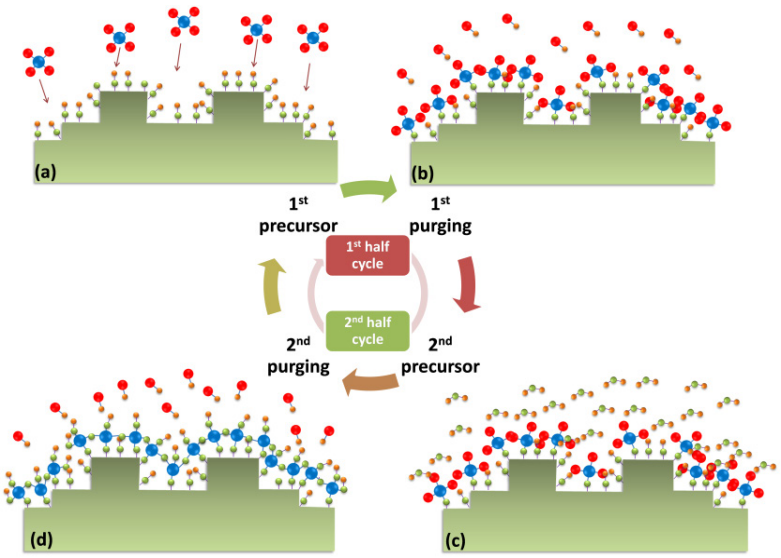

Figure 1.1: *Schematic diagram of atomic layer deposition process: (a) the first precursor is inserted and chemisorbed on the surface, (b) purging with nitrogen to remove the remnants after chemisorptions, (c) insertion of the second precursor to react with the first one on the substrate and (d) final purging to remove by products* [47].

Only fraction amount of reactant reacts on the substrate because of the self-limiting characteristics of ALD procedure. This is why there is a need for purge steps after each half cycle to remove unreacted reactants. The purge gas should be inert to the substrate and the reactants, such N_2. During each cycle the fraction amount reacted on the surface is known as growth per cycle (GPC).Thus the thickness of the film can be adjusted with the numbers of cycles.

1.1.1. ALD Temperature Window

ALD-like some other deposition techniques based on the temperature activation of reactions. ALD temperature is defined within a bounded interval knowing as ALD temperature window. Although some ALD process can be established at a lower temperature.

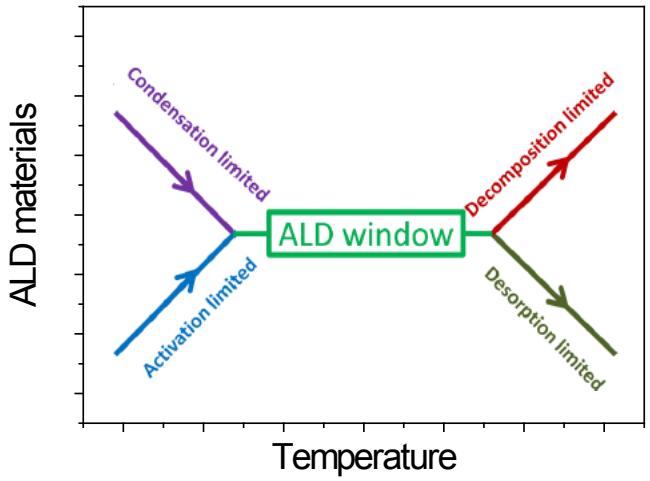

Figure 1.2: *Schematic representation of ALD processing window growth rate vs. substrate temperature and different regions of ALD processing temperature.*

The schematic diagram of ALD window presented in Figure 1.2. The growth rate and the film quality do not change so long as the temperature used is within the ALD window. Outside the temperature window at lower temperatures, there occurs either less growth due to insufficient thermal energy for reactions to occur or more growth due to condensation of precursors. At higher temperatures, if the material is volatile, desorption can occur which results in a reduction of GPC. Therefore ALD growth per cycle behavior differently at different temperatures. Several trends show how temperature may affect the amount deposited per cycle. Accordingly, GPC evolution with the temperature can be summarized in four ways.

The first case, the GPC can be constant with the increase of temperature which presents the ideal ALD growth, although it can be constant partially for every range of temperature. In the second case, GPC attend the highest value for lower temperature and then decreases linearly with the increasing of temperature. This behavior has been observed in many system such Al_2O_3 film, it can be explained by

the fact that with higher temperature the concentration of oxide group (-OH) decrease as consequence fraction of materials adsorbed decrease. In contrast to this behavior, the GPC behavior can be the other way round, where it's linearly depending on the temperature that's mean the decreasing of temperature increase the amount of the material deposited. The last case present a combination between second and third approach where the GPC start by increasing to reach a maximum and then decrease.

Those different kinds of dependencies of ALD to temperature are explaining in relation with the surfaces reactions, where the temperature of deposition has the role of surface reactivity activation. In ALD temperature was always presented as reactions catalyst, however, the surface temperature can favor also the diffusion of precursors unreacted on the surface leading to change the ALD -GPC.

1.1.2. ALD precursors

The choice of ALD precursors (reactants) isn't arbitrary but should be suited to ALD process. Therefore reactant should be volatile at range of temperature but not decompose before reacting on the surface, in addition, reactants should not desorb from the surface. Thus, preferably they must react in a saturating and irreversible manner with growth sites on the surface of the substrate. When gaseous reaction by-products are formed, they should be inert and not interfere with the ALD growth, on the other hand, the reactants should not dissolve in the film. They should be also noncorrosive towards the substrate and the reactor materials.

Many classes of compounds are used as metal reactants in ALD. The metal reactants used in ALD can be roughly divided into two groups, inorganic and metal organic.

- Metalorganic reactants: that contain a direct carbon-metal bond are classified as organometallic reactants. For example, alkyls, which are organometallic reactants containing a direct metal–carbon bond, are generally very reactive, but stable alkyls are not available for many metals and the deposition temperatures are limited because of the decomposition of the reactants.
- Inorganic reactants: Include elements and halides. Elements are an interesting class of ALD-reactants as steric effects and impurities arising from unremoved ligands are avoided.

Each type of reactant has its benefits and drawbacks regarding reactivity, stability, and impurities in the films. The variety in non-metal reactants is somewhat less than in metal reactants. The most typically used non-metal reactants are shown Table 1.1. The most commonly used types of non-metals reactants in ALD are the hydrides of the non-metal elements: water (H_2O), ammonia (NH_3), and hydrogen sulfide (H_2S), etc., which are used to grow oxides, nitrides, and sulfides, respectively. The advantage of these types of reactants is their generally high stability and reactivity in a broad temperature range, including high temperatures. Ozone is often used for deposition of oxides especially from compounds having bulky ligands that are not reactive with water. The drawback of

ozone is that it can oxidize also the surface of the underlying substrate. Ozone is also unstable, and its decomposition may be catalyzed by the film itself. In such cases, limitations arise for uniformity across large wafers and batches, and for conformality in high aspect ratio 3D structures.

***Table 1.1**: Examples of some precursors for different classes of reactants: inorganic and Metalorganic*

Inorganic	F M **Fluoride**	Cl M **Chloride**	Br M **Bromide**	I M **Iodide**	H M **Hybride**	O M **Oxo**
Metalorganic	$Al(CH_3)_3$	$Zn(CH_2CH_3)_2$	$Ta\{N(CH_3)_2\}_5$	$Ti(Cp^*)(OCH_3)_3$		

In deed, not all elements classified in this two category can be used as ALD-reactants due to lack of reactivity of most of them. In this thesis, we used two Metalorganic elements such as TMA and TDMAH. Mostly H_2O is used as an oxidant (like the case of this thesis), however, some reactants need others oxidant such as ozone, oxygen, oxygen radical. The film characteristics depend strongly on the choice of reactants and oxidant, in consequence growing the same film with different reactants leads to film with different growth parameters.

1.1.3. Reactants adsorption

The reactions on the surface result mostly on two kinds of adsorption that can be extinguished regarding the strength of interactions between the absorbed reactants molecules and the surface of the substrate. Those two kinds of reactions are physisorption and chemisorptions [48].

- **Physisorption** reaction originates from weak interaction where there is no strong exchanges bond between the surface and reactants molecules. This reaction is always reversible; therefore thickness of film can't be controlled because of the possibility high ratio nucleation that can result from surface diffusion.

- **Chemisorptions** reaction which describes a strong interaction between reactants and surface. In fact, chemical bond formed as exchanges ligand between the adsorbed molecules and the surface leading to a formation of a monolayer. The chemisorptions reaction can be both reversible and irreversible reactions. Multilayer formation should be prohibited in this mechanism of chemisorptions. This is due to the monolayer capacity, where the amount of materials adsorbed is related directly to the adsorption sites in consequence the materials deposited can't be condensing

in multi-layers but grow more in the horizontal direction to formed monolayer growth. The chemisorptions on the surface of the reactant can be described in three mechanisms: ligand exchange, disassociation, and association, are described in Figure (1.3).

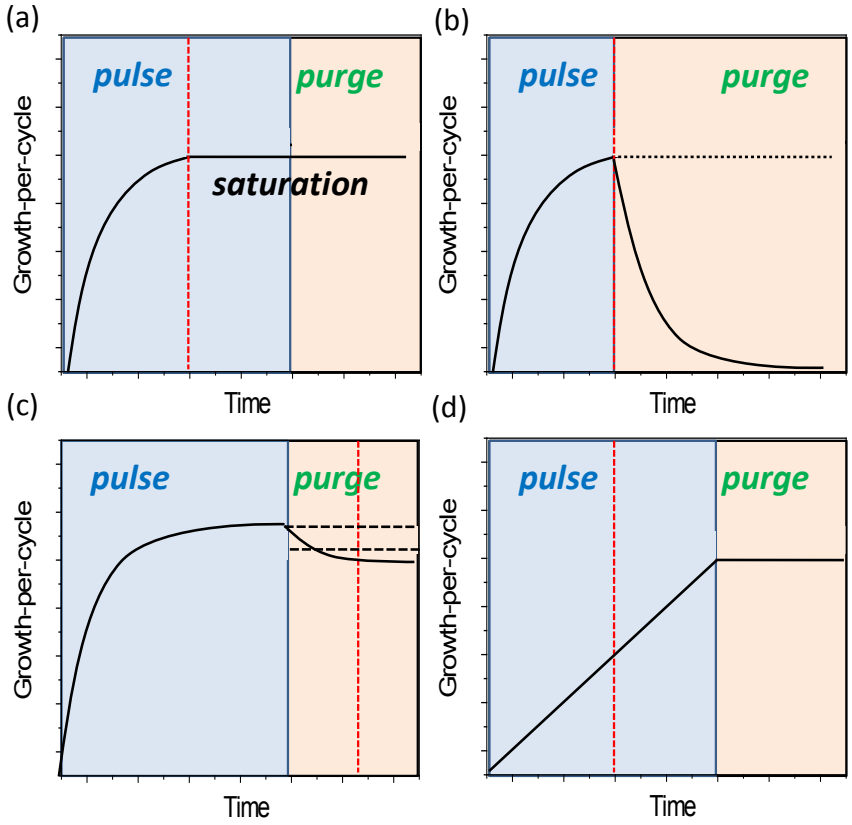

Figure 1.3: *Schematic illustration of different types of adsorption: (a) irreversible saturating adsorption (as required for ALD), (b) reversible saturating adsorption, (c) combined irreversible and reversible saturating adsorption.*

In Figure (1.3) the illustration of dependence reaction with time is presented. Figure 1.3 (a), is shown an irreversible saturation, where the growth increase with the time reaching a saturation point then be constant. This behavior illustrated the ideal ALD growth because with this reaction the amount deposited every cycle is constant then the GPC grow in a linear way with the number of cycles. The Figure 1.3 (b) is a reversible saturation reaction that the reaction in first increase with the pulse of materials and then decrease after first saturation with the purge means no growth can happen with the time.

If this reaction is reversible then as it shown in Figure 1.3 (c) reversible-irreversible saturation with t representing a practical transition time from reversible to irreversible saturation. Elam J W and George [49] show this reaction for the growth of Growth of ZnO/Al $_2O_3$ alloy films. finally, Figure 1.3 (d) presents an irreversible non-saturation.

Eventually, the nature of the deposition in ALD process is governed by the different mechanism of the adsorption on the surfaces, origin of the amount of materials deposited every cycle changes and

evolution during the film nucleations. This is the most important part of the surface reaction nature because it makes a direct cause-effect connection between the morphology of the film and the interface chemistry of the interaction surface-reactants. This will be explained next in Puurunen model combining the morphology of the ALD film grow and the different possible reaction between the substrate and the reactants.

1.1.4. Reactions mechanisms

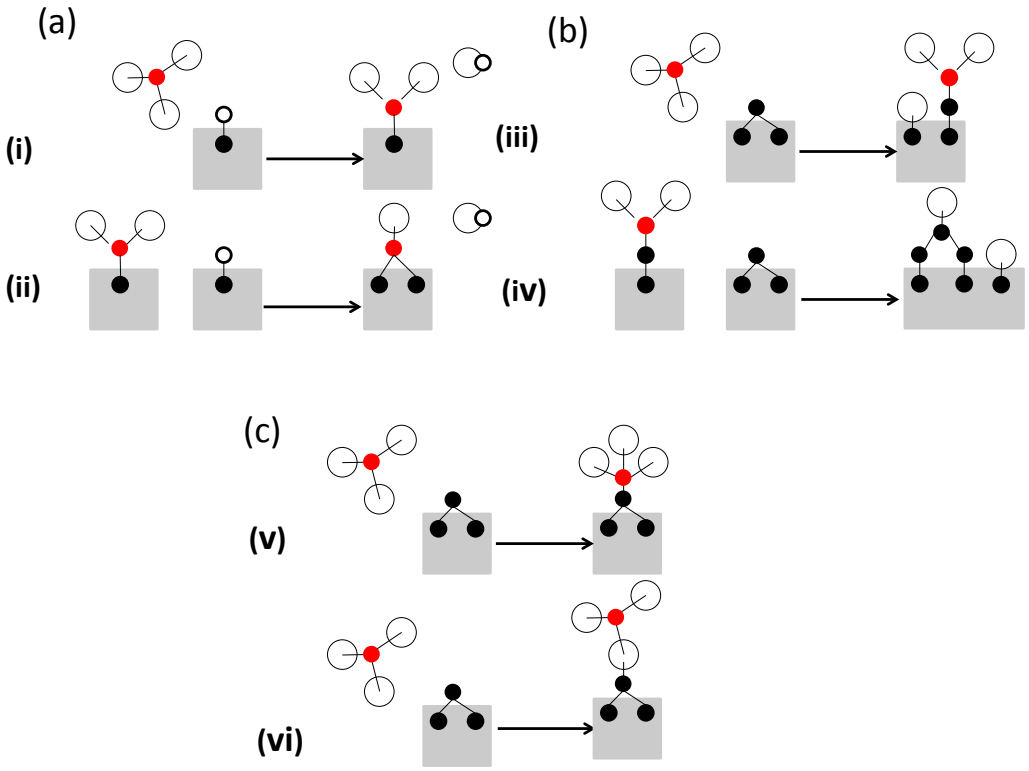

Figure 1.4: *The chemisorptions mechanism possible in ALD. (a) Ligand exchange reaction of the ML_n reactant with surface -A groups, releasing gaseous A_L (i) Ligand exchange can also occur between a surface ML_{n-y} complex and -A group (ii). (b) Dissociation of the ML_n in surface M-Z sites (iii). Dissociation can also occur between a surface MZn-y complex and M-Z sites (iv). (c) Association can occur through formation of a coordinative bond between the central M ion and the surface (v) or perhaps the ligands and the surface (vi).*

The saturation of the gas-solid system leads to a bonding of the reactant with the surface, where the adsorption occurs.This reaction can display different mechanism that can be summarized in 5 possible [50]. Three chemisorptions mechanism can be distinguished on the surface. The reactant molecules noted as (Ml_x) once adsorbed on the surface can occur ligands exchanges leading to the split of molecules by the combination of (L) with the surface group || -A to form volatile component (AL) and the reset part ML_{x-1} of the molecule adsorbed on the surface. In the ligand exchange between the

reactant and the substrate can also lead to the bond between the materials $ML_{x\text{-}1\ and}$ ||-A, show another ligand is released as AL. The two reaction of the ligand exchange 1 and 2 are presented in Figure 1.4.

- Ligand exchange

The reactant molecule (ML_n) exchange ligand with the surface, where it split on the surface to MLn-1 molecules attached to surface group A-│ │. The ligand (L) detached from the molecules Ml_n reacted with species A from the surface and realized as a gaseous product. The flowing equations describe this reaction as :

$$\text{(i) } \mathrm{ML_n(g)} + \ ||-\mathrm{A} \ \leftrightarrow \ ||-\mathrm{ML_{n-1}} \ + \mathrm{AL(g)} \qquad (1.1)$$

As it shown in Figure, the ligand exchange reaction can happen between a complex $Ml_{n\text{-}y}$ and the surface A-│ │, where ligand is released but does not result in bonding more metal species on the surface.

$$\text{(ii) } ||-\mathrm{ML_{n-y-1}} + \ ||-\mathrm{A} \ \leftrightarrow \ \ ||-\mathrm{ML_{n-y-1}}-|| \ + \mathrm{AL(g)} \qquad (1.2)$$

- Dissociation

The reactant molecule is split onto reactive M´-Z sites on the surface, as shown in reaction. Just as the ligand exchange reaction, dissociation may proceed further on the surface, but this reaction affects neither the number of bonded M atoms nor the number of bonded ligand

$$\text{(iii)} \left|\left|M'-Z\right|\right| + ML_n\,(g) \leftrightarrow ||M'-L + ||Z-ML_{n-1} \qquad (1.3)$$

- Association

The reactant molecule forms a coordinative bond with a reactive site on the surface and is chemisorbed without release of ligand as shown in the reaction

$$\text{(iv) } || + ML_n\,(g) \leftrightarrow ||\ldots ML_n \qquad (1.4)$$

Of these three mechanisms, ligand exchange would often be preferred, because its equilibrium can be driven towards the product by removing the gaseous reaction products. When a compound reactant chemisorbs on a solid substrate, saturation of the surface with absorbed species is typically caused by either of two factors, which are illustrated in Figure 1.5

- *Steric Hindrance of the ligand*

The ligand of the chemisorbed MLz adsorbed on the surface may create an umbrella effect, where the part covered on the surface can extend to prohibit the coming precursors to nucleate in nearby the

adsorbed molecules. This process leads to saturation of the surface and prohibited molecules to grow. As consequence, the surface can be considered as being full

- *Limited Number of Bonding Sites*

The number of bonding sites on the surface is lower than the number of ligand that can lead to bonding with the surface. Then the reactive sites are all consumed before the complete reaction that is required for achieving full ligand coverage. The free surface can be existent but not covered with precursors as there is no bond possible to favor the nucleation.

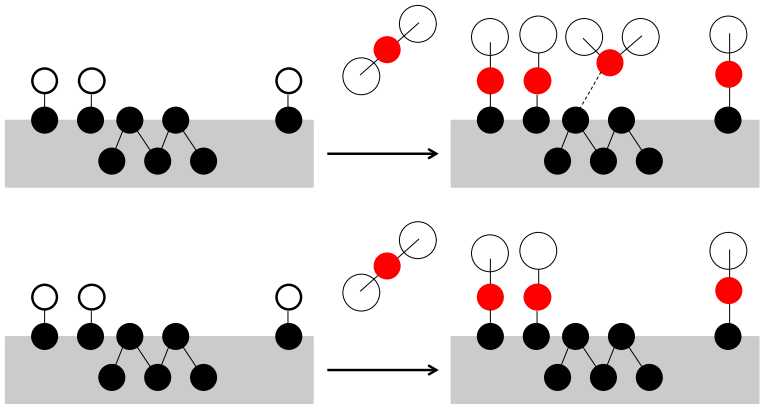

Figure 1.5: *A schematic illustration of the factors which may cause saturation of the surface with species chemisorbed from reactant MLn. (a) steric hindrance by the ligand and (b) a limited number of bonding sites on the substrate.*

1.1.2. ALD growth model: Growth-per-cycle (GPC)

1.1.2.1. Substrates and growth model

ALD mode growth still under investigation, where no model defines or describes how the film from ALD process grows. However, the assumption about the model growth are mostly concentrated about the fact that the ALD grow as two-dimensional layer-by-layer mode [22-29] (Frank–van der Merwe growth) islands growth [32-34] (Volmer–Weber growth) and or as random deposition (RD). The way of the film nucleation and growth has an important effect on the quality of the grown film than the performance of the film. Layer-by-layer (LBL) growth would result in the smooth films pin-holes free, which are consider as the best morphology for best films performance. The thickness of the ALD-grown film is often directly proportional to the number of ALD reaction cycles carried out, especially when thicker films are grown. Those numbers of reaction are limited by the self-limiting process that stops the reaction at some moment during the precursor's deposition. The three model of ALD growth are presented in Figure 1.6.

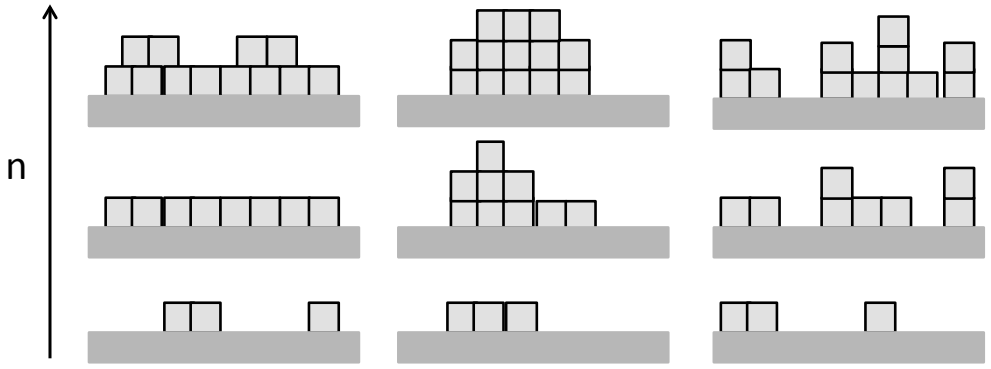

Figure 1.6: *Schematic illustration of the ALD growth models with the number of reaction cycles n that can occur on the surfaces. (a) layer-by-layer (LBL), (b) islands growth and (c) random deposition.*

The growth per cycle (GPC) was found to behavior in a complex way depending on the surface reactive sites. The number of reactive sites can be invariant with the number of cycle leading to the linear evolution of GPC with the number of ALD cycles. This numbers or reactions are related directly to the numbers of reactive sites. The two cases of increasing or decreasing this number of sites affect directly the GPC but also the model of the growth of film model. The number of reactive sites is then the origin of the different classification of the growth model of ALD. Three model of substrate are consequence of these parameters

- Substrate ALD ideal growth: with no changes of nucleation sites numbers that lead to layer by layer growth. The GPC on this growth is constant with the ALD cycles
- Substrate enhanced-growth: which enhanced the GPC in beginning of the deposition process where the growth reaches a peak on increase. This is related to an excess of reactive sites number in the front of the deposited materials.
- Substrate-inhibited growth: this is known as the most common substrate for ALD where the number of nucleation sites is to lower in front of the materials coming on the surface that leads mostly to the formation of islands of ALD where the molecules also can diffuse to defect then nucleated and then expanded with the number of cycles.

The substrate-inhibited is a model of growth of most ALD system where the consumption of the reactive sites by the materials deposited leads to reduce the number of the reactive sites, however, the deposition of oxide can in the same time generated new nucleation sites for the rest of molecules to grow on it.

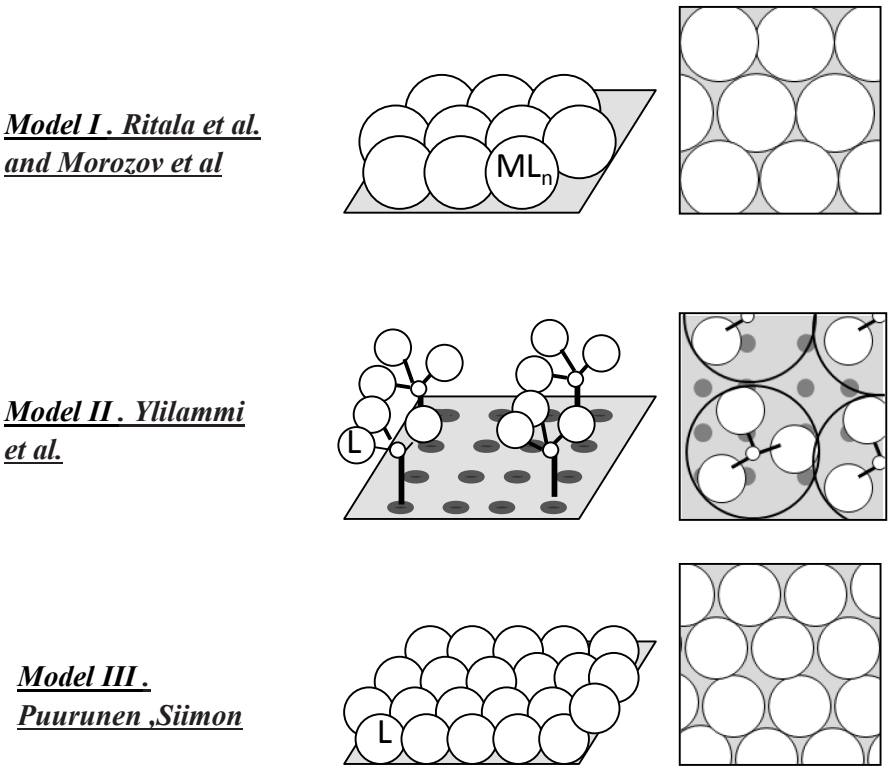

Figure 1.7: *Ritala et al. and Morozov model, a close-packed monolayer of reaction MZx by physisorption.(b) Ylilammi model of the arrangement depending on the reaction possible for the saturation of ligand of the surface coverage. (c) Siimon and Puurunen, model based on the chemisorption of the reactant on the active reactive sites on the substrate with ligand exchange that is calculated theoretically from Puurunen model.*

The classifications of substrate-inhibited ALD growth are then associated with the regime of growth. Different kind of model was given for the growth in relation with the GPC that directly depends on the nucleation sites. The GPC curve evolution depends on the islands fraction formation so it is divided into a different phase. These phases summarize in four phases

- Phase I: Start on islands nucleation and formation without overlaps between those formed ones. The islands coverage and the growth per cycle increase.
- Phase II: Overlaps of islands and coalescence leads to a reduction of the number of islands. Here the GPC also decrease but not less than the first cycle.
- Phase III: This phase start once all the islands formed are overlaps and no distinct islands features still given the place to formatted layer. The GPC increase and then decreases.
- Phase IV: Linear growth with the GPC is becoming constant.

This behavior and mode of growth are related almost in all the work done on the ALD to the islands growth models that are direct results of nucleation of the precursors on the surface after chemisorptions with the species on the interfaces. The ligands exchanges lead to the formation of this

islands basing on this model of ligands and how this affected to the GPC per cycle same model was introduced. Figure 1.7, is the illustration of three model of ALD process growth in relation with the chemisorptions of the ligand on the surface.

The model I: Ritala et al. [50-51] and Morozov et al. [52] developed a model, which define the GPC in relation with the size of the reactant ML_n. The density of the reactant is a fundamental parameter that leads to calculate the number of the reactant that covered a fraction of the surface in a closed packed on the monolayer. The main reaction of a reactant in this model is assumed to be a physisorbed monolayer of the molecules. The molecules adsorbed becomes MZx differ from the reactant ligands ML_n because on the reaction that occurs with the surface species. As consequence, the description based on just ML_n reactant is given a broad estimation of the GPC in this model. This model presented a limit in defining the real GPC of the ALD film.

Model II: This model has been developed by Ylilammi et al [53]. New parameters are introduced in the calculation of the GPC in this model where the geometry becomes included in the description of the process of the chemisorptions reaction. The size and the geometry, the length of the bond and angles of the chemisorbed MZx are important to define the model. Here the GPC increase with the steps of reaction with the existent molecules.

Model III: This model is based on the ligands exchanges and adsorption in close-packed monolayer as a physisorbed monolayer of ligands. This model was developed by Siimon et al [54] and Puurunen [55]. The model is calculating the theoretical maximum of the coverage with the ligand that leads to define the number of atoms metallic of the precursors M attached to the surface. The GPC increase with the size of the adsorbed materials.

In this work we will try to apply Purrunen model that is described empirical mathematical equation for the calculation of the number of metal atoms attached to the surface, leading to the calculation of the exchange number of ligands.

1.1.2.2. Puurunen model:

Riikka L. Puurunen is one of a pioneer in the ALD field. She has important contribution to the description of the ALD growth mechanisms. In many of her publications, she described the growth basing on islands model. Here, we introduce the model developed by Puurenen which was introduced in 2013 as ‘‘Growth per Cycle in Atomic Layer Deposition: A Theoretical Model" Chem. Vap. Deposition, 2003, 9, No.5. The main idea that she mathematically related in the equation the GPC and the reaction that occur on the surface.

- **Mathematical Model**

The growth per cycle has a direct relation to the different mechanism of precursor's reaction on the surfaces. ALD occur mainly tow type of chemisorptions on the surface, where the first one resides in ligand exchange between the ML_n and the interface group and dissociation or association mechanism. Puureen model describes the different type mechanism of growth with the GPC evolution. The GPC is the height of materials deposited in the direction (Z) and the lateral growth on (X, Y) directions. The determination of the GPC so is to determine first the heights of islands formed every cycle and also the surface islands coverage. The number of ligands attached to the MZx surface in one saturation MLn reaction ΔC_L[nm^{-2}], is , according to mass balance, proportional to : (1)The number of metal atoms attached to the surface ΔC_M [nm^{-2}] (2) the number of ligands in the MLn reactant ,n, and (3) the number of ligand released in the ligand exchange reaction with -A groups, that is , the number of reacted -A groups, ΔC_a [nm^{-2}], as the equation

$$\Delta C_L = n\Delta C_M - \Delta C_a \quad (1.5)$$

The amount of metal M attached to the surface in one saturation ML_n reaction is accordingly given by

$$\Delta C_M = \frac{1}{n}(\Delta C_L + \Delta C_a) \quad (1.6)$$

The theoretical upper limit for the ligand packing and ΔC_L^{maxthr}[nm^{-2}], is obtained from the filling area of one ligand, A_L [nm^{-2}] is

$$\Delta C_L^{maxthr} = 1\,(-A_L)^{-1} \quad (1.7)$$

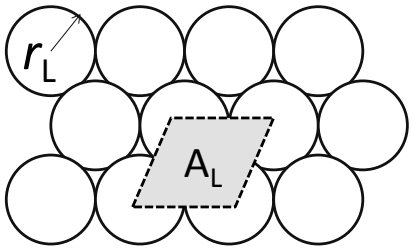

***Figure 1.8**: Filling area A_L of ligand L with radius r_L for close packing growth.*

The assumption of spherical ligands should be valid in most cases. Ligand coverage, (θ) defined then by the equation

$$\theta = \frac{\Delta C_L}{\Delta C_L^{maxthr}} \quad (1.8)$$

The theoretical maximum of the ligand coverage, θ^{maxthr} , is unity , though this should normally not be reached , because (1) a void larger than the size of one ligand is required for the ML_n molecule to interact with the surface, and (2) the location of the reactive sites on the surface may not allow a full

coverage . The coverage when steric hindrance defines saturation, and the ligand packing is therefore at its real maximum, is denote, θ^{max}, and the corresponding real maximum ligand packing is denoted ΔC_L^{max}. When the limited number of bonding sites defines saturation, θ is below,θ^{max}, and the surface remains partly uncovered. So that the model can discriminate between varieties of reaction models with –A groups, f is introduced to denote the fraction of –A groups reacted with ML_n as

$$f = \frac{\Delta C_a}{C_a} \tag{1.9}$$

The C_a [nm^{-2}] is the number of –A groups on the surface before the reaction of ML_n. The combination of Equations (1.6), (1.8) and (1.9) is obtained that relates ΔC_M to the size of the ML_n reactant (n, ΔC_L^{maxthr}), its reactivity with the MZ_x material (θ, f) and the amount of –A groups on the surface (C_a)

$$\Delta C_M = \frac{1}{n}\left(\Delta {C_L}^{maxthr} + f\ C_a\right) \tag{1.10}$$

The growth per cycle is often measured as thickness increment per ALD reaction cycle, Δh [nm]. The thickness increment per cycle is related to ΔC_M through the molar mass of the material, $\boldsymbol{M}$ [g mol^{-1}], the density of the materials, ρ [g nm^{-3}] , and the number of atoms per mole is N_A = 6.02214 x 10^{23} mol^{-1} by the Equation (1.11)

$$\Delta h = \frac{M}{\rho N_A}\ \Delta C_M \tag{1.11}$$

The combination of Equation (1.10) and Equation (1.11) results in the equation related the thickness increment per cycle, Δh to the chemistry of the growth as

$$\Delta h = \frac{M}{\rho N_A n}\left(\theta \Delta {C_L}^{maxthr} + f\ C_a\right) \tag{1.12}$$

- **Model application**

Table 1.2*: The equation of different cause of reaction saturation occurs in every possible reaction between the surface and the reactants. Mathematical approach shows the dependence of the saturation caused by the temperature (T), where* $C_a^{eq}(T) = \frac{(-1)}{(100)}\ T + 10$.

		Saturation cause by	
		Steric hindrance	**Number of –A groups**
Reaction 1[a]	ΔC_M	(1/n)[$\theta^{max}{\Delta C_L}^{maxthr} + C_a^{eq}(T^*)$]	$C_a^{eq}(T)$
	ΔC_L	${\theta^{max}\Delta C_L}^{maxthr} = {\Delta C_L}^{max}$	(n-1) ΔC_M
	$\Delta C_L/\Delta C_M$	n-1	n-1
	f		1
	θ	$C_a^{eq}(T^*)/\ C_a^{eq}(T)$ θ^{max}	$\frac{\Delta C_L}{\Delta C_L^{maxthr}}$
Reaction 2[b]	ΔC_M	(1/n)[$\theta^{max}{\Delta C_L}^{maxthr} + C_a^{eq}(T^*)$]	
	ΔC_L	${\theta^{max}\Delta C_L}^{maxthr} = {\Delta C_L}^{max}$	
	$\Delta C_L/\Delta C_M$	n-2	n-2
	f	$C_a^{eq}(T^*)/\ C_a^{eq}(T)$	1
	θ	θ^{max}	$\frac{\Delta C_L}{\Delta C_L^{maxthr}}$
Reaction 3[a]	ΔC_M	(1/n)[$\theta^{max}{\Delta C_L}^{maxthr} + C_a^{eq}(T)$]	$C_a^{eq}(T)$
	ΔC_L	${\theta^{max}\Delta C_L}^{maxthr} = {\Delta C_L}^{max}$	(n-1) ΔC_M
	$\Delta C_L/\Delta C_M$	$(\Delta C_L/\Delta C_M)$	n-1
	f	1	1
	θ	θ^{max}	$\frac{\Delta C_L}{\Delta C_L^{maxthr}}$
Reaction 4	ΔC_M	(1/n)[$\theta^{max}{\Delta C_L}^{maxthr} + C_a^{eq}(T)$]	-
	ΔC_L	${\theta^{max}\Delta C_L}^{maxthr}$	-
	$\Delta C_L/\Delta C_M$	$(\Delta C_L/\Delta C_M)$	-
	f	1	-
	θ	θ^{max}	-
Reaction 5	ΔC_M	(1/n)[$\theta^{max}{\Delta C_L}^{maxthr}$]	-
	ΔC_L	${\theta^{max}\Delta C_L}^{maxthr} = {\Delta C_L}^{max}$	-
	$\Delta C_L/\Delta C_M$	n	-
	f	0	-
	θ	θ^{max}	-

T* denotes the temperature where change occurs from one factor causing saturation to another. In this case, the number of reactant on the surface is then $C_a^{eq}(T^*) = \frac{\theta^{max}\Delta C_L^{maxthr}}{n-1}$ in [a] and $C_a^{eq}(T^*) = \frac{\theta^{max}\Delta C_L^{maxthr}}{\frac{n}{2}-1}$ and [b]

The effect of selected reaction chemistries on the growth per cycle in ALD has now illustrated for the growth materials MZ_x from reactant ML_n and ZH_m surface species. The ML_n reaction attaches metal atoms and ligand on the surface, according to the chosen chemistry. The chemistries are chosen to be representative of ALD process. The ZH_m reactant removes the ligands L, realizing them as HL, and leaving behind (Z)H groups. The ZH_m reactant can also dissociate or combine, releasing ZH_m and leaving behind a Z bridge. The number of (Z)H groups at saturation is assumed to depend on the growth temperature, that is, C_a=$C_{(Z)H}$=$C_{(Z)H}{}^{eq}$. Equation then transforms into

$$\Delta C_M = \frac{1}{n}\left(\theta\, \Delta C_L{}^{maxthr} + C_{(Z)H}^{eq}\right) \quad (1.13)$$

The reaction of ML_n is assumed to fulfill the criteria of ALD growth in the temperature interval 0-1200°C. The maximum ligand coverage, θ^{max}, is assumed to be 0.7, independent of temperature. The $C_{(Z)H}^{eq}$, is assumed to decrease steadily from 10 nm^{-2} at 0°C to zero at 1000°C. The application of this model gave different kind of reaction are illustrated in the Table 1.2. The reactions possible with the application of those models, also introduced above in Figure 1.4 are then derived from the model equations. According to the model, the reactions presented in Table 1.2 are detailed.

- **Reaction 1**

The ML_n reactant chemisorbs on the surface through ligand exchange so that one ligand is released. No dissociation or association occurs. The ΔC_L to ΔC_M ratio is n-1. Depending on $C_{(Z)H}{}^{eq}$, which in turn depends on temperature, saturation of the surface with adsorbed species is define (1) by steric hindrance ($\theta = \theta^{max}$) or (2) by the number of (Z)H groups on the surface ($\theta < \theta^{max}$).

- **Reaction 2**

The ML_n reactant chemisorbs on the surface through ligand exchange so that two ligands is released. No dissociation or association occurs. The ΔC_L to ΔC_M ratio is n-2. As in the reaction 1, saturation of the surface with adsorbed species is defines by steric hindrance or by the number of (Z)H groups, but the temperature where the limiting factor changes differs from reaction 1

- **Reaction 3**

The ML_n reactant chemisorbs on the surface through ligand exchange so that all (Z)H groups on the surface are consumed, $f = 1$. No dissociation or association occurs. Saturation on the surface with adsorbed species is again defined by steric hindrance or by the number of (Z)H groups.

- **Reaction 4**

The ML_n reactant chemisorbs on the surface through ligand exchange so that all surface (Z)H group are consumed, $f = 1$. Dissociation and/or association may also occur. Saturation of the surface with adsorbed species is defined by steric hindrance of the ligand $\theta = \theta^{max}$

- **Reaction 5**

The ML_n reactant chemisorbs through dissociation and association. No ligand exchange occurs. The ΔC_L to ΔC_M ratios n. Saturation is defined by the steric hindrance imposed.

This model applied by Puurunen [58] in the case of Growth of Aluminum Oxide from $AlMe_3$ and H_2O, Yttrium Oxide from $Y(thd)_3$ and O_3 and Titanium Dioxide from $TiCl_4$ and H_2O where she shows that the results obtained, fit with the experimental data of those ALD system measured experimentally.

1.2. Scanning tunneling microscopy (STM)

The main experimental method used in this thesis is scanning tunneling microscopy (STM), which is a technique for imaging conducting surfaces and its adsorbents with atomic resolution. The method was invented 1982 by Gerd Binnig and Heinrich Rohrer at the IBM research labs in Switzerland [56]. It was the first method capable of atomic resolution on flat surfaces in real space. In 1986, the two inventors were awarded the Nobel Prize in physics together with Ernst Ruska, the inventor of the electron microscope.

STM is a powerful microscopy technique that based on the quantum mechanical phenomenon known as tunneling. In which the wavelike properties of electrons permit them to "tunnel" beyond the surface of a solid into regions of space. This phenomenon is forbidden in the classical physics rules. The tunneling current increases exponentially with the decrease of the distance between the two materials. This high sensitivity makes STM an important tool for the morphology of ALD film growth.

1.2.1. Tunneling Theory: Quantum effect

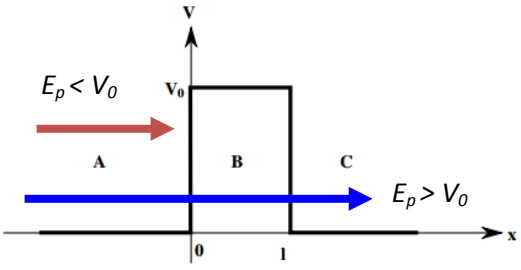

Figure 1.9: *Particle tunnel through uni-dimensional potential V_0 (B) from region A to region C.*

In classic physics, if a particle approach a potential barrier it can't go through it if the potential is higher than the particle energy, however in quantum mechanics, this is not necessarily the case.

Quantum physics introduce the tunneling effect, thus particle, as wave nature, doesn't stop at the barrier but present a probability of transmission.

In Figure 1.9, the module of the path of the wave function of the particle traveling from region (A) to region (C) with are separated by a potential barrier (region B) with a width (d). This particle can either be reflected by the barrier or tunnel to the region (C). Thus, if the particle has E> V, here wave function oscillate with constant probability density, in contrast when E<V, wave function shows an exponential decay. That affirmation about the behavior of the particle in barrier potential case are based Schrödinger Equation solution of wave function φ(x)

$$\frac{d^2}{dx^2}\,\varphi(x) + \frac{2m}{\hbar^2}\,(E - V_0)\,\varphi(x) = 0 \tag{1.14}$$

For E >V, the general solution is

$$\varphi(x) = Ae^{ikx} + A'e^{-ikx} \text{ , where } k = \sqrt{\frac{2m(E-V)}{\hbar}} \tag{1.15}$$

E < V:

$$\varphi(x) = Be^{\delta x} + B'e^{-\delta x} \text{ , where } \delta = \sqrt{\frac{2m(V-E)}{\hbar}} \tag{1.16}$$

In both region (A) and (C) the energy of the particle is higher than the barrier the effect of barrier existed only in the region (B). Thus, wave function is defined in each region as the three equation of each region

$$\varphi_A(x) = A_1e^{ikx} + A'_1e^{-ikx} \tag{1.17}$$

$$\varphi_B(x) = A_2e^{\delta x} + A_2'e^{-\delta x} \tag{1.18}$$

$$\varphi_C(x) = A_3e^{ikx} + A'_3e^{-ikx} \tag{1.19}$$

The wave function tunneling requires the continuity of the wave function and its first derivative between the three regions (A), (B) and (C). Also, the reflection terms in the equation should be annulled. Thus, calculation of the transmission probability between region (A) and (C) is given as

$$T = \left|\frac{A_3}{A_1}\right|^2 = \frac{4\,E\,(V_0-E)}{4\,E\,(V_0-E) + V_0^2\,sinh^2\frac{\sqrt{2m(V_0-E)}d}{\hbar}} \tag{1.20}$$

If we consider that the case of Vacuum (infinite potential high), the transmission probability *T* become exponentially depending on the width (*d*) of the barrier given by

$$T \approx \frac{16\,E\,(V_0 - E)}{V_0^2}\, e^{-2\delta d} \qquad (1.21)$$

Due to the wave nature of the electrons, the amplitude of the wave function of an electron does not end at the surface but decays exponentially into the vacuum. When two materials conductors or semiconductors [57] are brought into close, the wave function of one material reaches into the second one, giving rise to transmission probability of the electron to the second metal. This is the basic of STM measurement, where applying a potential difference (U) between the tip and the metal lead to tunneling current (I) flows through the vacuum, with an exponential dependence on the distance (*d*).

1.2.2. Junction tip-sample

The current (I) flowing not only depends on the distance between the two materials but also on the local density of states of them surfaces. Thus, the current (I) is providing information on the electronic structure of the surfaces of the materials. If the junction experiments of two planar materials, no spatial resolution can be achieved.

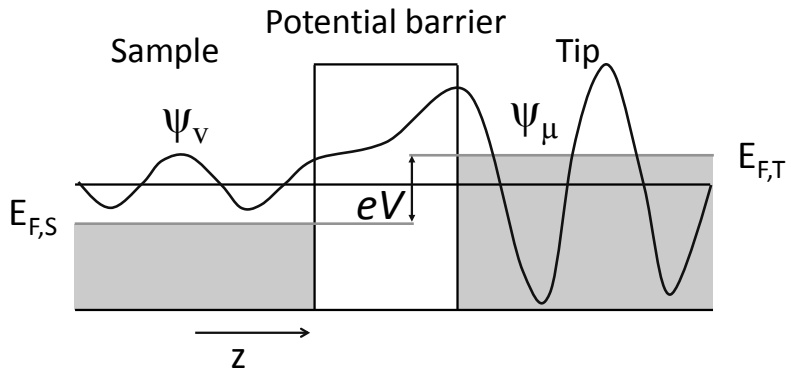

Figure 1.10: *The wave function of particles tunnels in the junction sample-tip. The electron tunnels from an occupied tip state* ψ_μ *into an unoccupied sample state* ψ_v.

Thus for spatial resolution, a tip with few atoms at the apex is used in STM. The current flows highly localized through a few atoms at the apex of the tip, causing the high spatial resolution of the STM. Fundament of a detailed understanding of the STM is the first-order perturbation theory, using Fermi golden rule

$$I(\mathrm{U}) = \frac{2\pi e}{h} \sum_{s,t} \left|M_{s,t}\right|^2 \times \delta(E_t + U - E_s) \times \left(f(E_s)[1 - f(E_t)] - f(E_t)[1 - f(E_s)]\right) \qquad (1.22)$$

Where the summation goes over all unperturbed quantum levels of the sample (s) with energy E_s and of the tip (t) with energy E_T. U is the potential difference between sample and tip. The Fermi-Dirac distributions (*f*), at the sample and tip temperature T, are ensuring that only tunneling from occupied to

unoccupied electron levels occur. According to Bardeen [58], the probability of transition from level t to levels is given by the tunneling matrix element $M_{s,t}$

$$M_{s,t} = -\frac{h^2}{2m_e} \int dS \, (\psi_t^* \, \nabla \psi_s - \psi_s \, \nabla \psi_t^*) \tag{1.23}$$

This expression for the tunneling current (I) can be simplified by assuming a step-like behavior of the Fermi-Dirac distribution, which is in principle correct at a temperature of 0K and a good approximation at low temperature.

$$I(U) = \frac{2\pi \, e^2}{h} \sum_{s,t} \left| M_{s,t} \right|^2 \times \delta \, (E_s - E_F) x \, (E_t - E_F) \tag{1.24}$$

Where introduced the Fermi energy E_F. To evaluate $M_{s,t}$, Tersof and Hamann [59] made the assumption that the tip wave functions are s-orbital's the sum of the absolute squares of the wave-

$$I(U) \propto \int_0^{eU} \rho_s \, (E, x, y) x \, \rho_t (E - eU) x \, T \, (E, U, z) dE \tag{1.25}$$

A function yields the local density of states (LDOS) of the sample ½s and the LDOS of the tip ½t at the position (x; y).

The tunneling current I(U) depends on this model on the density of states of the tip at the applied voltage U, on the density of states of the surface at the Fermi-level and on the transition matrix T. Making the approximations that the tunneling is purely vertical and disregarding all surface contributions other than of s- or p_z-symmetry, one can write T in the following form

$$T(E, U, z) = \exp(-2z \times \sqrt{\frac{m_e}{h^2} \times (W_S + W_t - 2E + eU)}) \tag{1.26}$$

This equation can be further simplified to the final result of this approach to calculate the tunneling current (I) by assuming $-2E + eU << W_s + W_T$ what allows to put T in front of the integral. The equation can be written as:

$$I \propto e^{-2kz} \int_0^{eU} \rho_s \, (E, x, y) x \, \rho_t \, (E - eU) dE \tag{1.27}$$

This is the final result for the Tersoff-Hamann [60] approach for the tunnel current (I) in Scanning Tunneling Microscopy. This equation consists of two parts: an exponential factor describing the dependence of the tunnel current on the tip-sample distance (the topographic information) and an integral factor describing the dependence of the tunneling current from the LDOS of sample and tip.

In Scanning Tunneling Spectroscopy, one can directly evaluate the sample LDOS at the position (x, y) as a function of energy. The tip is kept at the position (x, y) and a sample-tip distance z. The bias voltage U is ramped while recording the tunneling current I and the differential conductance dI /dU. The differential conductance can be calculated by taking the derivative of Equation

$$\frac{dI}{dU} \propto \left(\left[-\int_0^{eU} \rho_s(E)\frac{dp_t}{dE}(E-eU)dE\right] + \rho_s(eU)\rho_t(0)\right) \quad (1.28)$$

It is typical to assume that the tip-DOS is not depending on the voltage. Then the integral in vanishes and one obtains for the differential conductance

$$\frac{dI}{dU} \propto \rho_s(eU)\rho_t(0) \quad (1.29)$$

This Equation (1.29) states that the dI/dU signal is proportional the sample LDOS at the bias voltage U.

1.3. X-ray photoelectron spectroscopy (XPS)

X-ray photoelectron spectroscopy (XPS) is a surface analyzing technique to study the elemental composition of the surface. Due to the elemental specific application of XPS, it is also known as electron spectroscopy for chemical analysis (ESCA). The XPS system was first developed by Siegbahn and co-worker in 1960's at the University of Uppsala, Sweden [61]. The principle of XPS measurement based on the electrons emission from the substrate with different energy that can be correlated to a different component of the substrate. This electron emission requires an illumination of the substrate with a monochromatic light source such X-ray sources (Mg Kα and Al Kα). XPS techniques present high surface sensitive technique with low attenuation length of photoelectrons

1.3.1. XPS theory

Electrons from core levels and valence band states can be excited by X-ray emission, leading electrons to leave the substrate to the vacuum with a kinetic energy that will analyze referring to the vacuum level via an electron analyzer. Koopmans' Theorem demonstrates that the energy of the electrons does not change with the excitation. Thus, the kinetic and binding energies of the electron have the following relation:

$$h\nu = E_B + E_k + \emptyset_{substrate} \quad (1.30)$$

There is no a defined value for the work function since it changes from material to other. Therefore, Fermi level can be used as reference point. The energy equation become

$$h\nu = E_B + E_k \quad (1.31)$$

The emitted electrons from substrate contain not only information about orbital but also about the martial its self. Indeed, the binding energy of electron depend on the chemical environment (next neighbor) of the atoms ($\Delta E_{chem.}$), the electron correlation (ΔE_{corr}), the relativistic energy (ΔE_{rel}) and the relaxation and/or screening of the core hole – multi-electron effects (ΔE_{Relax}).

$$E_B = \Delta E_{atomic} + \Delta E_{chem} + \Delta E_{relax} + \Delta E_{corr} + \Delta E_{rel} \quad (1.34)$$

Excitation process produces empty states lead to the non-equilibrium system. That's why, the final state of system required relaxation process that can occur through two processes. In first case orbital vacancy filled up with the electron from higher orbital accordingly extra amount of energy released as photon. In second case , the vacancy can be filled with electron from high sub shell and the produced difference amount of energy occur electron ejection for relaxation known as Auger electron.

1.3.2. Application of XPS

The photoelectron spectroscopy present a powerful spectroscopy technique for high surface sensitive owing to the out-come information's about the properties of the subject materials surfaces. The data analyses lead to determine not only, the chemical composition of single component more than this it's give the information about the quantity of each component in a chemical compound, known as elemental ratio.

1.3.2.1. Chemical composition

The photo emitted electrons from same orbital have different energy for different elements. The equation offers a unique value for each element, which makes possible to have information about the elemental composition on the surface.

On the other hand the binding energy can shift due to the chemical environment or the chemical state of the element in the material. The shift in binding energy depends on number of electrons taking part in chemical bonding and as well as type of chemical bonding. Due to the chemical bonding when the population of electrons in the outermost shell decreases the effective charge experienced by the core electron increases and hence the binding energy shift to higher binding energy position. On the other way around when the population of electron in the outer most shell increases the effective charge experienced by the core electron decreases and hence the binding energy moves to lower energy. The shift in binding energy (ΔEB) is given by equations

$$\Delta E_B = \left(E_f^{A(N-1)} - E_i^{A(N)}\right) - \left(E_f^{B(N-1)} - E_i^{B(N)}\right)$$

$$\Delta E_B = \left(E_i^{B(N)} - E_i^{A(N)}\right) - \left(E_f^{B(N-1)} - E_f^{A(N-1)}\right) \quad (1.35)$$

1.3.2.2. Elemental ratio of the surface

In the quantitative analysis, the information about the quantity of each component in a chemical compound (elemental ratio) and composition of a surface into the surface (depth profile) can be obtained.

$$I = \varphi n\sigma \int_0^\infty e^{-\frac{x}{\lambda cos\theta}} dx$$

$$I_\infty = \varphi n\sigma\lambda \, cos\theta \quad (1.36)$$

Photoelectron spectroscopy can also be used to determine the elemental ratio on the surface of the material. The intensity of the spectra depends on the concentration of the element present. More physically the intensity depends on certain factors like incident photon flux (φ), atomic density (n), atomic cross section for the transition to occur (σ), the inelastic mean free path at the desired photon energy (λ), the distance (x) and the angle (θ) at which the photoelectrons are collected. For different elements the above factors are different and hence when the intensity of two elements is compared these factors must be taken into consideration. Considering two elements A and B on the surface the intensity of these two elements can be given as IA and IB. The physical parameters affecting the intensity of the PES can be defined as atomic sensitivity factor S. The values for inelastic mean free path and the atomic cross-section can be obtained from the data base [62-63]. The ratio of the two elements present on the surface can be determined by taking the ratio of peak intensity after back ground correction as shown as

$$\frac{A}{B} = \frac{I_A / S_A}{I_B / S_B} \quad (1.37)$$

1.4. Scaling surface theory

This mathematical theory is used in physical approach to undrstand the growth of different films deposited by the differetn techniques such as CVD and sputtering. Different growth of film as results of various deposition techniques can occur a non equilibrium condition that leads to rough surface morphology and complex evolution of the surface morphology. The molecules/atoms reaching the surface can behavior in different way (diffusion, relaxation...) that is responsible on non-equilibrium growth by producing a front roughness. These roughness's compete with the smoothing of the surface, such as diffusion. The coming molecules also can attached to higher point of the surface and then do not adsorbed or grow in lower layer leading to the enhanced of the roughness. Those complex behavior of the roughness are then subjected to a conventional statistical mechanic treatment cannot describe the complex behavior of the growth. Scaling theory come here as an mathematic model that can explain the growth of different kind of film and describe the roughness evolution of the surface.

The dynamic scaling hypotheses present the basic of this concept, the model call self-affine scaling. Many investigation and study based on this approach of different kind and techniques of film deposition have been done in the last two decades [64-70]. The dynamic scaling theory was developed and reported in many reviews such as Fractals, Scaling, and Growth Far from Equilibrium by P.

Meakin (Cambridge University Press, 1998) [71] and Fractal Concepts in Surface Growth by A.-L. Barab´asi and H. E. Stanley(Cambridge University Press, 1995) [72].

1.4.1. Statistical components of surfaces

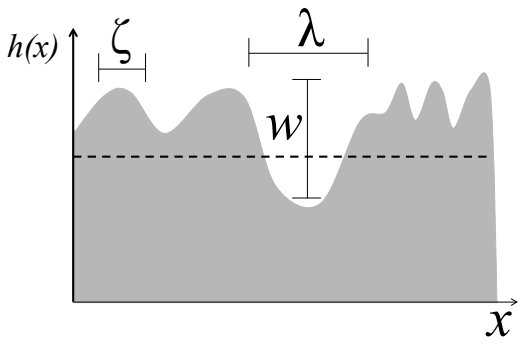

Figure 1.11: *Illustration of surfaces statistics used to describe rough surfaces: The mean height (dashed line), surface width w, lateral correlation length ξ, and wavelength λ .*

The surfaces roughness can be described through a mathematical model based on *h(x,t)*, where *h* present the height profile of the measured surfaces profile at position *x* at time *t*. The different statistics of the surfaces roughness can be determinate in use of the height profile *h(x,t)* of the surfaces. In Figure 1.11, the different statistics components that characterized the surface.

1.4.1.1. Surface width or standard deviation (w)

This surface width is the most used statistical parameters of the surface that describe the roughness in relation with the growth process. It is define as a function of the height profile h(x) by

$$w = \sqrt{\langle [h(x)]^2 \rangle} \tag{1.38}$$

This width is then varies as the average values of the height, mean higher the width is higher the surface is rough .The growth process lead to evolution of the width with the increase of time depositions. The dynamic of the film grown can affect the surface width by reducing / increasing it lead to non-stationary growth or keep it constant with the deposition process which is a stationary growth. The diagram (Figure 1.12) shows the kind of growth dependent on the surface width evolution during film growth.

First stationary growth is the case if the (w_1) of the film in C_n cycle is equal to the surface width of w_2 of C_{n+1} ALD cycles means $\frac{w_{n+1}}{w_n} \cong 1$. In other case $w_{n+1} \ll w_n \rightarrow \frac{w_{n+1}}{w_n} \ll 1$, or $w_{n+1} \gg w_n \rightarrow \frac{w_{n+1}}{w_n} \gg 1$, then the growth is non-stationary.

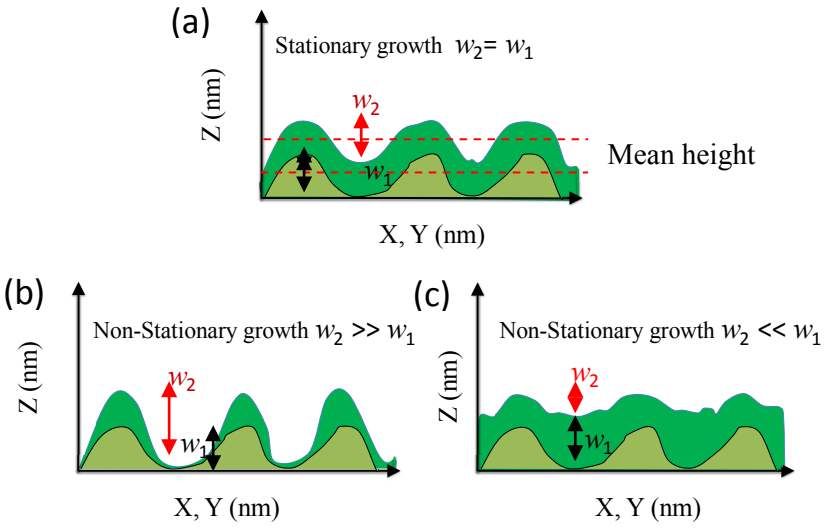

Figure 1.12: *The three cases of the surface widths evolution.(a) stationary growth where surface width is constant. (b) and (c) non stationary growth.*

This case can be meaningful in the case of discrete growth as ALD. Therefore the dynamic evolution of the surface width with the time is define as

$$w(t) \sim t^{\beta} \tag{1.39}$$

β is the growth exponent. The behavior of w evolution with time as power of β is based on the dynamic scaling theory that is used to describe the film dynamic properties. Many growths model and are associated to different values of β. in the discussion part we discuss the different values obtained of β.

1.4.1.2. The lateral correlation length (ξ)

The lateral correlation length (ξ) is the distance that has correlated height. In another way, two surface heights are correlated on average if their lateral separation is less than the lateral correlation length. The measure the values of (ξ), the autorotation function (ACF) or the Height-height-correlation function (HHCF) can be used making (ξ) manful to describe the film morphology and dynamic of growth ((HHCF) used in this theses). Figure 1.13, present the illustration of the different relation between the lateral correlation length evolutions.

Similar to the width evolution the lateral correlation present the same analyses, in contrast to the surface width which describe the growth on the height direction, the lateral correlation is the growth in the horizontal direction. The values as illustrated shows the three case of the evolution of, ξ it can be constant it which display a stationary growth with no surface morphology changes. The coloration length can extend as $\xi_2 > \xi_1$ leading the extending of correlated height in horizontal dimension or reduction of this scale length where $\xi_2 < \xi_1$ and front roughness is results in this case .The evolution of

the lateral correlation length is similar to the interface width, where ξ vary as power-law with the time as

$$\xi(t) \sim t^{1/z} \tag{1.40}$$

Where $1/z$ is the roughness dynamic exponent with β both describe the dynamic of the grown film and the model occurs for this competition between growth in height and in lateral direction.

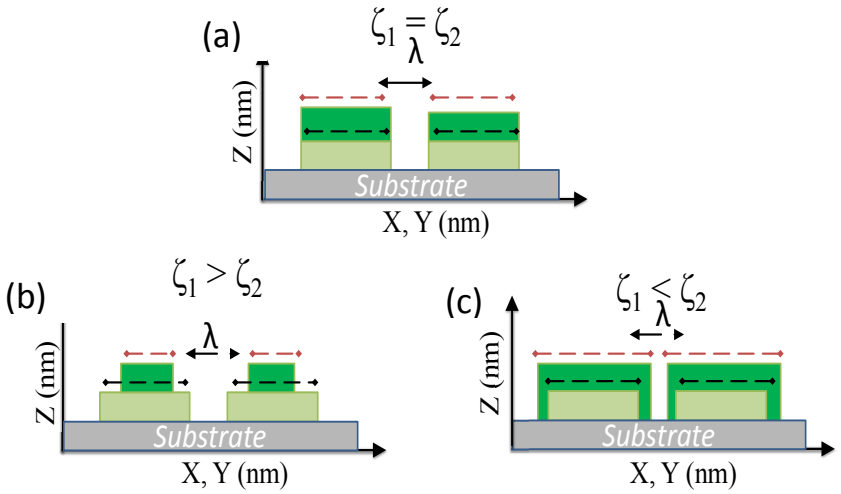

Figure 1.13: *Illustration of lateral correlation length evolution(a) Constant length scale of the nearest correlated height. (b) Reduction of sale of correlated height. (c) the extending of the lateral height correlated.*

1.4.1.3. The roughness exponent (α)

The exponent roughness as illustrated in Figure 1.14 is in both case describing the presence of nosy growth that can happen during the deposition of materials [73]. The simplest description of this roughness exponent is by the classification of the values in the range [0,1]. Some theoretical calculation of α, show that this roughness exponent can be affected also by the geometry of the grain/islands of the materials deposited. The relation between the roughness exponent and the growth model lead to definition of two kind of model conservative growth model where the relaxation process is the chemisorptions and the surface diffusion is neglected, i.e. universal range non-conservative growth 0.4-0.5 and non-conservative model that allowed the creation of voids, where the relaxation mechanism are not competitive with the defects in film grown. Eden model and ballistic deposition model or the (KPZ) model describes volume non-conservative growth when α ≈ 0.4-0.5. For the determination of the exact model, the others roughness scaling would be discussed.

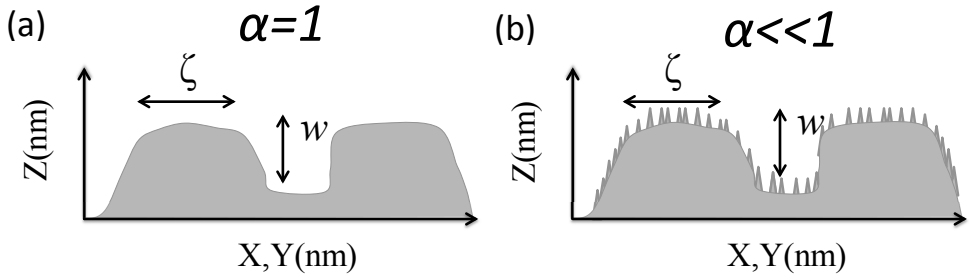

Figure 1.14: *The illustration of the surface morphology for surface roughness exponent α=1 of non-noisy growth (a). For α<<1 the surface then describe an important noise (front roughness) of deposited film (b).*

1.4.2. Scaling functions

This concept has been used as a powerful tool that accommodates considerable simplification leading to the description of the film roughness. The scaling function is mostly used for the scaling description. Through this function the surface roughness can be described in details. This function can be invariant or variant under scaling changes [74]. Here, the height-height correlation function (HHCF) is the chosen function for the analyses of the surface roughness.

1.4.2. 1.Height-height correlation function HHCF

First, the autocorrelation function is introduced, which measures the correlation of surface heights separated latterly by the vector *r.* Is define by the Equation (1.36)

$$R(r,t) \equiv w^{-2}\langle h(x,t)h(x+r,\mathrm{t})\rangle \qquad (1.41)$$

The statistical evolution depends on the surface directions. In results if the behavior does not depend on specific orientation of the surface , then the surface is isotropic and the autocorrelation function is depend only on r. in another hand if the evolution behavior in different way regarding to different orientation of the surface then the surface is anisotropic [75]. In these theses the direction of the surface is measure parameters on the study so the function evolution calculated as it would be shown in section discussion (Chapter 4), where the sample presented two define orientation, so the calculation of the statistical components was calculated for both orientations separately.

The properties of this function are derived from the behavior in tow limit points. For r =0 then $R(r,t)=1$. Now when the (r) is large, surface height become uncorrelated, because in this case $\langle xy\rangle = \langle x\rangle\langle y\rangle$ are uncorrelated variables.The height-height autocorrelation function is define as :

$$H(r,t) \equiv \langle (h(x+r,t) - h(x,t))^2 \rangle$$
$$H(r,t) = \langle [h(x+r,t)]^2 \rangle + \langle [h(x,t)]^2 \rangle - 2\langle h(x+r,t)h(x,t) \rangle$$
$$H(r,t) = 2w^2 - 2\left(w^2 R(r,t)\right)$$
$$H(r,t) = 2w^2[1 - R(r,t)] \quad (1.42)$$

The (HHCF) properties derive from the autocorrelation function, having the same property as the dependence on the surface orientation. The height–height correlation functions a function of $r = |r|$ only for isotropic surfaces, which allows the height–height correlation function to be expressed as *H(r, t)*$\sim 2w^2$ for large r define as r>> ξ and *H(0,t)=0*. The important thing about the (HHCF) is that for the small value of r the function evolution can describe the variation of the correlation between the height at small length range so the correlation between the nearest neighborhood at small range. The autocorrelation term in the equation of HHCF has different expression regarding the nature of the surface. In this theses tow kind of surface are shown which are self-affine surface and mounded surfaces.

1.4.2.2. Self-affine surfaces

For self-affine surface [76], one profile height h(x) for small value of r, i.e. r << ξ , is describe as

$$|h(x+r) - h(x)| \sim (mr)^{\alpha} \quad (1.43)$$

$(mr)^{\alpha}$ is surface local roughness, and α is the roughness exponent, (Figure 1.14). From the Equation (2.38) , the height function HHCF in the case of self-affine surface become

$$H(r) \equiv \langle \left(h(x+r) - h(x)\right)^2 \rangle \sim \langle |(mr)^{\alpha}|^2 \rangle \sim (mr)^{2\alpha} \quad (1.44)$$

This equation leads to the evolution of *H(r) as*

$$H(r) \propto \begin{cases} (mr)^{2\alpha} & if \quad r << \xi \\ 2w^2 & if \quad r >> \xi \end{cases}$$

Now the typical evolution of self affine surface HHCF function is presented in the following Figure 1.15. In the case of self-affine surface the functional for of the *H(r)* can be written as

$$H(r) = 2w^2 \left[1 - exp\left(-\frac{r}{\xi}\right)^{2\alpha}\right] \quad (1.45)$$

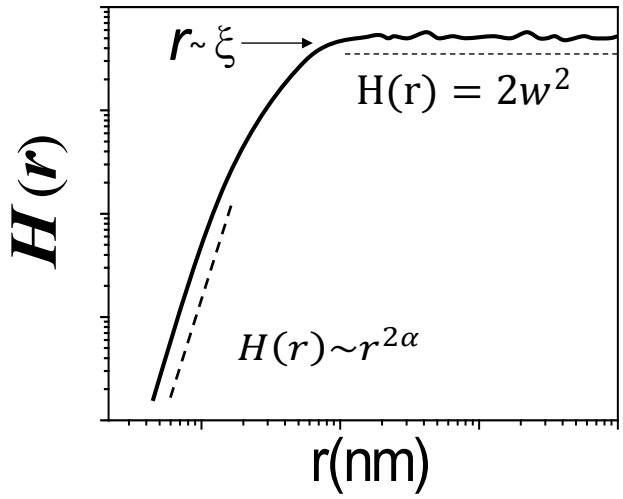

Figure 1.15: *Typical height–height correlation function curve obtained from self-affine surface. The plot is on a log–log scale, which gives the height–height correlation function a linear behavior for small r with slope 2α. For r>ζ , the curves reach a constant value plateau of $2w^2$.*

This functional form was proposed by Sinha et al.[77] the Equation (2.40) allows writing for r << ξ

$$H(r) \approx 2w^2\left[1-\left(1-\left(-\frac{r}{\xi}\right)^{2\alpha}\right)\right] \approx \frac{2w^2}{\xi^{2\alpha}}\, r^{2\alpha} \sim r^{2\alpha} \qquad (1.43)$$

This approach lead to the form of the (HHCF) for small value as $H(r)\sim r^{2\alpha}$, means that the determination of the roughness exponent α is the slope of this function.

- **Local slope**

The local slope presented the correlation between the vertical growth such the surface width *w* and the lateral growth presented on the lateral correlation (ζ), included the exponent roughness α**.** For the smaller r the behavior of the HHCF is then $H(r)\sim(mr)^{2\alpha}$. In the first regime of HHCF the function curve depend on the local slope *m* where it is define as

$$m^{2\alpha} \equiv [r^{-2\alpha}\, H(r)]_{r=0} = 2w^2[r^{-2\alpha}(1-R(r))]_{r=0} \qquad (1.47)$$

In the dimension (1+1) the local slope is then

$$m = \frac{(w\sqrt{2})^{\frac{1}{2\alpha}}}{\zeta} \qquad (1.48)$$

1.4.2.3. Dynamic roughness exponent

The growth of film that shows self-affine surface are described as local growth model, where the dynamic roughness exponents α, β and 1/z. The solid-solid model of growth is based on the equation

belongs to the class of contentious growth. The stochastic Equation (1.49) describe this kind of growth is known as Langevin- Equation,

$$\frac{\partial h(r)}{\partial t} = \Phi(r) + \eta(r) \quad (1.49)$$

η is the noise in the system and Φ is function of the height profile which reflect the growth process. The evolution of the profile with time defines the growth dynamic residue on the behavior of Φ(r). This function is the key of the dynamic growth and contain information about the non-local and local effect, all the models of growth discussed this function in relation with the non-local effect of the growth. The local models that can describe the evolution of the film are summarized in the Table 1.3.

Table 1.3: *Universal equations of the growth and the dynamic exponent solutions.*

Φ	***Equation***	***α***	***β***	***z***	***Reference***
$\nu\nabla^2 h$	Edwards-Wilkinson	0	0	2	[78]
$\nu\nabla^2 h + \frac{\lambda}{2}\lvert\nabla h\rvert^2$	KPZ	0.38	0.24	1.58	[79-80]
$-k\nabla^4 h$	Surface diffusion	1	0.25	4	[81-83]
$\Omega_0 j_z$ $\nu\nabla^2 h - k\nabla^4 h$	Bulk diffusion	0.5 / 0-1	0-0.25	3.33 /2-4	[84]
$-k\nabla^4 h + \frac{\lambda}{2}\nabla^2\lvert\nabla h\rvert^2$	Lai-Das Sarma	0.66	0.2	3.33	[85]
$\nu\nabla^2 h - k\nabla^4 h + \frac{\lambda}{2}\lvert\nabla h\rvert^2$	KS	0.75-0.8 0.25-0.28	0.22-0.25 0.16-0.21	3.0-4.0	[86]

1.4.2.4. Mounded surfaces

Form to the height–height correlation function for a self-affine surface. The only notable difference in behavior arises at length scales beyond the lateral correlation length, or for $r > \xi$. In the self-affine case, the height–height correlation function is constant in this region, but for mounded surfaces it is oscillatory. A frequency peak implies that the surface profile has a quasi-periodic behavior at the peak frequency, and this quasi-periodic behavior leads to oscillations in the height–height correlation function at large distances. One functional form for the height–height correlation function that behaves in this manner is given in Figure 1.16 for a (1+1) dimensional surface.

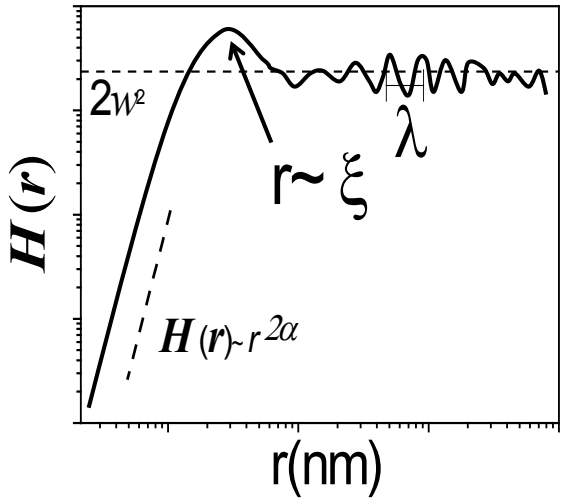

Figure 1.16: *Representative height–height correlation function for a mounded surface. For r~ ζ the HHCF display a peak then decrease to constant plateau for r>ζ with an oscillation of λ period. The constant value is 2 w.*[2]

The Figure 1.16 presented the HHCF curves evolution on the case of mounded surfaces that are obtained in the case where non local effect occurs. The HHCF evaluated then with respect to the Equation (1.50) [87]

$$H(r) = 2w^2\left[1 - exp\left[-\left(\frac{r}{\zeta}\right)^{2\alpha} j_0\left(\frac{2\pi r}{\lambda}\right)\right]\right] \qquad (1.50)$$

This growth behavior display more complicated growth mechanisms which are a result of non local effect. In contrast to the local growth the values of the dynamic roughness exponents has different behavior and values from the local models. Some prediction about the dynamic values α, β, and 1/z are not consisting with the values obtained for the local model growth for some deposition techniques such as CVD, sputter deposition [88-92]. The local model is not able to explain many measurement of β that are not fitting with the same values universal showed in Table 1.3.

- **Length scale λ and Local slope *m***

There has been extensive research and examples of experiments performed on mounds formed by the step barrier diffusion effect during molecular beam epitaxy (MBE), also known as the Ehrlich–Schwoebel barrier effect. This effect does not allow atoms to diffuse over the edge of a step on the surface, which creates an overall uphill current of diffusive particle flux. [93-99]This effect is a characteristically local growth effect because it involves the diffusion of particles on the surface [102-104]. Diffusion, by definition, only affects atoms near the diffusing particle, and as a consequence the effects of diffusion are localized. However, the step barrier diffusion effect creates mounds on the

surface, with the average mound separation λ evolving as a power law, $\lambda \sim t^{p}$, where the experimental values of the wavelength exponent p lie in the range from 0.16 to 0.26. In addition, the growth process can be modeled by a local stochastic continuum Equation (1.60)

$$m = \frac{(w\sqrt{2})^{\frac{1}{\alpha}}}{\zeta}\left[1+\left(\frac{\pi\zeta}{\lambda}\right)^{2\alpha}\right]^{\frac{1}{2\alpha}} \tag{1.60}$$

- **Shadowing and Reemission**

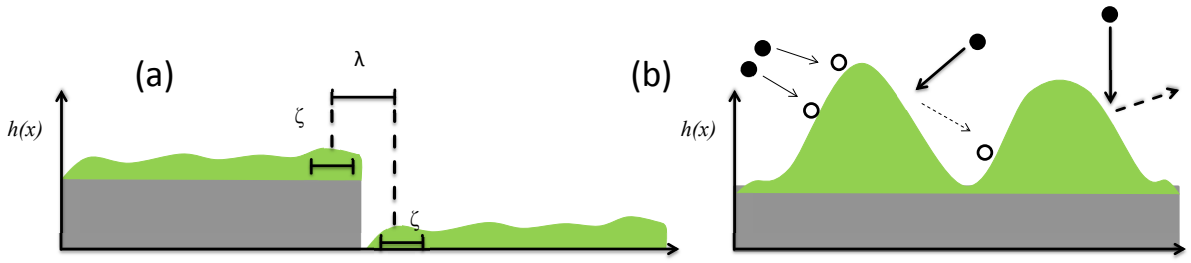

***Figure 1.17**: Illustration of the origin factor of mounded surface. (a) Steps effect and (b)shadowing effect of relative tall structure in the surface that lead to different motion of the particles/molecules reach the surface. The distributions are not conformal and particles can leave the surface or attached in the top/lower part depending of the energy of striking to the surface.*

The steps effect in figure 1.17 is also an important surface parameters that lead to non equilibrium growth. The molecules coming if they do not react and adsorbed in sites over the surface important surface diffusion can occur. The defect regular such as steps with the barrier on the steps. The difference is the barrier effect on the bottom and top of edges leads to non continuity of the film orphology and creating important growth in lateral position with the condensation of materials. In many common thin film growth techniques such as sputter deposition and chemical vapor deposition (CVD), the growth dynamics are dominated by where taller surface features block incoming flux from reaching lower-lying areas of the surface. A diagram of the shadowing effect is seen in Figure 1.17(b). The shadowing effect is active because, in sputter deposition and CVD, the incoming flux has an angular distribution. This allows taller surface features to grow at the expense of shorter ones, leading to a competition between different surface features for particle flux. This competition ultimately leads to a mounded surface as shorter surface features receive little or no particle flux and "die out". Shadowing is an inherently nonlocal process because the shadowing of a surface feature depends on the heights of all other surface features, not just close, or local, ones.

Chapter 2: Experimental and materials

This chapter is dedicated to the description of experimental set-up of in-situ STM. The STM experimental and the tip preparation used in this thesis. The experimental part is divided into two parts: techniques used for preparing sample and techniques used for characterizing the samples. The technique involved in synthesis of Al_2O_3 and HfO_2 is the atomic layer deposition (ALD). The grown samples are investigated with scanning tunneling microscopy and an x-ray photoelectron spectroscopy (XPS) using laboratory.

2.1. In situ ALD-STM set-up

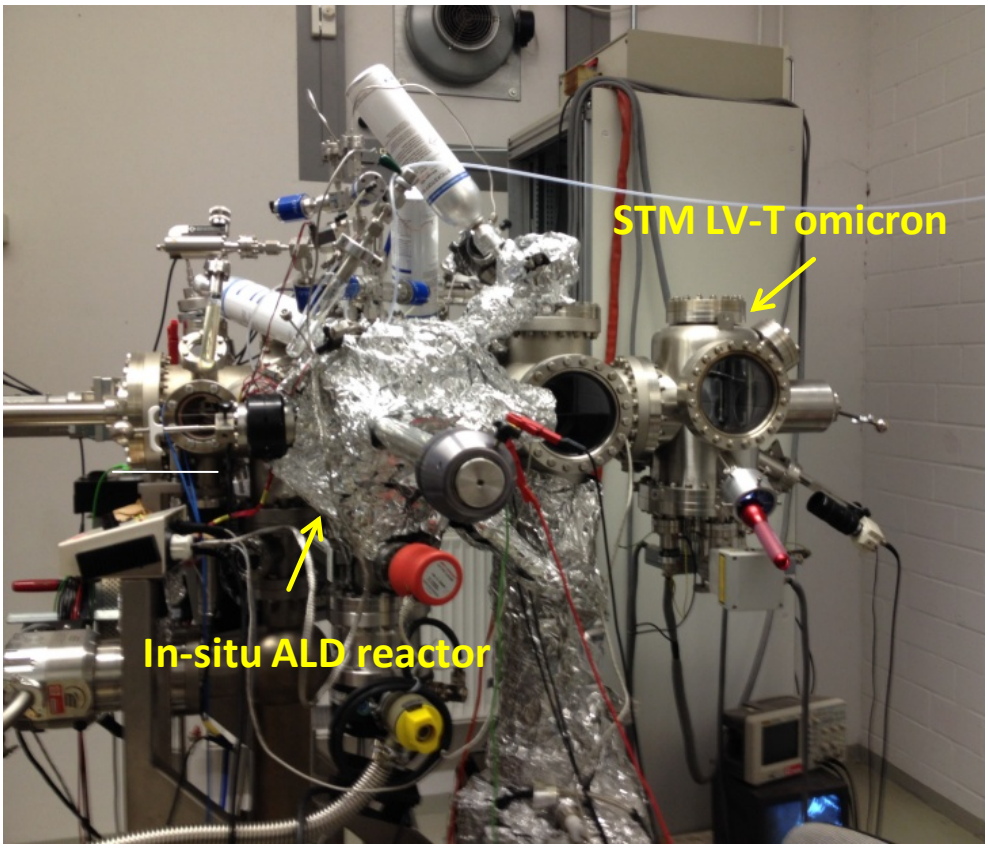

***Figure 2.1**: (Photo) The in-situ ALD reactor attached to the STM .The deposition is done at high vacuum with a pressure of 7 x10^{-8} mbar. Then the sample transferred to the STM (omicron LV-T) chamber where the pressure is 9 x10^{-10} mbar.*

Our set-up contain the STM chamber, in-situ ALD attached to preparation chamber and the preparation chamber that is at pressure of 10^{-8} mbar. The used STM is an Omicron LV-T at ultra high vacuum ~ 10^{-10} mbar. This STM is equipped by a system anti-vibration that prohibited the oscillation of the tip as consequence no noise can affect the imaging data. This system is highly stable against mechanical noise such as pre-pomp. All the STM measurements are done at room temperature, not important drift is obtained at this temperature. All the STM pictures were recorded at the resolution of 800 x 800 raster points scan lines. With STM, we measured different area from the sample and the data analysis performed with WSxM software [100].

The in-situ ALD reactor attached (Figure 2.2) to the STM is maintain at 7 x 10^{-8} mbar which presence an ultra high vacuum. Three ALD valves are connected to the reactor that contains the precursors.

These valves are automatically opened for define duration that are adjusted refereeing to the precursors used. This ALD is home made in our group that was used in many ALD in-situ investigation that shows distinct results among the ALD fields.

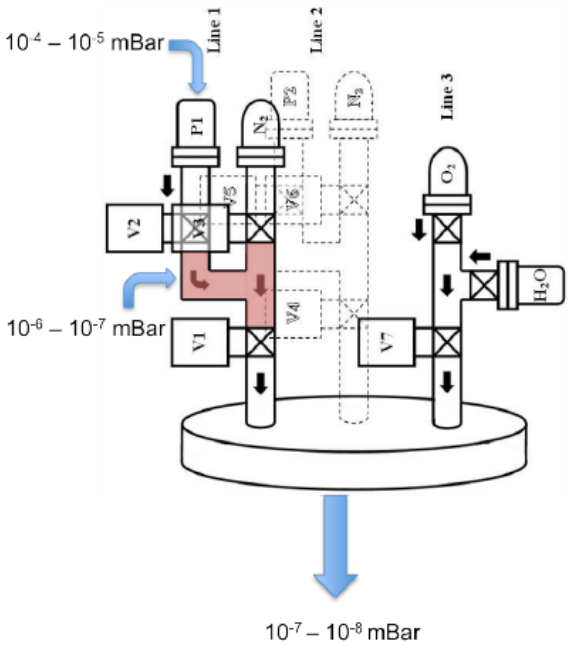

Figure 2.2: *Schematic drawing of the gas delivery system used for the in-situ reactor* [101]

The ALD of HfO_2 was performed in the in-situ ALD reactor equipped with valves for the regulation of the Hf-precursor and the oxidant, in this case H_2O. The pulse length of Tetrakis-(dimethylamido)-hafnium (IV) (TDMAH) half cycle was 1.5s pulse followed by a two step nitrogen purge pulse (after 1 and 5 seconds) to eliminate un-reacted precursor molecules. The reaction saturation of the TDMAH standardized in our system to be 1.5 second. In the literature the time of saturation can varies with the reactors but in this range of time. The second half cycle consists of an oxygen source pulse (H_2O in our case) with duration of 0.5s.

The reactor is equipped by heating system where the substrate is installed and through resistance heating the temperature increase to reach the temperature needed. The heating process is done with very small steps of current increase to not create an strong gradient of temperature in the substrate. After the deposition the sample is then transferred to the STM .To get full insight of the HfO_2 growth we started the STM study on fresh Si-H terminated surfaces and investigated the growth for each half cycle up to the fourth one at room temperature. For the second cycle the deposition is done at 280°C temperature of the substrate.

2.1.2. STM tip preparation

The STM measurement is fundamentally based on the quality of the tip that is used to probe the surface. The tip used in STM is important for the realization of successful microscopy, where no good tip lead to lousy imaging. The tip should be extreme sharps with an apex of single atom for ideal measurement; this can resolves details in atomic scale. The small aspect ratio of the tip reduces the vibration that can occur during the probe then stable atomic resolution is obtained. Different kind of metal are used as tip such as gold and platinum however the tungsten is the most metal used as tip. The tungsten tip present high stable tunnel junction in ultra high vacuum that why in this work the tip that was used is prepared from tungsten materials. The procedure of tip preparation is based on electrochemical etching of tungsten wires has different protocols and experiments where no only way to prepare the tip. In the Figure 2.3, the producer of our tip preparation is detailed

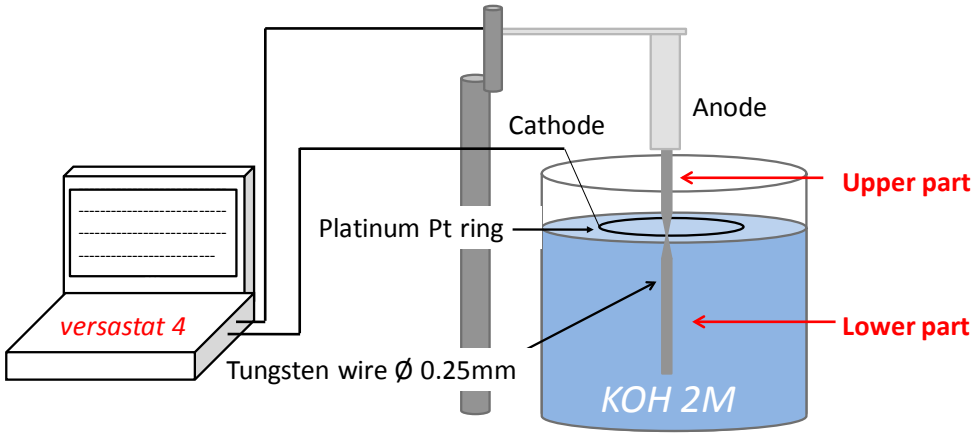

Figure 2.3: *Set-up of electrochemical etching of Tungsten (w) (Anode) wires in 2M KOH solution with Pt ring as cathode with application of 5V for 15min. The electrochemical process is controlled by versastat 4.*

The tip was made by electrochemical etching in 2 M Potassium hydroxide (KOH) solution from 0.025mm tungsten wires. The tip is emerged in this solution in vertical position in center of platinum wire made in circular shape. The tip and the counter electrode are connected to versastat 4 that control the current applied where it stops the alimentation once the etching reaction is done, this lead to the reduction of oxidation of the tip apex. The bias voltage applied between the anode and the cathode is 5V DC, which is necessary to generate the flowing etching reactions [102]

Cathode: $6\,H_2O + 6e^- \rightarrow 3\,H_2(g) + 6\,OH^-$

Anode : $\underline{W(s) + 8\,OH^- \rightarrow WO_4^{2-} + 4H_2O + 6e^-}$

$$W(s) + 2\,OH^- + 2H_2O \rightarrow WO_4^{2-} + 3H_2(g) \quad (2.1)$$

Afterward the tip was cleaned with ethanol and isopropanol in ultrasonic bath then immersed in 49% HF solution for 5s that lead to the remove the WO_3 oxide layer formed from the electrochemical etching of the tip. After every step with dry the tip with running N_2. Before installing the tip in the STM a sputter with Ag+ is done to remove the contamination and lead to well define sharp tip.

2.1.3. STM resolution and calibration

The STM station is equipped by feedback system that is highly sensitive to the electronic density changes over the surface. The tip oscillated according to the fine changes of the surface morphology at atomic scale delivering well defines images of surface. The scanning is controlled in three-dimension (3D) by a piezo-scanner either bound to the tip. The speed of this feedback is essential for good measurement; therefore via the interface omicron controlling the speed is required.

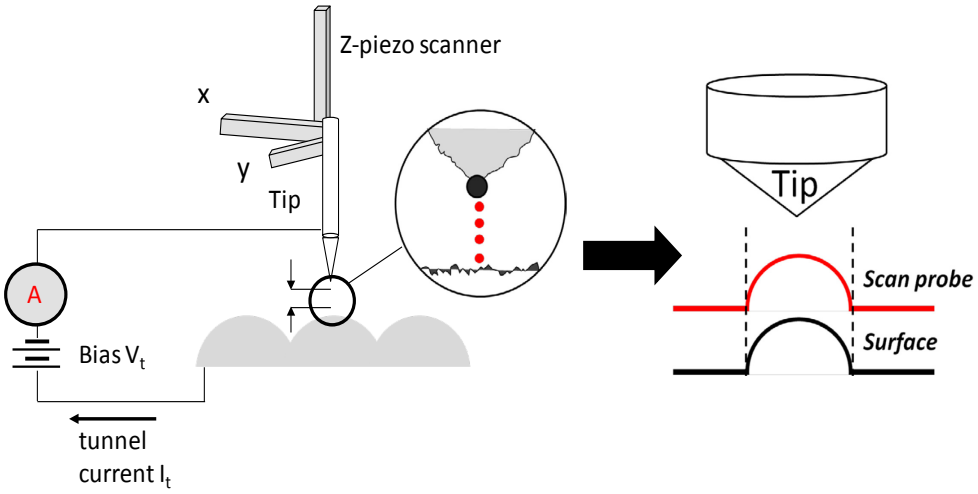

Figure 2.4: *Illustration of the STM system of measurement. The current applied on the sample and surface lead to current tunneling between the tip and surface. The feedback is controlled by piezo scanner which assures the movement forward/backward from the surface to maintain constant height/current. Best scan parameters implies better and higher resolution of the feature probe.*

For the measurement tow kind of procedures can be used: constant current mode where the piezo-scanner changes in the (Z) direction when the tip probes the surface to keep the same tunnel current between the surface and the tip. The second mode is used at fixed distance (z) so then the images is

obtained with the changes of the electronic density in other way the tunneling current between the surface and the tip. In our investigation, the first approach is used which is better for rough surface because at mode with fixed (z) the tip can be easily crushed.

In Figure 2.4, the illustration of the 3D of piezo-scanner and the set-up of the current bias for the STM. The voltage applied between the tip and the surface is important for the good prove. The set of the current and the voltage should be calibrated to get good results, where the tunnel current obtained should describe the right changes of the electronic density over the surfaces. The Tip during the scan over the surface responds to the local electronic density in every (LDOS) point on the surface. Spatial movement of the tip, assigned to the changes of (LDOS) on the surface.

In summary to get good results that revile real surface morphology, suited tip should be made and then calibration of the current and voltage applied between the substrate and tip should be done according to the different measured surfaces.

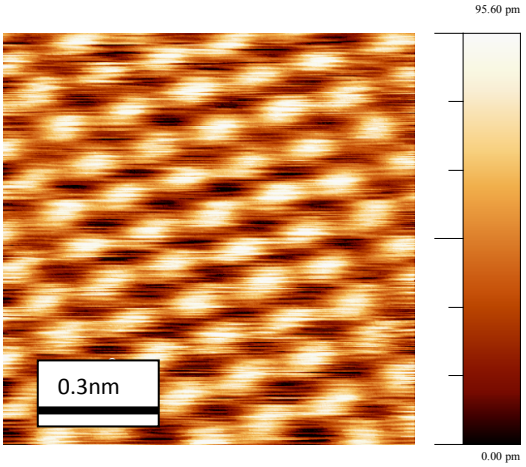

Figure 2.5: *HOPG nano-resolution STM images (1.2nmx1.2nm). Gap voltage V=0.3V and current I=-1.41nA and the scan speed 50nm/s.*

We used HOPG substrate that is cleaved with scotch type as substrate reference for the calibration of the STM and to be sure about the tip resolution. In Figure 2.5, nano-resolution of HOPG measured with tungsten tip that was homemade indicated that our tip is ideal for the investigation that is done with our STM.

2.2. Materials

2.2.1. Precursors

2.2.2.1. Tri-methyl-aluminum: TMA

Al_2O_3 is one from the most studies high-k film grows by ALD. Since the first attempt at growing Al_2O_3 ALD using tri-methyl-aluminum (TMA) and H_2O precursors late in the 1980s. Extensive studies have been establishing to determine different growth parameters of Al_2O_3 [103-107] owing to the impressive application of this film in the semiconductor industry. The chemical properties, used in this thesis, of the TMA, are presented in Table 2.1

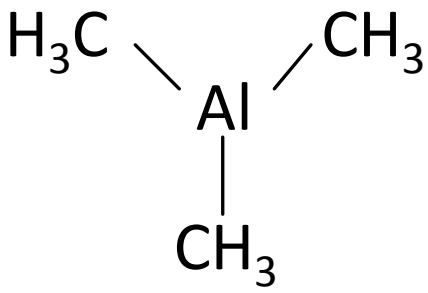

Figure 2.6: *Tri-methyl-aluminium (TMA) molecules*.

The reaction of the precursors TMA ($Al(CH_3)_3$) and H_2O leading to the Al_2O_3 growth is described by the flowing Equation (2.2) [108-112]so long as Al-O bond are strong.

$$2 \text{ x } Al(CH_3)_3 + 3H_2O \longrightarrow Al_2O_3 + 3 \text{ x } CH_4 \qquad (2.2)$$

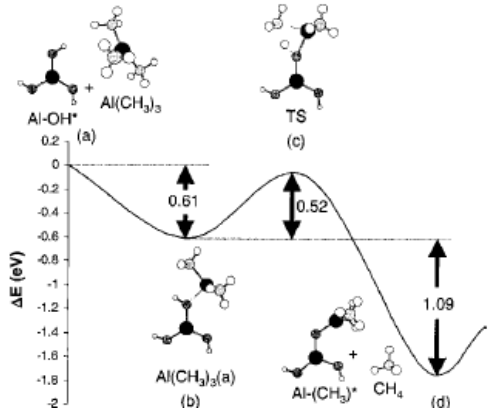

Figure 2.7*: Reaction path and predicted energies for the reaction of $Al(CH)_3$ on the Al-OH* surface site calculated using the $Al(OAl(OH)_2)_2$ –OH cluster* [113].

The TMA precursors are highly reactive this why the reactions efficiency increase, accompanied by the self-limiting growth. As consequence of the reaction efficiency different reactions path can results in relation with the surface potential energy. DFT modeling was done by Widjaja et al [113], present a

predicted reaction path of TMA and water ALD. The energetic diagram (Figure 2.7), shows that Al_2O_3 growth has different reaction process in relation with the energy. The reaction path of $Al(CH)_3$ favor the formation of Al-OH on the surface. The surface reaction of TMA during ALD process showed that the AlOH* molecules increase in front of the increasing of $AlCH_3$* species. However, the other ways round happen when the surface is exposure to H_2O, the AlOH* gain in an increase in front of $AlCH_3$*. This surface chemistry was showed in many studies of ALD film growth from TMA and H_2O.

The ALD-Al_2O_3 film parameter has been investigated for different deposition condition, such as the temperature, deposition time. Most studies report that the growth of Al_2O_3 presented a perfect linear growth with the number of cycles, with a growth per-cycle 0.11-0.12 (nm). This growth is less than the growth of monolayer Al_2O_3. The monolayer, as it was shown in the first chapter, can be estimated from the model of height (see section) using the density (Table 2.1). The density of Al_2O_3/cm^3 is then:

- $\rho = 1.7 \times 10^{22}$. Units/cm^3.
- $\rho^{\frac{2}{3}} = 6.8 \times 10^{14}$. units/cm^2
- $\rho^{\frac{1}{3}} = 3.8 \times 10^{10}$. units/cm

The monolayer is then about 0.38nm, this value is much higher than the measured film thickness of the growth per cycle, i.e. 0.11-0.12nm.

Table 2.1: *Chemicals properties of the molecules Al_2O_3 that can be formed from the TMA+H_2O.*

Parameters	Molecular weight (g mol^{-1})	Density ρ(g nm^{-3})
TMA	58	$3.8\ 10^{-21}$

2.2.2.2. Tetrakis(DiMethylAmino)Hafnium TDMAH

The HfO_2 film grown by ALD has been the subject of many studies because of the important properties, e.g. dielectric constant, of these high-k films [114-115]. As consequence, HfO_2 thin oxide film is an alternative candidate for silicon dioxide gate. As Al_2O_3 ALD film, HfO_2 film grown achieved high conformality film growth on height-aspect-ratio structures [116-118]. The reactant use for the build-up of the film by ALD process varies for different ligand attached to the -Hf atoms. The most popular Hf precursors for ALD at present are hafnium alkylamides. Due to the relatively weak Hf-N bond and their high volatility, this enables efficient deposition at relatively low temperatures.

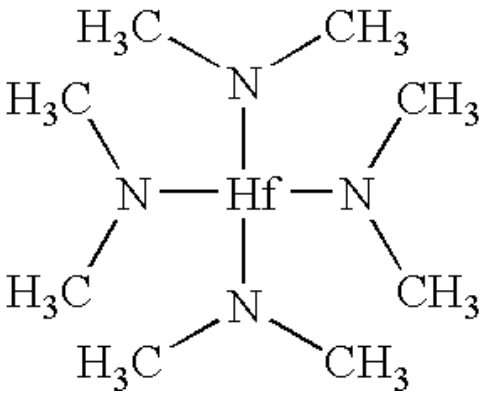

Figure 2.8: *Tetrakis[DiMethylAmino]Hafnium Hf[N(CH$_3$)$_2$]$_4$ (TDMAH) molecule.*

Tetrakis-Ethylmethylamino Hafnium (TEMAH), Tetrakis-Dimethylamino Hafnium (TDMAH). Hafnium chloride ($HfCl_4$). For the deposition of high-k films, with O_2, O_3 and H_2O being the most common oxidant precursors. TDMAH has been widely studied for the ALD of HfN_x and HfO_2 on Si surfaces is used essentially for the deposition of pure HfO_2 or in conjunction with silicon sources or aluminum sources to form silicates and aluminates respectively. TDMAH can be used both in ALD or MOCVD mode for the deposition of high-k films, with O_2, O_3, and H_2O being the most common co-reactants. In this thesis, H_2O is the oxidant used in the HfO_2 ALD growth. TDMAH fulfill reactant properties for ALD reaction, where a low melting point TDMAH reacts immediately once its exposure to H_2O. As consequence strong bond formed between -Hf and -OH. As it shown in the Figure 2.8, TDMAH composed from one atom of -Hf and four group of -NCH_3.The ALD reaction leads to the dissociation of the x-NCH3 group and create a Hf-OH bond.

Table 2.2: *TDMAH molecular weight and density.*

Parameters	Molecular weight (g mol^{-1})	Density ρ(g nm^{-3})
TDMAH	354.8	9.6 x 10^{-21} gnm^{-3}

The density of the reactants and the bond length showed in the Table 2.2. Would be used, like for Al_2O_3, to determine the monolayer of HfO_2. The reported values of the growth per cycle on HfO_2 are about 0.1nm/cycle. The surface termination was shown to be important for the film growth where mostly the systems used are –OH terminated.

- ***HfO_2: TDMAH+H_2O on Si-H terminated***

The growth of the many ALD precursor on Si-H terminated is one from the important field in the understanding of the ALD as the important of Si-H substrate in growing gates for the semiconductors industry. Many investigations were done by the comparison between the growth on Si-H and Si-OH, where it's known that -OH group are reactive sites for ALD precursors to nucleate on the surface. The

first reaction between the precursors (AlMe, ZnMe, $HfCL_4$ ...) and Si-H revile complicated behavior of chemical reaction with the surface.

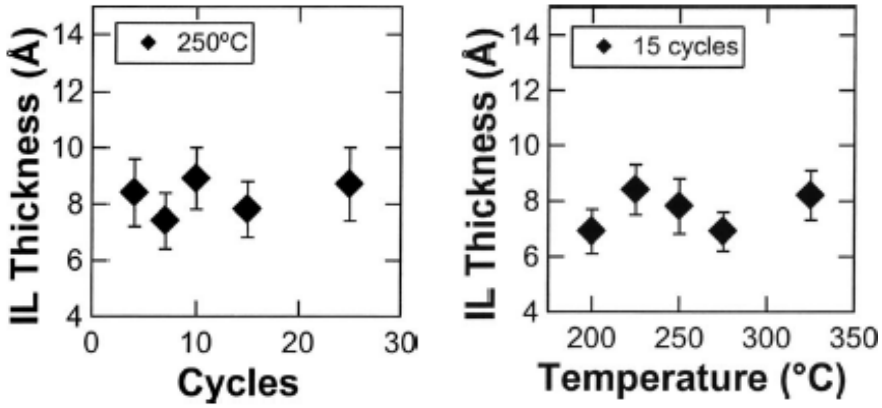

Figure 2.9: *(a) The thickness of the interfacial layer as a function of cycle number for HfO_2 films on Si–H surfaces. (b) Interfacial layer thickness measurements for a series of 15 cycle HfO_2 films deposited at substrate temperatures ranging from 200 to 325 °C* [119].

C. Hackley et al. [119-121], deeply investigated the growth of HfO_2 from TDMAH and H_2O on both Si-OH and Si-H terminated surfaces. They showed that the growth of HfO_2 at 275ºC on Si-H, display in early growth stage an interface of 0.8nm of SiO_2, this layer hence then the growth and tune the nucleation of HfO_2. The thickness measured of the film is constant from the 4^{th} to the 25^{th} cycles. In Figure 2.9, the film thickness is shown with the number of cycles and with the temperature evolution. The formation of the HfO_2 on the early stage of ALD is still far from being understood from a chemical point of view where many reaction mechanisms can occur this was especially observed for Al_2O_3 grown on Si-H terminated.

The energetically reaction Recently C. Longo et al [122], calculated the chemical composition and the growth rate in the use of density functional theory (DFT) used density-functional theory methods with the aim of investigating the selective reaction growth of HfO_2 on Si-H terminated and (-OH) through the deposition of two precursors TDMAH and H_2O. M.-T. Ho et al. show the growth of HfO_2 on Si(100)-H terminated display a bond creation between Si-H and Hf- atoms leading to the growth of Si-Hf-OH bond. Therefore, no observed important difference between both termination, (-H) and (-OH) species, still the idea about the poorer growth of HfO_2 on the Si-H terminated still remain the major problem of ALD on Si-H surfaces.

M. Jason Kelly et al [123], studies the growth of HfO_2 on Si-H terminated by in-Situ Infrared Spectroscopy and DFT modeling of hafnium alkylamine Adsorption on Si-H. They show that a ligand exchanges between Hf-N(Me) and Si-H occur. Accordingly, TDMA-Hf reacts with a fully hydrogenated Si-(100)-H surface, involving hydrogen abstraction that occurs by direct interaction

between the Si-H and –Hf metal atoms, leading to the formation of reactive Si radical surface sites and H-N(Me) gas product.

In this theses, the microscopy is done to show the possibility of nucleation of the first 4th cycle (This part still dark in the ALD process) of HfO_2 on Si-H. The height of the feature and the coverage and density of the formed ALD nucleation can prove if there is ALD or now and theoretical model are used to investee if the compounds formed is Hf-Si or it's just a formation of the Si-OH group from the H_2O pulses.

2.2.2. Substrates

2.2.2.1. Si (111) - H-terminated: etching at NH_4F 40%

We used P-type Si(111) samples one side polished, the resistivity of 10 Ω cm, miscut with an angle of 0.5° toward [$\bar{2}$11] direction industrial provided from PI-KEM Ltd Company. A complete process for the passivation of the Si(111) was flowed to obtain ideal Si-H stepped surface. NH_4F 40% is one of the most used processes for the etching of Silicon.[124-126].

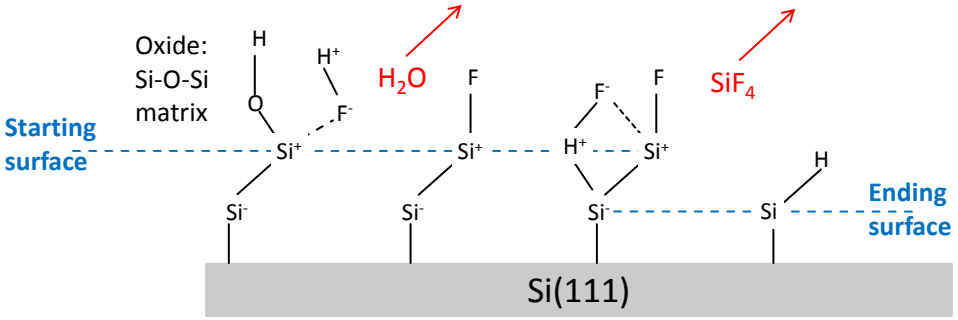

Figure 2.10: *Illustration of the reaction between the HF ions and the Si-OH surface. This reaction starts with the bonding of F^- to Si^+. The H^+ bond with –OH species leading to the formation of H_2O that leaves the surface with Si^+F^- bond. With the coming HF ions bond with the Si created strong electronegativity that results in SiF_4 that leave the substrate. As results passivated surface Si-H is created.*

In Figure 2.10, an illustration of the reaction occur during the wet etching with NH_4F (Figure 2.10 (a)) that lead to Si-H bond, in Figure 2.10 (b) in the case of stepped surface on the terraces (flat surface) vertical bond of Si-H however on the steps edges formation of monohydride and dihydride can results.

First, the initial Si (111) wafer must be clean without any organic contamination to form a uniform oxide layer, the sample was cleaned with acetone and isopropanol in an ultrasonic bath as a first step to remove big contamination from the wafer and then clean it in hot water for 20min. Then the sample was emerged in 120°C of Piranha solution (H_2O_2: H_2SO_4, 1:3) for 15min to eliminate the contamination as metallic ions and particles and organic, in this process, the surface is etched and

oxidized leading to growing layers of oxide. The sample was then carefully transferred to the RCA1 solution (H_2O: H_2O_2: NH_3, 4:1:1). Then we emerge back the sample in Piranha solution for 10min. After each step of the cleaning process, we rinsed the wafer by running Ultra pure water and dry it with running pure N_2. The sample was then reemerged in a vertical position in 40% NH4F for 10 min.

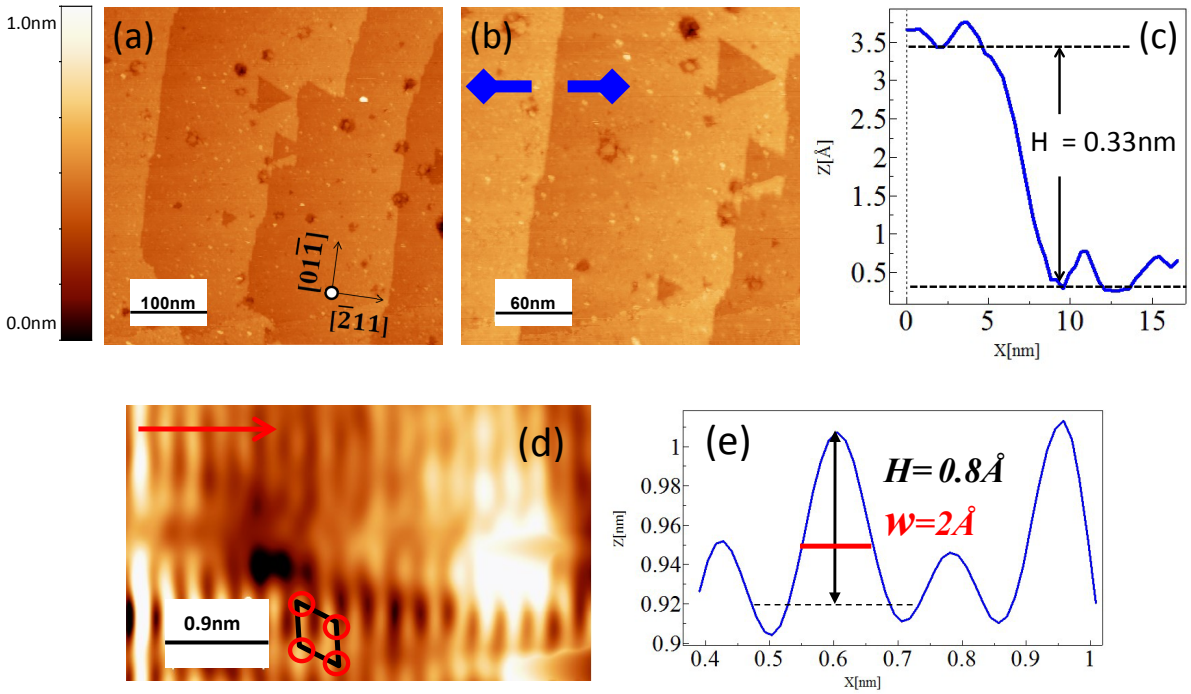

Figure 2.11: *(a) large field of Si-(111)-H substrate prepared by NH_4F 40% wet etching reaction lead to a flat surface on the terraces with a roughness of RMS =0.02nm. The step height is 3.3Å which is identical to the distance inter-planer of Si-Si layer in the direction perpendicular to the surface. The crystalline structure of the prepared Si(111)-H is presented in the STM images (d), the structure of the silicon is (1×1) structure which of (111) facet of the silicon etched. The profile o shows the Si-H in the perpendicular with the Si-Si under layer.*

The remove of oxygen from the solution is important for better etching process where the O present can lead to the formation of pitch on the surface. The installation of the sample is similar to the one reported by Wade and Chidsey [127]. After the etching, we dried for 2 min by running N_2. To avoid the effect of oxygen in the etching reaction we bubble the NH_4F solution with N_2 for one hour before the emerging of the wafer to dissolve O in the solution. All those parameters are so important to get the flat Si-H terminated with regular terraces and steps flow. The sample is transferred within some second to UHV, where we attached an ALD reactor made by our group.

Terraces were, therefore, expected to be about 100nm wide on average. In this state's, the wafer has an interface of Si/SiO_2. In our study we are investigated Si-H terminated surface, this is why we need an

etching of the surface to remove the SiO_2 layers. The chemical preparation of vicinal Si(111) is too delicate, dependent on many parameters, the most important parameter is the speed of the etching, the higher that the pH of the solution is, the faster etching of surface will be. Despite the height of barriers which is at the level of atoms scales, this effect of smoothing can lead to an intrinsic surface tension proper to the substrate orientation.

2.2.2.2. HOPG / Ag- HOPG

- Highly oriented pyrolytic graphite: HOPG

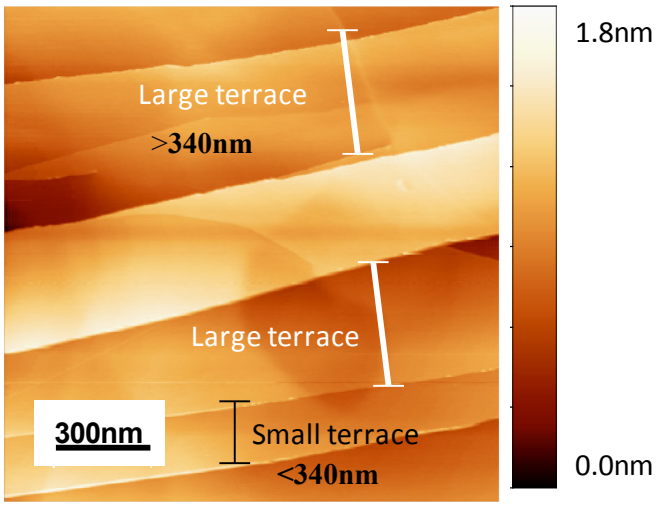

Figure 2.12: *STM image (1.5µm x 1.5µm) of HOPG cleaved in atmosphere with scotch type and cleaned with N_2 in vacuum.*

The HOPG sample (supplied by Veeco) was cleaved several times using Scotch tape right before the introduction into the vacuum system and the measurement. The cleaved substrate lead to an internet stepped surface with different widths scale of terraces. We define tow kind of terraces (Figure 2.12): Large terraces for widths >340nm and small terraces for widths <340nm. The definition of terraces widths is regarding the diffusion length of the precursors as it will be discussed in chapter 4, where the grown film displays different features of growth depending on the widths of terraces. A model will be introduced in the chapter 4.

- Ag-HOPG

For the second substrate, we deposited Ag on the HOPG surface. This growth was done in a UHV chamber equipped with a cell for thermal deposition consisting of 0.5mm pure silver wire (99.99%) subjected to a direct current of 17.1 A at a voltage of 0.9 V. For 1 min of thermal deposition, at pressure of 10^{-8} mbar, Ag nanoislands grow on the steps edges of HOPG surface.

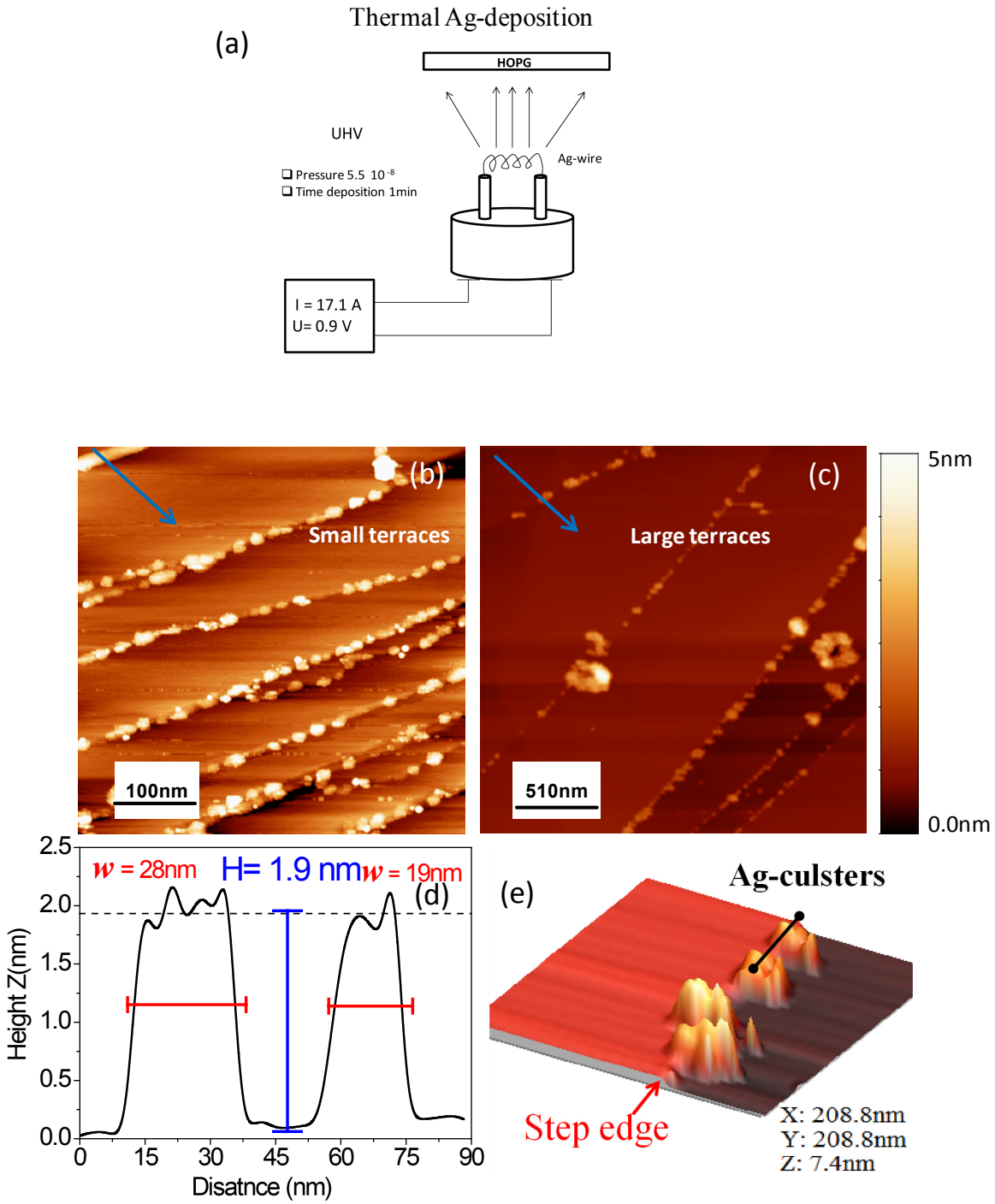

***Figure 2.14**: Silver PVD deposition on the HOPG. (a) the station of thermal evaporation of silver (b) and (c)STM images of the deposited Ag on the steps edges on small and large terraces respectively.(d) the profile of 2 adjacent Ag-clusters on the steps from figure (e) 3D of the two islands on the steps edges.*

We grow ALD on Al_2O_3 on Ag-HOPG which the same deposition parameters and then scanned with STM. Figure 2.14 shows the distribution of the silver on the HOPG substrate. The growth of Ag-cluster grows on the steps edges and decorated them along the parallel to the steps. Figure 2.14 (b-c),

presents a scan area of (500nm × 500nm) and (2.4μm × 2.4μm) and depicts that an agglomeration of silver on the edge of steps occurs; the height of these clusters varies between 1-5nm. Figure 2.14 (d) and 2.12 (d) show STM 3D one step large terraces shows two Ag-cluster with a height of 1.3nm for both.

Chapter 3 Results

In this chapter the results of ALD growth on the three different substrates Si(111), HOPG and Ag-HOPG will be described in details. This chapter is divided into two main parts.

The first part is dedicated to the characterization of in-situ ALD growth of TDMAH and H_2O on Si(111) at room temperature and at 280°C, using STM. The ALD growth features, parameters, nucleation and islands formation would be the main results that describe the morphology evolution of the film on the different substrate in relation with the Si(111) crystallinity (stepped surface, the direction of the surfaces flow).

The growth of Al_2O_3 on HOPG is pure as its is predicted for the ALD on HOPG. The results are mainly dedicated to the investigation of the nucleation and the grown features the (2D and 3D, stripes) observed on the terraces using scanning tunneling microscopy. Those results are dictated to examine the assumption about the ALD growth on inhibited surface to cheek the growth per cycle evolution with the number of ALD cycles.

3.1. HfO_2 ALD on Si-H surfaces

The results presented in the flowing part have two different resolutions of the area scanned. First, large area of 500-700nm^2 to get an overview of growth. Then high resolutions of the step region and on the planar surface (terrace) , to investigated the islands formation and surface coverage at nano-scales. The profiling of the different ALD features is done for the step and islands height.

3.1.1. Cycle -by-cycle STM

3.1.1.1. Si (111)/HfO_2 growth at RT

- **First ALD cycle**

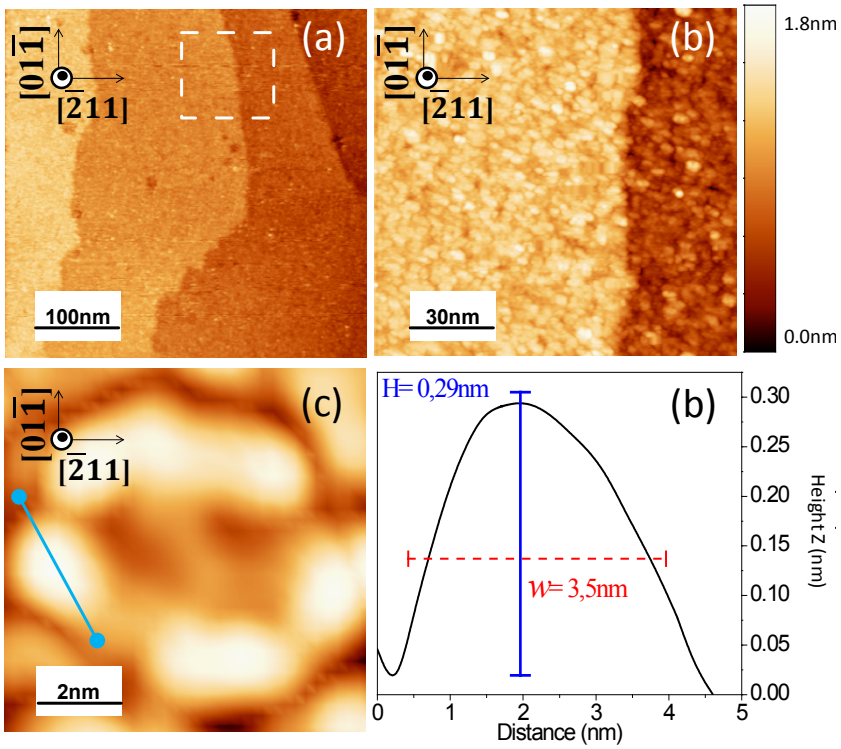

Figure 3.1: *Constant-current STM images of the first TDMAH deposition: (a) an overview (500nm × 500nm) of the surface coverge by the deposited molecules, homognious deposition at large scale. (b) Step region (150nm ×150nm) zoomed in on the spot marked by dashed square from (a) shows a replica growth of the steps. (C) High resolution of (10nm × 10nm) of group of islands arranged in flower structure. (d) Profile of single islands (blue line Figure (c)) with the dimension of 0.29nm of height and 3.5nm of width.*

In the first half cycle (Figure 3.1) of TDMAH deposition, the growth displays high homogeneities over the terraces or on the steps edges. The surface coverage of islands with height 0.2-0.3nm is ~90%. In this half cycle the root-mean-square (RMS) roughness of the substrate increase from 0.02nm (initial roughness substrate) to 0.15nm. The roughness is in relation to the increase in height of ALD deposited materials. STM measurement of single group of nucleated islands presented in the Figure 3.1 (c) on surface fraction of $10nm^2$. A single island has width of ~4nm and 0.29nm of high as it is shown in profile Figure 3.1 (d). Those islands are distributed randomly with no preferential direction.

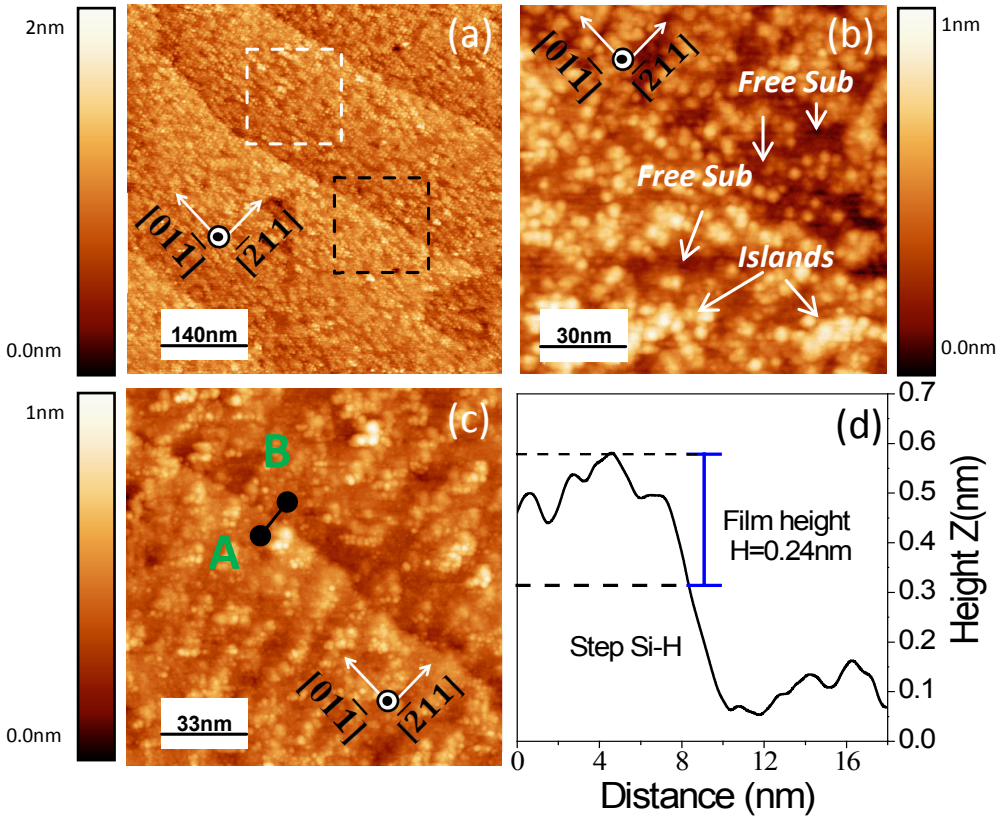

Figure 3.2: *Constant-current STM of the complete cycle of TDMAH and H_2O deposition. (a) An overview (700nm ×700nm) an increase of the surface roughness over the terraces. (b) and (c) zoomed in on the spot marked by dashed white and black square, respectively in (a). (b) the distributions of islands over the planar surface with coverage of 71% of surface fraction of (150nm × 150nm). (c) Magnification of step region of one step with height of 0.24nm on the top of edges for scan line A-B. (c) Profile of the steps height of A-B line.*

Within the second half cycle, H_2O pulse is so interesting; it's obvious that the agglomeration started really with the deposition of H_2O. While the film features display high agglomeration over the surface of islands with dimensions variying from 0.24nm in the steps region to 0.4nm in the terraces(see

Figure 3.3). The RMS roughness increase with small amount from 0.15nm to 0.18. Thus the deposition of H_2O changes slightly the height of islands with a decrease in height of islands with about of ~0.05nm. However the surface coverage becomes 71% of islands (Figure 3.2(b)) with a height in the range of 0.20-0.46nm. This behavior can be related to the fact that the OH group subtract the ligand $N(CH_3)_2$ from $Hf(N(CH_3)_2)$ leading to reduce of the film heights(see discussion Puurunen model application).This height of materials deposited on the steps edge of the A-B scan line in Figure 3.2 (c) shows the film height is 0.24nm on the top edges (Figure 3(d) profile). The ALD film formed shows different features of agglomeration of islands, on the bulk of the terraces ether in the region of the steps.).

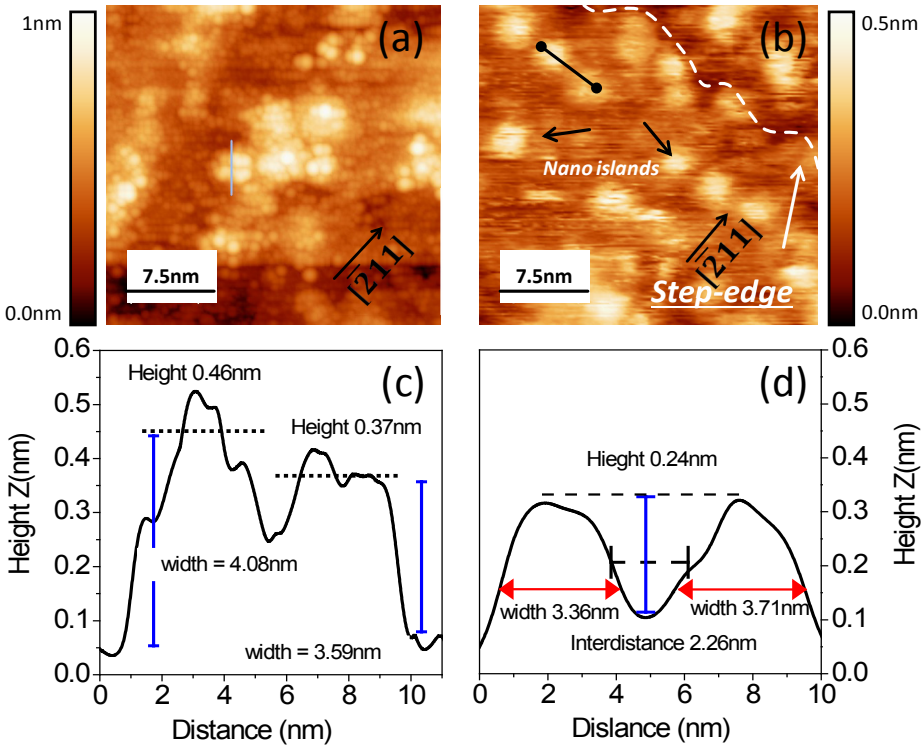

Figure 3.3: *Constant-current STM High resolution (a) and (b) (37.5nm × 37.5nm) of nucleation of HfO_2 on planar surface and step regions. (a) Nucleation in terrace of molecules in flower structure on the terraces. From the profile in (c), the height varies between 0.37-0.46nm. The feature of ALD on the steps region is clear to be isolated islands with the same dimension of 0.24nm of height and 3.3-3.71nm as it is shown in the profile (d).*

Figure 3.3 (a) shows one example of islands formation. It is clear that the growth of those islands has the same pattern of the first half cycle (see Figure3.1 (c)). The dashed white circles show the formed islands fraction. The height increase from 0.27nm to 0.37-0.49nm. As like as the width from 8nm to10nm the coverage fraction of the surface by this islands agglomeration. The HfO_2 islands are presented on the steps edges of the steps are presented in Figure 3.3 (b). They are aligned with respect

to the direction parallel to the edges, direction [1-2 1]. These islands height and width are respectively 0.42nm and 4nm

- **Second cycle**

In the second half deposition of TDMAH molecules, the overview of 700nm^2 (Figure 3.4 (a)) shows no changes of the surface with the deposited TDMAH. The surface roughness increase to reach 0.26nm means that the islands heights changes during the deposition. In Figure 3.4 (b), magnification(160nm x 160nm) of the steps region is showed highly arranged islands distribution in the direction of the steps flow, which mean that TDMAH molecules once at the surface are not drove by the orientation of the previous growth then affect the ALD agglomeration to be selective. No steps decoration obtained where the islands still just nucleated on the top and bottom of the steps. The high of islands here are homogeneous from the steps toward the middle of terraces.

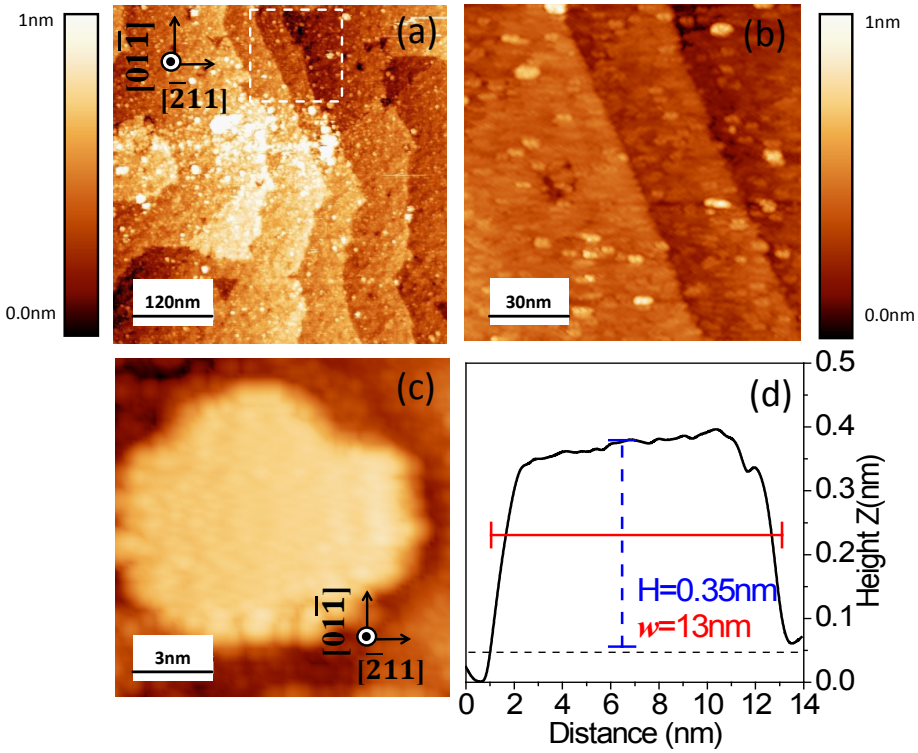

Figure 3.4: *Constant-current STM (a) STM image (600nm × 600nm) of the second half deposition of TDMAH molecules (b) STM image (150nm ×150nm) magnification on the step region shows conformal growth of closed film. (c) fraction of surface covered by 2D islands for 13nm of width and 0.35nm of height (Profile (d))*

The high of islands are about 0.35nm, this is higher than the heights of the 1st cycle .Accordingly the molecules grown on the previous materials deposited in first cycle but also covered more the free

surface that was non covered previously. In comparison between the single islands obtained in the first cycle and after the second deposition of TDMAH the free surface fraction are covered leading to the increase of the islands dimension that reach 14nm. The complete surface coverage here increases to 75% of islands with the high of 0.2nm.

The complete 2nd cycle shows a growth of complete layer, where the coverage is about 94% of islands with the height of 0.24nm. Within this cycle the RMS roughness decreases to 0.17nm. The Figure 3.5 (a), overview field display non nucleation on the steps edges. The magnification terraces (plane surface) and steps region and are then respectively presented in Figure 3.5 (b) and (c) of is the field of dashed white square in Figure 3.5 (a). On the high index terraces (A) conformal growth is observed on the terrace with existing of 3D islands far from the steps edges by distance >20nm . In this cycle, no nano-islands isolated as the first cycle is seen (Figure3.3 (b)), this means that the materials has been grown more on the free space substrate. Figure 3.5 (d), field 100nm^2, the film is closed but with some hole (black spot circled in white) , the height of the film calculated from those hole is about 0.24nm with the presence of small nano islands that can be correlated to the apex of previous materials deposited.

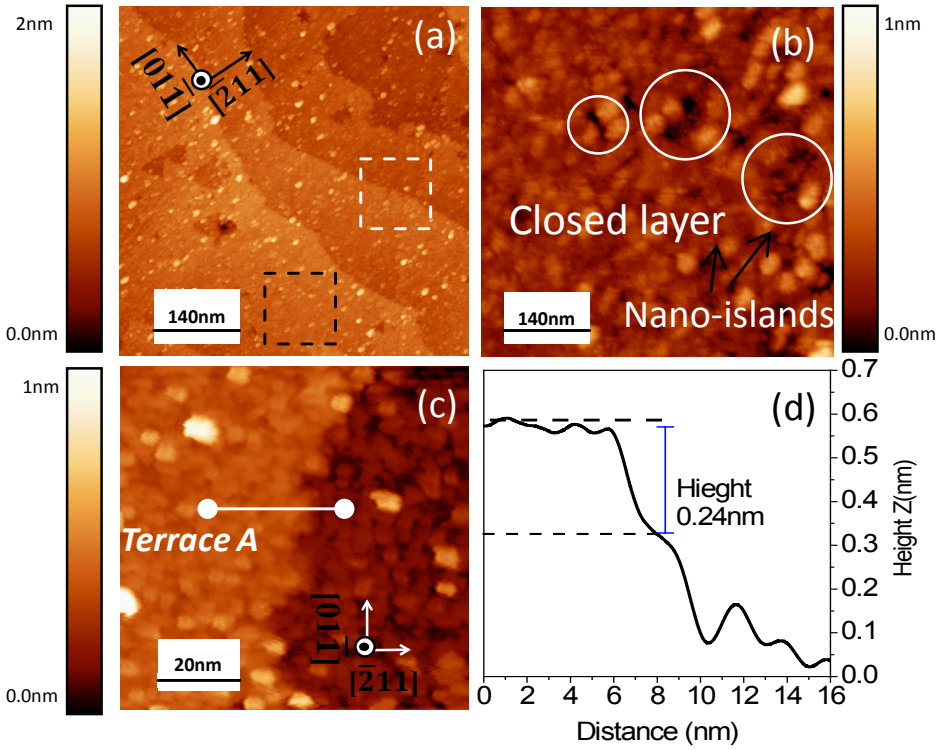

Figure 3.5: *Constant-current STM images (a) overview field of the 2nd complete cycles. (b) and (c) zoomed in on the spot marked by dashed squares black and white, respectively in (a). (b) STM of covered surface of (155nm × 155nm). The surface is covered at 94% with the presence of hole in the film (white circle). The figure shows a presence of some islands apex with height ΔH= 0.05nm. (c) STM (100nm × 100nm) of the growth in the steps*

region, no high agglomerations observed. (d) Profile of the steps (white line) shown that the film height is 0.24nm which is remain constant from the 1st cycle.

The steps region growth is observed in Figure 3.5 (a) display high ratio aspect of the surface morphology. The coverage on the top terraces (A) seems to be more compact then the materials grown in the bottom of the steps. Here the STM shows decoration of the steps edges but with non important deposited materials. Small changes of the edge termination however the height of the steps didn't changed from the first cycle. The profile in Figure 3.5 (d) shows that the height of the growth is 0.24nm with conformal growth in the region of the steps.

- **Third cycle**

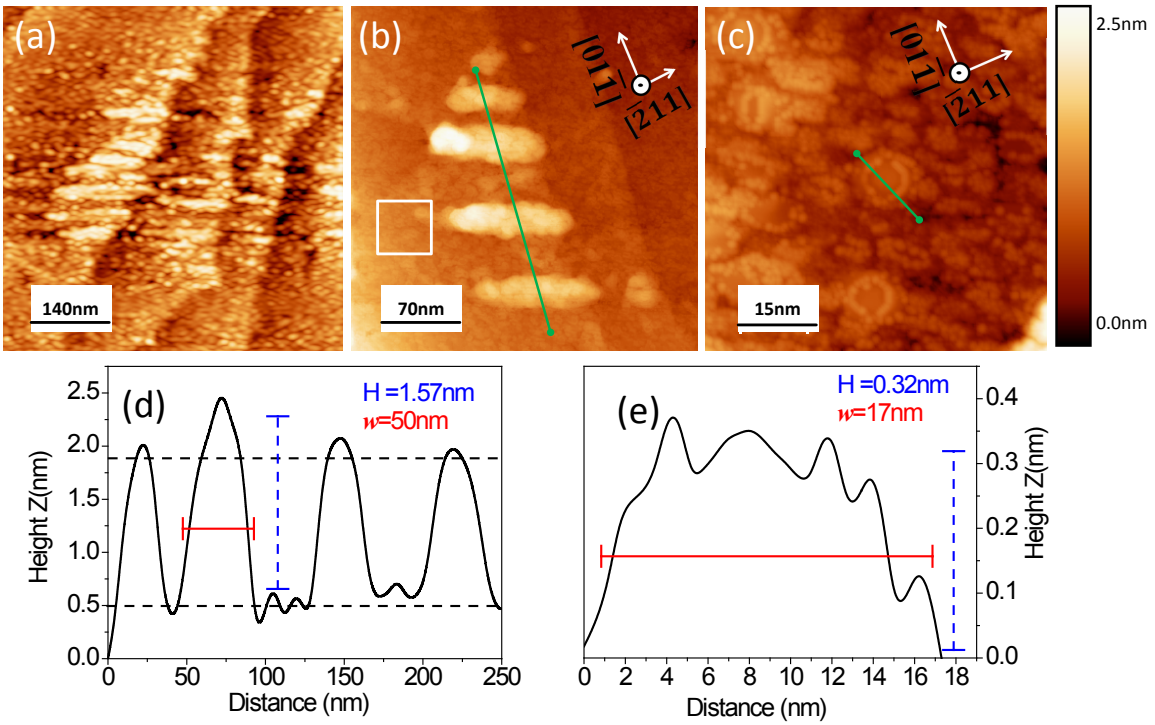

Figure 3.6: *Constant-current STM images (a)-(c) of the ALD film growth after the 3rd half cycle of TDMAH. (a) (750nm ×750nm) shows high nucleation of the materials on the steps edges.(b) STM (350nm × 350nm) of the arrangement of the materials grown in stripes features on one steps edges, the heights of these features (profile (d))varies in the same range with, e.g., 1.57nm. The STM image (65nm × 65nm) (c) is a zoom in the white square in (b) of the growth on the terraces far from the formed stripes has the height of ~0.32nm.*

The third TDMAH deposition deliver a growth morphology that is non similar to two previous cycles. New features appear with this half cycle of deposition. In Figure 3.6 (a) an overview of the filed shows that the growth of theses stripes happen on many steps (3 steps in this Figure). A decoration of the

steps edges is observed. In Figure 3.6 (b), a magnification of the steps region shows better the growth of high agglomeration of materials with the height of 1.57nm and an average width of ~30-50nm as shows the profile in Figure 3.6 (d). Those strips are arranged in the direction of the steps flow with a distance of 20-35nm of inter distance. A barrier effect of the steps can be considered as the effective surface feature on this nucleation on the stop of the steps (see discussion). This effect of the steps is clear from a morphology description, the application of the statistical mathematic model of the surface growth show that the presence of the steps affects the dynamic process.

The STM of the complete 3rd cycle in different scanned spots from the surface is presented in Figure 3.7 (a), (c) and (d). The strips increase in length on the region near to the bottom of the steps leading to coalescence between stripes on higher index terraces with the lower index ones on the same direction of the steps flow leading to the formation of continues self-arranged islands.

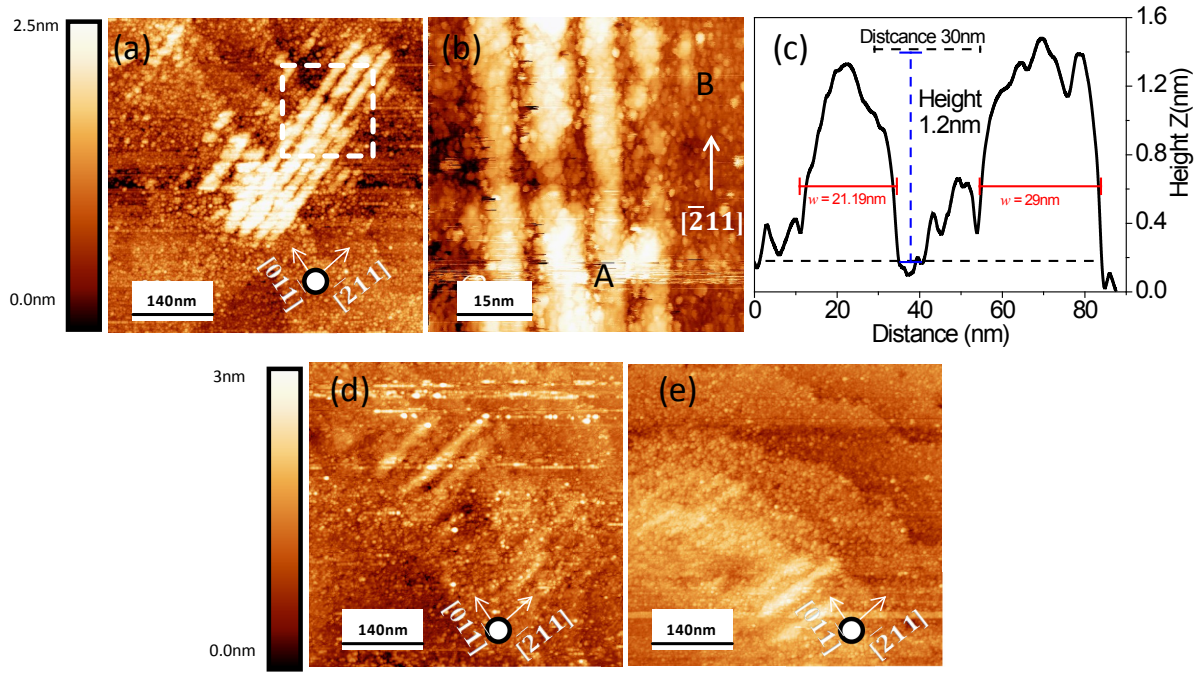

Figure 3.7: *Constant-current STM images (a-d) STM images of the complete 3rd cycle. (a) (b) and (c)(700nm × 700nm) are recorded from different spot of the substrate. In (a) the growth shown an extending in the formatted strips feature grow already with the TDMAH pulses. (b) magnification of the region of dashed white square in (a). The dimension showed in the profile (d) of 2 adjacent stripes.*

In Figure 3.7 (b), shows the morphology of the strips in between two terraces A and B. The growth is clear stopped on the edge of the steps with a clear repetitive pattern of grown islands. The stripes have the height is about 1.2nm and width of 30-40nm. The spaced distance between stripes in the direction is about 20-40nm. Surface coverage with these strips is about less than 20% of the surface.

In addition the growth of new small strips on the edge of the steps. The roughness of the complete third cycle is 0.738nm which is logical with the amount of H_2O molecules coming on the surface that react with TDMAH on the surface. The increasing in dimension of the strips between the half and the complete cycles gave an assumption about the possibility of surface diffusion that depend on the surface reaction, where week bon between -Hf and Si surface diffuse during the deposition to agglomerate in the preferential direction. This behavior is not like ALD assumption that based to the saturation reaction that not allows formation of high growth per cycle.

- **Fourth cycle**

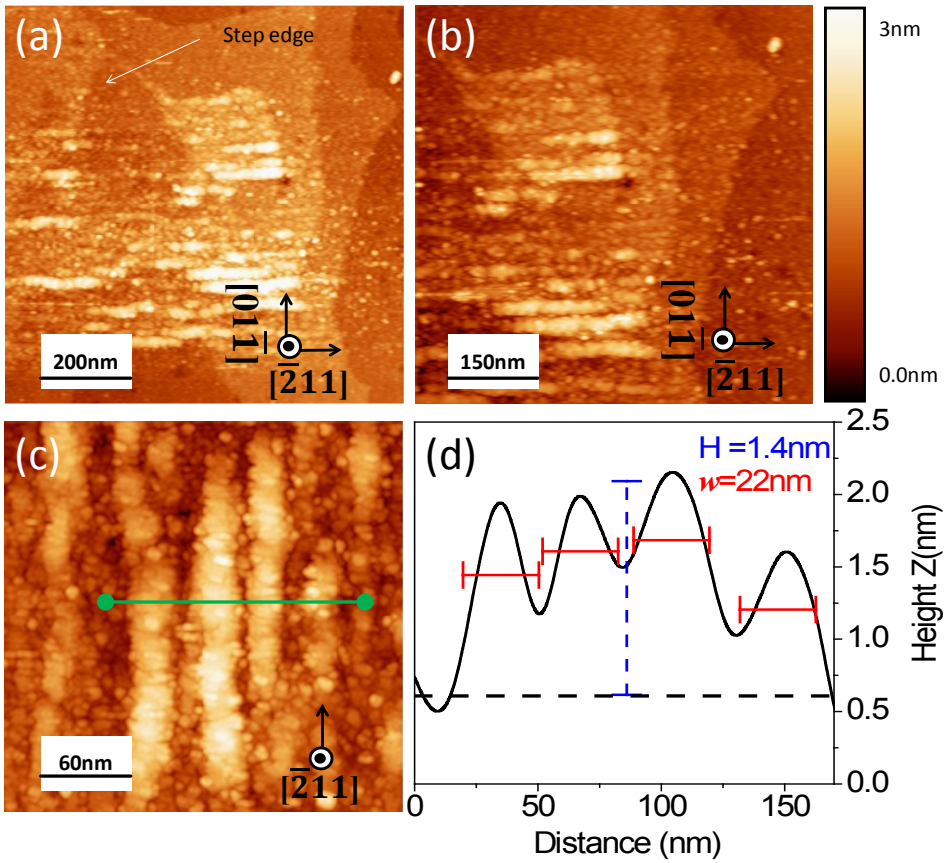

Figure 3.8: *Constant-current STM images (a-c) of the growth during the 4th TDMAH deposition. The strips formed decrease in height as it show profile (d), and the inter-distance between the strips reduced to~ 5nm.*

From the profile (Figure 3.8 (d)), the high of the islands decrease, reason of the decrease free space within the deposition of TDMAH that are localized as clear in this vacancies. The widths average decrease to 20nm. Figure 3.8 (a) and (b) shows the 4th TDMAH pulse a presentation of fraction filed of surface from the terraces. Within the deposition of TDMAH, the stripes formed are denser but with smaller dimension then the 3rd cycle this means that the growth happed in the free space covering the stripes formed. The surface coverage become 40% which is higher than in the third cycle.The

magnification of Figure 3.8 (c) from the terraces region display high distribution of the stripes on the planar surface with dimension of 1-1.4nm of heights arranged in aligned line parallel to the steps direction [$\bar{2}$11]. The inter-distance between the strips is fully with the materials deposited from the TDMAH molecules that lead to an increase of the inter distance between strips and makes the surface more homogeneous. The roughness of the surface decrease to reach 0.58nm. Thus, the strips length decrease and create complete closed domains of complete layer of islands in the same direction

The completed 4th cycle results are presented in Figure 3.9. First observation is the high surface coverage that is about ~ 47%. The roughness decreases slightly from 0.58nm to 0.42nm. The overview field (Figure 3.9 (a)), show that steps start to be coverage with high rough surface.

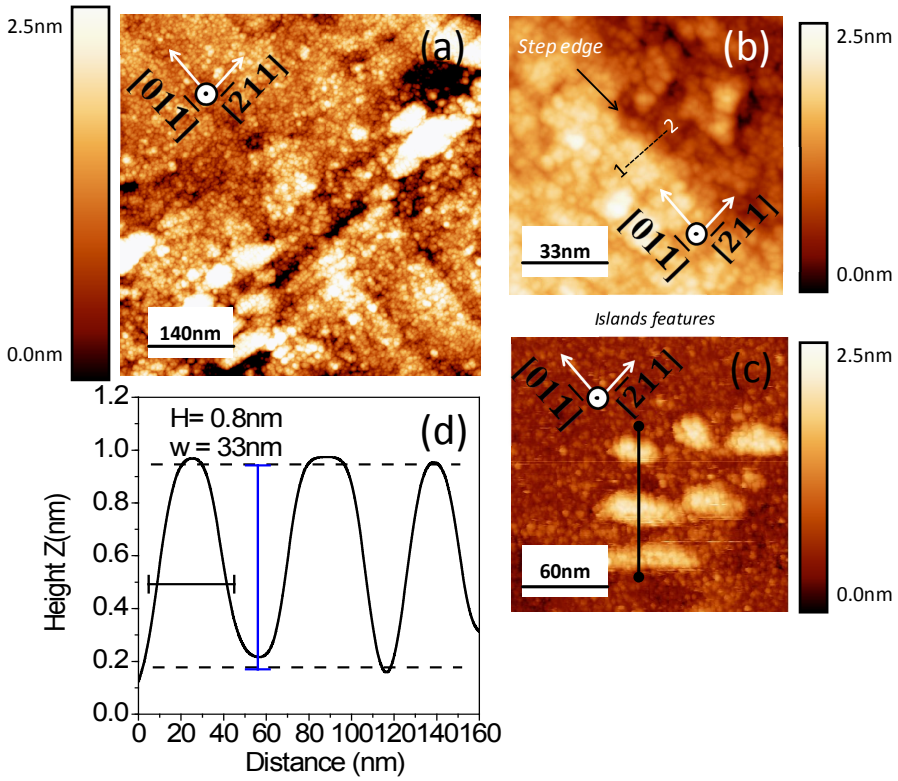

Figure 3.9: *Constant-current STM images (a-b-d) STM images of the 4th complete cycles of HfO_2 on the Si. (a) Overview field (700nm ×700nm). Important nucleation are observed but with height of ~0.95nm and 35nm of width. Same steps still are able to distinguish on the surface the magnification of the steps region shows the steps edges (b). (d) The islands grown on the terrace with height of 0.8nm, profile (c).*

For the steps region, same part of the steps can be observed and distinguish as it showing in the Figure 3.10 (b), where the growth in the top and bottom of the steps edges in homogeneous and growing materials are deposited on the two side of the steps without any agglomerations of large islands. In contrast other regions of steps are completely covered and mixes with the surface thus it can't be distinguish. Large islands formed in the same region from the previous strips formation. This is related

to the materials growing between the strips and the film morphology is drove to fit with the substrate. Those islands have respectively ~0.95nm of height and ~ 35-40nm of widths.

3.1.1.2. Si(111)/HfO_2 growth at 280°C

- **First cycle**

The HfO_2 growth is observed in the first cycle on large scale, i.e. 700nm, Figure 3.10. As first observation, agglomerations observed over the surface, with islands distributions. The steps profile of three spaced steps from Figure 3.10 (a) is kept without non agglomeration on the steps bottom; however the growth occurs on top of the steps. The profile shows that the steps height increase from the 0.33nm, i.e. Si(111)-H steps height, to reach 0.59nm. The difference in height is 0.26nm on the steps edges. The profile of the surface height shows that island formed in region of 120nm from the steps. The height is about 0.2nm of islands.

The islands nucleate at the terraces has different value of heights. Those values can be overestimated because of the low resolution at this dimension (700nm). To extract more resolution, a magnification scan region showed in Figure 3.10 (b) and Figure 3.10 (c) presented respectively the STM scan of the region with white dashed white square and the region black dashed shows the growth on the terraces in Figure 3.10 (a). The growth on steps region of the Si(111)-H after ALD cycle with an interesting results where the growth in upper steps region (top-edges) present a high density of deposited materials HfO_2.The profile (Figure 3.10 (d))shows that at the edges of the steps the height increase with 0.1nm , equivalent to the theoretical growth of one cycle of HfO_2, however with the distance the growth is increasing from the steps edge to reach islands with height of ~0.5nm .On the bottom steps there is no direct nucleation but the presence of same nano islands of HfO_2 with 0.1-0.2nm height and 2-5nm widths. The grown material in the bottom of the terraces shows important vacancies in the film black spot indicated by white dashed circles.

The growth on the terraces region with black dashed token to show the growth nucleation the island distribution shows a conformal growth but with rough surface, the islands are divided to kind large one of 0.4nm of height and other with smaller height 0.1-0.2nm. Figure3.10(b) is a map filtering of height with the green line , distinguish between three layer , the dark brown is the substrate the first layer is the lighter brown scaled at 0.2-0.3nm the third layer is the bright islands that are at 0.3-0.4nm. The coverage is 54% of the materials at lower scale, i.e. islands 0.2nm. The formation of partial layer is shown here, this is in accord with the growth fraction of ALD model as O.Nilson and Puurunen prediction.

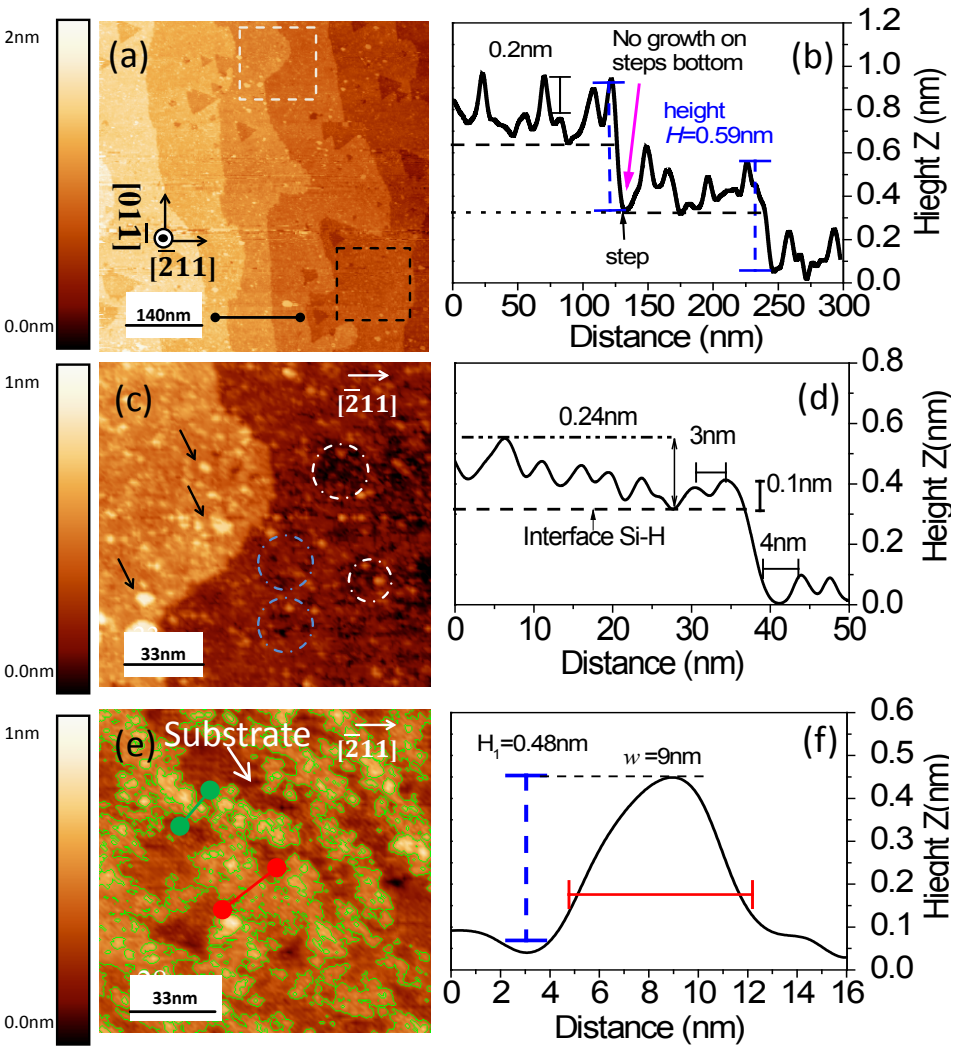

Figure 3.10: *Constant-current STM images. (a) STM (700nm × 700nm) on the first ALD cycle at 280° C. Substrate height decrease front light to dark scales. b) Profile on the height line of three adjacent steps. The height is referred to the substrate where the calculation of the steps height after the first cycle is 0.59nm (the Si-H blank steps height 0.33).(c) and (e) (165nm × 165nm) zoomed in on the spot marked by dashed squares black and white, respectively in (a). The growth on steps edges keep the same shape and the materials grow with 0.1nm in height. (c) Coverage of the terraces by 54% of molecules with maximum height of 0.48nm as it is shown in (f) from green line in (e).*

- **Second cycle**

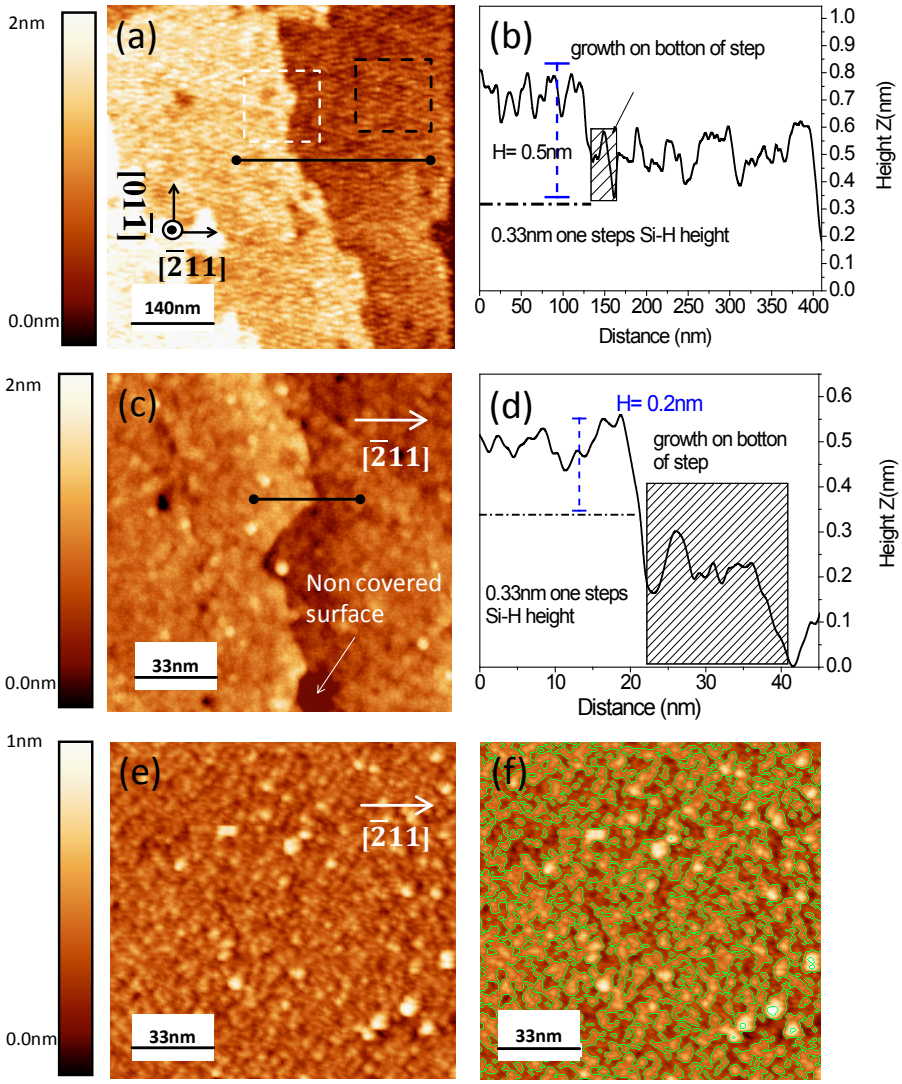

Figure 3.11: *Constant-current STM images of the 2nd HfO_2 ALD. The film displays a continuum growth on the terraces and steps. (c) and (e) (165nm × 165nm) zoomed in on the spot marked by dashed squares black and white displays high conformal growth on the steps and of the terraces. However, growth in the bottom of the terraces occur but in homogenous distribution.*

The growth of the materials in the second cycle shows more homogeneous coverage at large scale. The steps edges still clear with the direction of the steps flow. No height agglomerations on the terraces are presented. The profile, Figure 3.11, display grown materials direct on the steps edges (dashed square in the profile). The height on the bottom of the steps is 0.2nm .The steps region Figure 3.11 of the steps region shows no agglomeration on the steps edges. High homogeneity of the growth on the steps and also on the terraces region, with so important coverage reaches ~100%. In Figure 3.11

(e) of the terraces shows how the film is closed at these cycles with nano islands of 0.05nm height in average. The roughness decrease in this cycle to reach 0.18nm (almost the same roughness for the 2nd cycle at RT).

- **Third cycle**

Figure 3.12, shows the growth morphology of HfO_2 nucleation in the 3rd cycles of deposition. The roughness increases in this cycle to reach 0.25nm. This roughness is results from agglomerations of important features height over the surface. Also, the formation of important defect over the surface as important hole in the film. The steps morphology shows an irregularity en the edges of the steps with effect on the deposition in the region of the steps. The height over the steps varies from 0.2nm in the second cycle to 0.31nm. This height varies also from a region to another as it shows in Figure 3.12 (b), where the height (black line) is about 0.17nm and fro the region (red line) its decrease to 0.38nm.

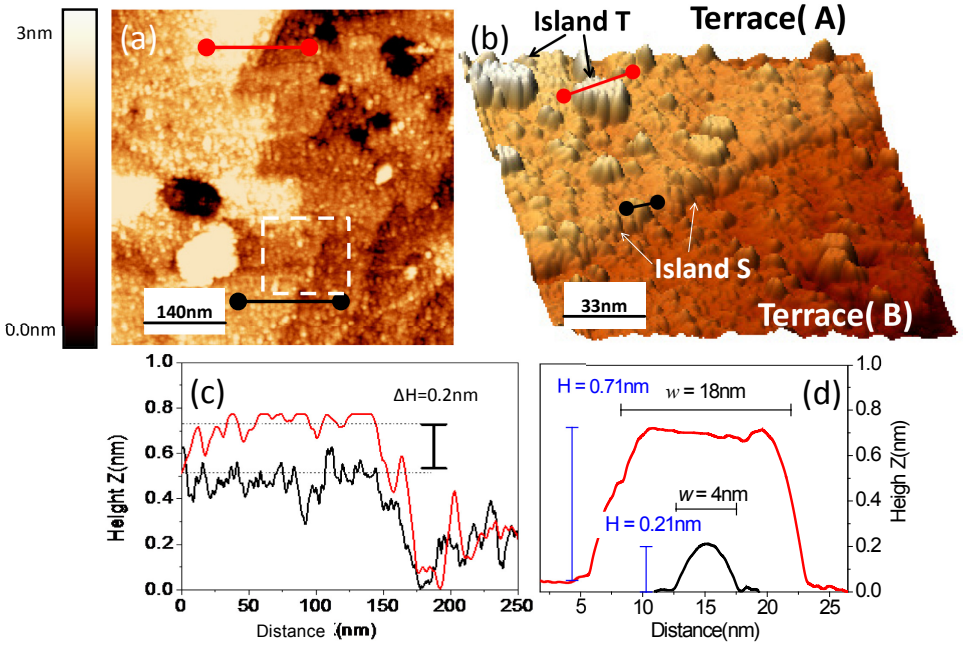

Figure 3.12: *Constant-current STM images of the 3rd HfO_2 ALD. (a) large field surface fraction shows a changes of the steps and start to change the surface structure. the steps changes of height for different position as it is shown in profile in (c) of red line and black line in (a), ΔH= 0.24nm. The zoom in white square spot shows in (b) present 3D image of one single steps separating terrace (A) and (B) of the islands growth on the edge of step which ahs 0.2nm of height and 4nm of width and (profile(b)). The formed islands heights are increasing from the steps to the edge were island T has about 0.71nm height/18nm of width.*

As it clears from the Figure 3.12 (c) of nano-resolution (3D) of the steps regions there is an increasing of the islands height from the steps to the terraces. From terraces (A) to terraces (B) with the decrease of distance from the steps to the middle of the terraces the islands formed from the ALD growth increase. The height on the terraces is about 3 times than the islands decorated the steps, where the heights profiles shows that is in the terraces 0.71nm and on the steps edges is 0.21nm as it is shown in Figure 3.12 (d).

- **Fourth cycle**

In Figure 3.13 presented the STM measuring of the growth after 4 cycles of TDMAH and H_2O cycles. In the 4th ALD cycle, the first observation is that the surface morphology is affected by the deposition of ALD. The surface is rougher with high density of holed on the terraces. The steps are almost diluted in the surface and start vanishing. In contrast to this density of holes the film grown still compact and dense with high aspect ratio of surface coverage. The steps start to vanished still in same region the steps that still be observed reach the height of 0.6nm.

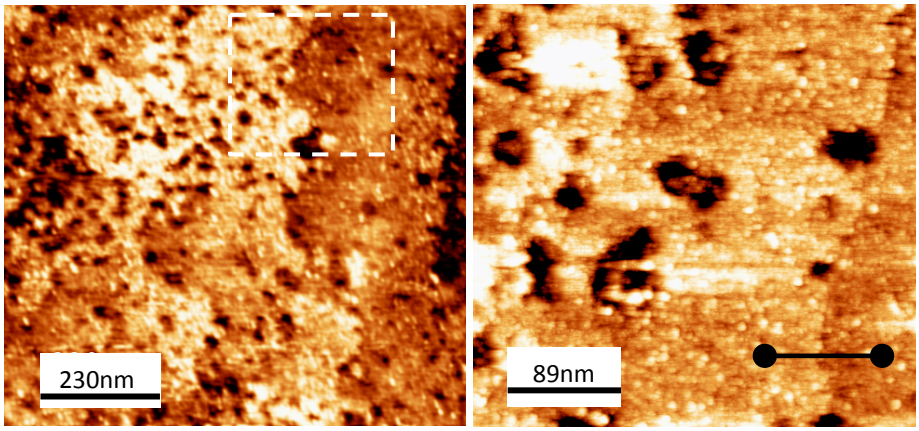

Figure 3.13: *Constant-current STM images (a) and (b) STM images of large field of the 4th ALD cycle (700 × 700µm) and (445nm × 445nm). The surface display higher roughness with the presence of many holes in the film on the terraces. The profile of the steps (c) shows an important height in the top of the steps with 0.6nm and also in bottom by 0.3nm.*

3.1.2. Data of surface morphology

3.1.2.1. Surface roughness

- **RMS roughness**

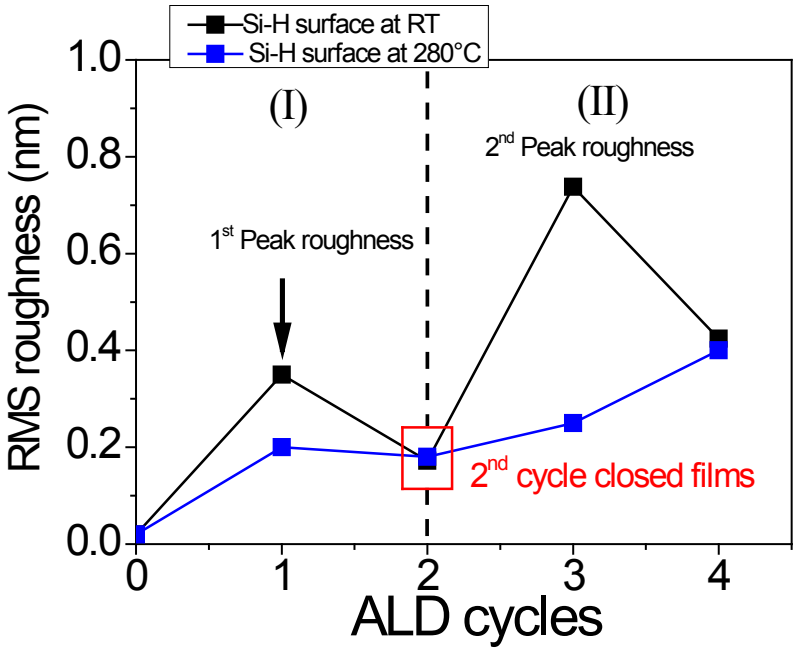

Figure 3.14: *Curves evolution of root-mean-square(RMS) roughness of the ALD film deposited for each cycles on the of Si(111)-H at RT (Red line) and at 280°C (Blue line).The evolution shows two different regimes : Regime (I) the RMS roughness shows a peak in 1st cycles and decreasing in the 2nd cycle (ALD film close for Si-H). Regime (II) RMS roughness increase in second peak in the 3rd cycle then decrease in the 4th cycle. In contrast a linear increasing of the RMS roughness for 280°C .*

In the first part of the curve (regime (I)), all curve shows an increase in the first cycle then decrease after the second cycle to reach the smallest value during the fourth ALD cycles. In the case of -OH terminated substrates the existence of this peak in the first cycle is related to the coverage percentage of substrate with -OH species of the substrate. Dkhissi et al. found that in optimal conditions for OH coverage reaching 100%, -Hf coverage of about 50% is possible on the surface after the first ALD [128]. Therefore the roughness should increase on the first cycles because the 50% of Hf coverage will lead to rough substrate. However in the case of the Si-H as it was demonstrated in the results section have the coverage rate of the surface is respectively 71.4% and 54% for Si-H at RT and Si-H at 280°C. The coverage values for Si-H go beyond the estimation of the coverage in the presence of the -OH species. From this result it can be assumed that the morphology of the substrate is more influencing the growth then the termination species. This deduction can be justified by the slope variation of the RMS curves in this first regime for all systems. Despite the similarity of the curve evolution, the

increasing and decreasing slope in the first regime is different for each system. The increasing slopes are respectively 0.16 and 0.32 for Si-H at RT and at 280°C.

In the second regime (II), the film deposited on the Si-H at RT show another peak in the 3rd cycle which is a result of the growth of stripes with important height then decrease in the 4th cycle as the materials deposited grow in the vacancies leading to the decrease of the height of the global film. Here the behavior of the roughness is kept unchanged however the values are more important than in the first regime. In contrast the roughness of the film at 280°C is increasing in linear way as the theoretical prediction of the GPC in ideal ALD growth.

In comparison with the Si-OH first 4th cycle investigated by Kolanek et al [48], the initial roughness can be related to this non similarity of the behavior of the film growth. The ALD film on Si(111)-H surface is closed in the 2nd cycles however for Si-OH the RMS roughness peak increase in the first cycle from 0.18nm to 0.23nm then decreased in linear way tell the 4th cycle where is reached the lowest values of 0.17nm. Accordingly the author concluded that the film was closed at the 4th ALD cycle. This would be more discussed in details in chapter 4.

- **.Roughness moment (R_{sk}) and (R_{sk})**

The Skewness (R_{sk}) is central moment amplitude of the profile function measured through large assessment length. This roughness parameter is sensitive for the deep changes in the profile such valley and height peak on the surface density. The mathematical and numerical Equations of Skewness (R_{sk}) [129]:

$$R_{sk} = \frac{1}{R_{RMS}^3}\int_{-\infty}^{\infty} z^3 p(z)\ dz \quad (3.1)$$

$$R_{sk} = \frac{1}{R_{RMS}^3 N}\left(\sum_{i=1}^{N} Z_i^3\right) \quad (3.2)$$

Z_i , is the height of the profile in each point of the surface profile. This equation lead to the reduction or removing the noisy high then the power of 3 will kept the singe of the profile, positive negative height. A negative value of (R_{sk}) indicates that the surface is made up of valleys, whereas a surface with a positive skewness is said to contain mainly peaks and asperities.

Kurtosis (R_{ku}) moment is the fourth moment of profile amplitude probability function and corresponds to a measure of sharpness of the probability density of the profile (reference). The mathematic equation is

- $R_{ku} = \frac{1}{R_{RMS}^4}\int_{-\infty}^{\infty} z^4 p(z)\ dz$ (3.3)
- $R_{sk} = \frac{1}{R_{RMS}^4 N}\left(\sum_{i=1}^{N} Z_i^4\right)$ (3.4)

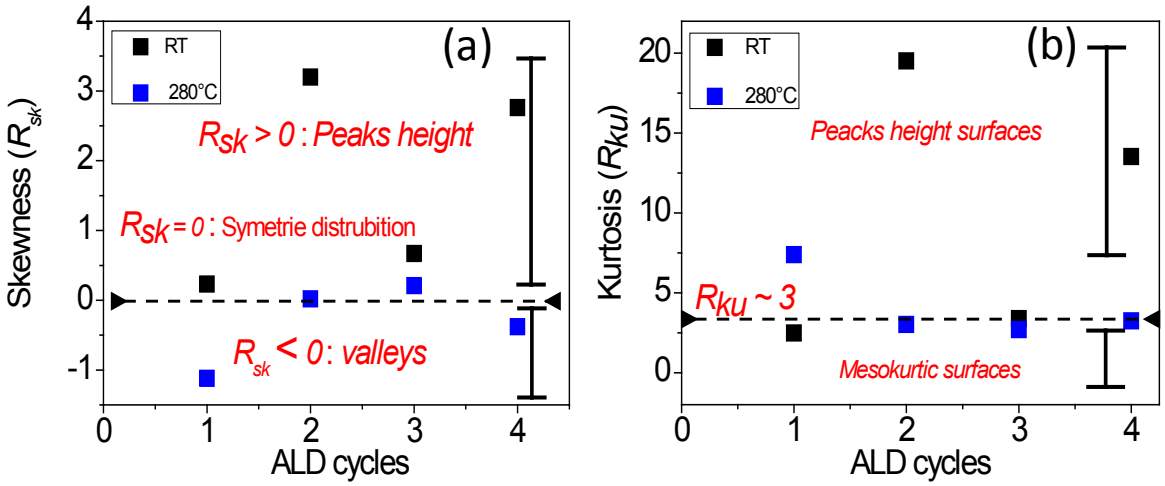

Figure 3.15: *Moment of profile amplitude probability density function calculated from STM for each cycle of TDMAH and H_2O for every cycle. The Skewness (R_{sk}) and Kurtosis (R_{ku}) values shows that for the film formed on Si-H at 280°C are similar and the fluctuation around the values R_{sk} =0 and R_{ku} =3 which are assigned to symmetrical growth. However the values for Si-H show that the surface is dominated by peaks of height.*

In the first cycle the values of (R_{ku}) are respectively 0.23 and -1.12 and for Si-H at RT and 280°C. The values of the (R_{ku}) in the first cycle are 2.48, 7.93 and. Both values obtained for the roughness parameters indicated that the Si-H at RT have the same profile geometry where the R_{Ku} for both surface are near to the values of 3. Means, that the profile height presented a Gaussian of symmetrical growth, that because the values of R_{sk} are near to 0. However Si-H at 280°C. When (R_{Ku}) is 3 indicates a Gaussian amplitude distribution, and the surface is called Mesokurtic, but if Kurtosis is smaller than 3 the surface is flat and called Platykurtic. If the Kurtosis is higher than 3, the surface has more peaks than valleys [129]. The calculation of those values for the HfO_2 film grown on Si-H at RT and 280°C film, with R_{sk} and R_{ku} respectively -1.12 and 7.39, describe a non-symmetrical growth dominated by the peaks height.

In the 2nd, 3rd and the 4th cycles, the profile height of the film deposited on Si-H at 280°C, shows simularity of (R_{sk}) and (R_{ku}) fluctuation, where the referential values of symmetrical distribution of the height , i.e. $R_{sk} \sim 0$ with similar shape, i.e. $R_{ku} \sim 3$. So it can be concluded that the geometry of the profile is remain mostly the same for the 2nd, 3rd and 4th cycles. This is correlated in the discussion part to the random deposition of the growth.The Si-H describe another profile height shape, in the 2nd, 3rd and 4th cycles, like in the first cycle positives values of R_{sk}, which mean that the distribution of height profile are not symmetric and then $R_{ku} > 3$, in less in the 3rd cycle with is about 3. The profile is dominated by th peak high in the 2nd cycle, this is what was observed with the STM.

3.1.2.2. Height-height correlation function (HHCF)

For the calculation of the (HHCF), for each ALD cycle we extracted 8 profiles at different positions of the surface in both direction of the Si(111)-H terminated stepped surface: The parallel $[01\bar{1}]$ and the perpendicular $[\bar{2}11]$ direction to the steps flow. We calculated the HHCF function from the average profiles token from the surface from the Equation 1.42. The profile heights are took for the same direction with same length scale which is 250nm. Those profiles are then subjected to the HHCF numerical equation to calculate the curves evolution for every cycle for ALD at RT and 280°C. These curves deliver a knowledge about the surface morphology, where the surface width *w*, lateral correlation ζ, roughness exponent *α* and local slope *m* as the surface statistics components.

For STM measurements, we usually evaluate the one-dimensional height-height correlation function based only on profiles along the direction $[\bar{2}11]$ and along the direction $[01\bar{1}]$. It can therefore be evaluated from the discrete STM data values as

$$H_{[\bar{2}11]}\ \left(r_{[\bar{2}11]}\right) = \frac{1}{N(N-1)} \sum_{n=1}^{N} (z_{n+1} - z_n)^2 \quad (3.5)$$

$$H_{[01\bar{1}]}\ \left(r_{[01\bar{1}]}\right) = \frac{1}{N(N-1)} \sum_{n=1}^{N} (z_{n+1} - z_n)^2 \quad (3.6)$$

Where n = τx/Δx and n = τy/Δy respectively for x and y positions. The two direction of the surface here are associated to the x-position faster direction of scan and the y-position lower scan speed respectively.

In second place the determination of the dynamic roughness exponent β and 1/z from the Equations (1.39) and (1.40) presented in first chapter (see HHCF part). For contentious growth deposition in time such as CVD and sputtering, the dynamic part of the growth can be determined as function of time, as t^{β} and $t^{1/z}$. However the ALD process is cycling deposition which makes it a discrete growth. The continuous film the material deposited amount is controlled by the material transport and the surface reaction, by analogy the amount deposited also is controlled by the ALD self-limiting reactions. Here in Table (3.1), the Thickness average from the mean height of the profiles used to calculate HHCF.

Table 3.1: *Film thickness (nm) of the ALD at RT and 280°C for every cycles of deposition .*

Cycle	1st	2nd	3rd	4th
RT	0.24	0.24	1.2	1.8
280°C	0.14	0.24	0.54	0.8

- **ALD at RT**

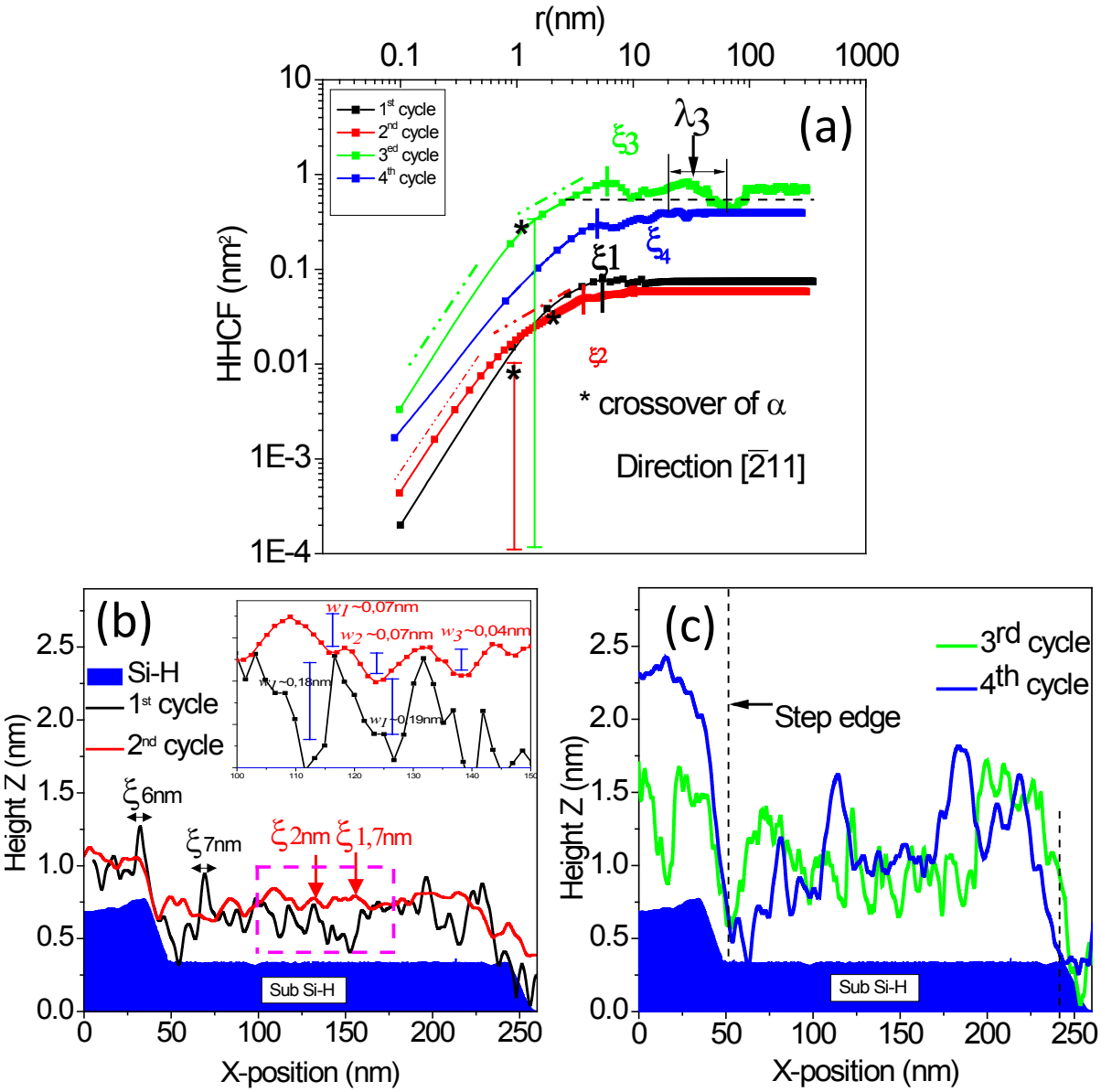

Figure 3.16: *(a) Log–log plots of the HHCF evolution during 1st- 4th, respectively. Black arrows indicate approximate positions where surface characteristics (Surface width (w), lateral correlation length (ζ) and the roughness exponent (α) are acquired. (b) The profiles (separated in 2 graphs) in the direction perpendicular to the steps* [$\bar{2}$11].

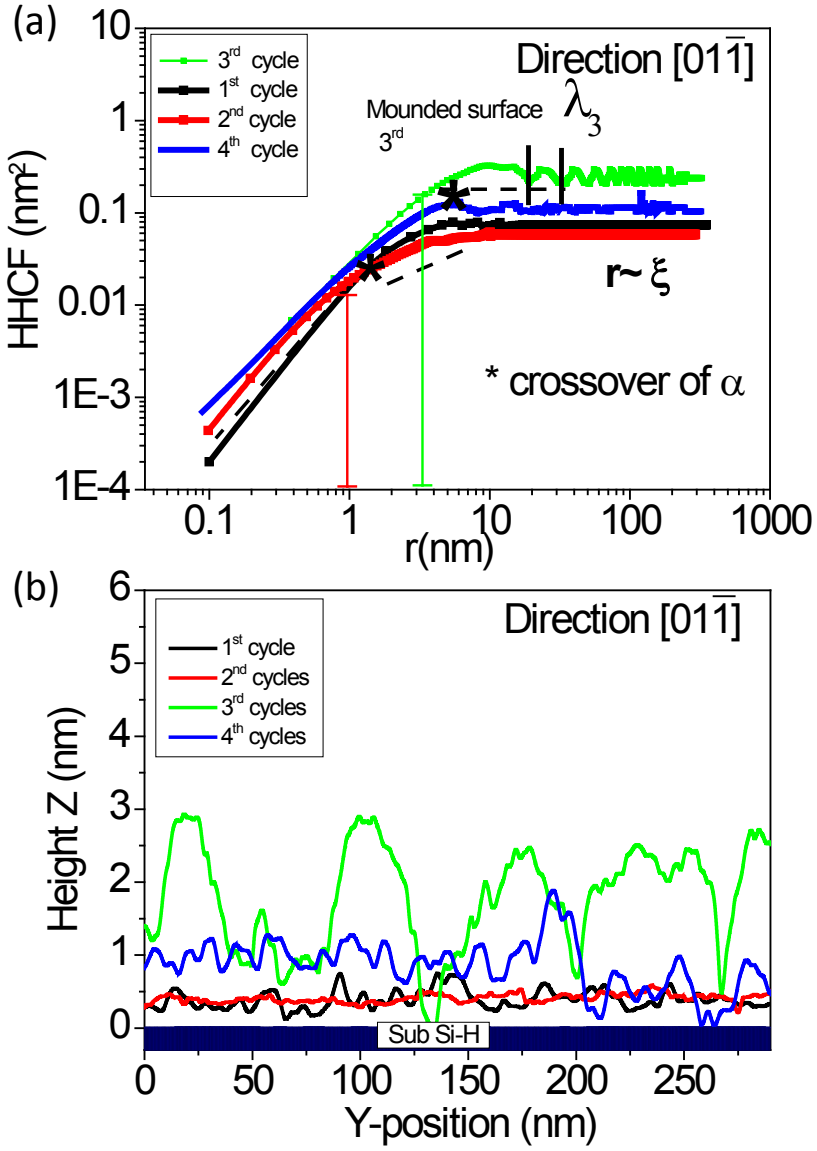

Figure 3.17: *(a) Log–log plots of the HHCF evolution during 1st- 4th, respectively. Black arrows indicate approximate positions where surface characteristics. (b) The profiles are in the direction perpendicular to the steps* [01$\bar{1}$].

The HHCF respectively for the both direction of the surface are shown in the Figure 3.16 and 3.17 described more complex surface, especially depending on the surface directions and the ALD cycles. In the direction parallel to the steps (HHCF) for RT and, the curves have linear growth for $r \ll \zeta$ and then plateau for $r \sim \zeta$. This behavior depicts a representative height–height correlation function for a self-affine surface in the 1st and 2nd cycles. In contrast, for the 3rd and 4th cycle obtained curves assigned to the mounded surface, this can be a consequence which of the surface morphology.

Roughness exponent α

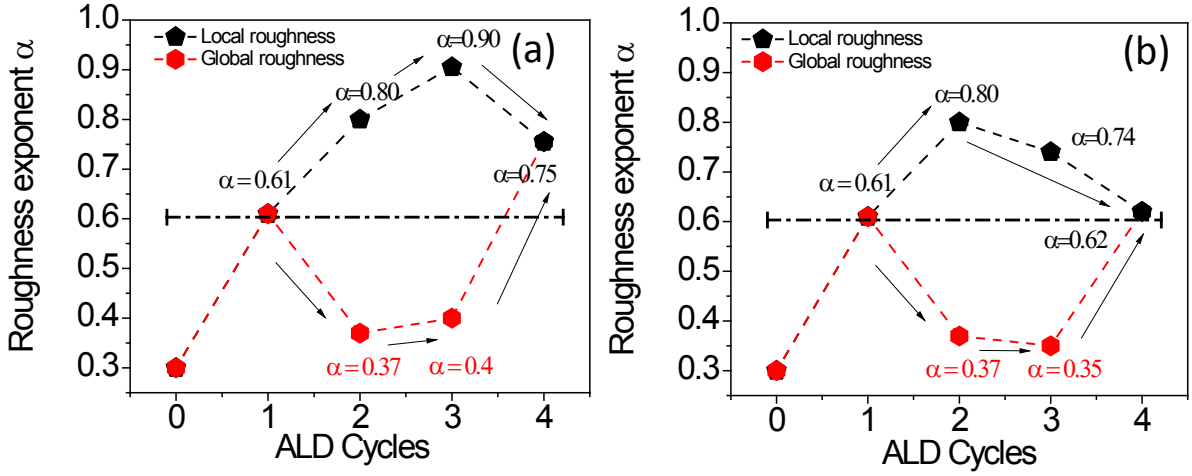

Figure 3.18: *The roughness exponent (α) evolution during ALD for Si-H at RT. (a) The roughness exponent evolution in the direction parallel to the steps* $[01\bar{1}]$ *and (b) in the direction perpendicular to the steps* $[\bar{2}11]$. *Black point shows the local roughness and red point the global roughness.*

The slope of the linear, .i.e.$|h(x+r)-h(x)|\sim(mr)^{\alpha}$ part with the increasing of the ALD cycles shows different values for different samples for different ALD cycles. From the curves HHCF in Figures 3.16 and 3.17, it is obvious that in the 2nd and 3rd cycle crossover existed in both directions.

In the Figure 3.18 the global and local roughness exponent are presented. As we shows the crossover exists in the 2nd and 3rd cycle in both directions. In the 2nd cycle the values of the local and global roughness exponent are identical that mean there is isotropic behavior in both directions, i.e.$\alpha^{1}_{[1-21]} = 0.80$ and $\alpha^{1}_{[1-21]} = 0.37$.

In contrast for the 3rd cycles the roughness exponent global and local are non isotropic, i.e. $\alpha^{1}_{[1-21]} = 9$ and $\alpha^{1}_{[-211]} = 0.74$. This means that the growth of islands geometry are changed with the direction this can be supported by the STM measurement where the width and length of the formed stripes leave important fraction of surface without materials deposited with means that the inter distance between the stripes has other features and this do not existed in the perpendicular direction which is more contentious agglomeration of islands. Where, that means the grain on the interface developed two features of grain during the ALD. These values would be discussed in the chapter 4.

Surface statistics (w, ζ, m)

The correlation length behavior as $H(r) \approx (mr)^{2\alpha}$ for short length scale r << ζ. Thus, HHCF depend on the local slope *m*. With dimensional analyses the local slope is determined from Equation (1.48) and (1.60) of self-affine surface and for mounded surface, respectively

$$m = \frac{(w\sqrt{2})^{\frac{1}{2\alpha}}}{\zeta}$$

$$m = \frac{(w\sqrt{2})^{\frac{1}{\alpha}}}{\zeta}\left[1 + \left(\frac{\pi\,\zeta}{\lambda}\right)^{2\alpha}\right]^{\frac{1}{2\alpha}}$$

The local slope presented the correlation between the vertical growth such the surface width *w* and the lateral growth presented on the lateral correlation ζ, included the exponent roughness *α*. The calculation of the local slope delivers information about two possible growth modes: stationary (normal) or non-stationary (anomalous). in the previous discussion those two mode of growth was studies separately for (*w)* and (ζ).

Table 3.2: *All the surface scaling component for different cycle at RT in both direction of Si(111).*

Scaling components	Direction	1st	2nd	3rd	4th
w	$[01\bar{1}]$	0,19	0,15	0,54	0,43
	$[\bar{2}11]$	0,19	0,15	0,31	0,2
ζ	$[01\bar{1}]$	6,91	2,82	6.35	4,52
	$[\bar{2}11]$	6,91	2,82	12,15	5,03
m	$[01\bar{1}]$	0,04	0,043	0,28	0,18
	$[\bar{2}11]$	0,04	0,043	0,03	0,02

- **ALD at 280°C**

In the Figure 3.19 and 3.20 of HHCF calculated for the film grown at 280°C for all cycles describe a self-affine morphology in both direction of Si(111)-H. However the statistics component differs in both direction of the surface. All the values of statistics component are summarized in the Table 3.3.

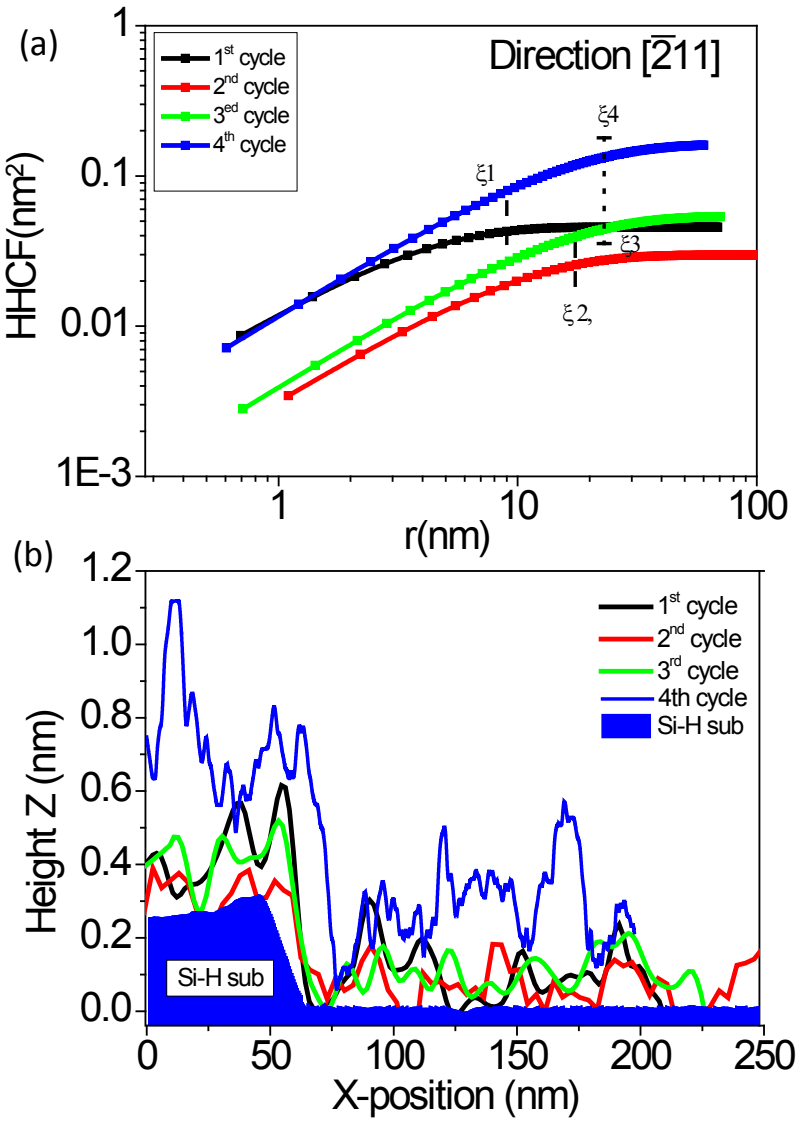

Figure 3.19: *(a) Log–log plots of the HHCF evolution during 1st- 4th, respectively. Black arrows indicate approximate positions where surface characteristics (Surface width w, lateral correlation length ζ and the roughness exponent α are acquired. (b) The profiles are in the direction perpendicular to the steps* [$\bar{2}$11].

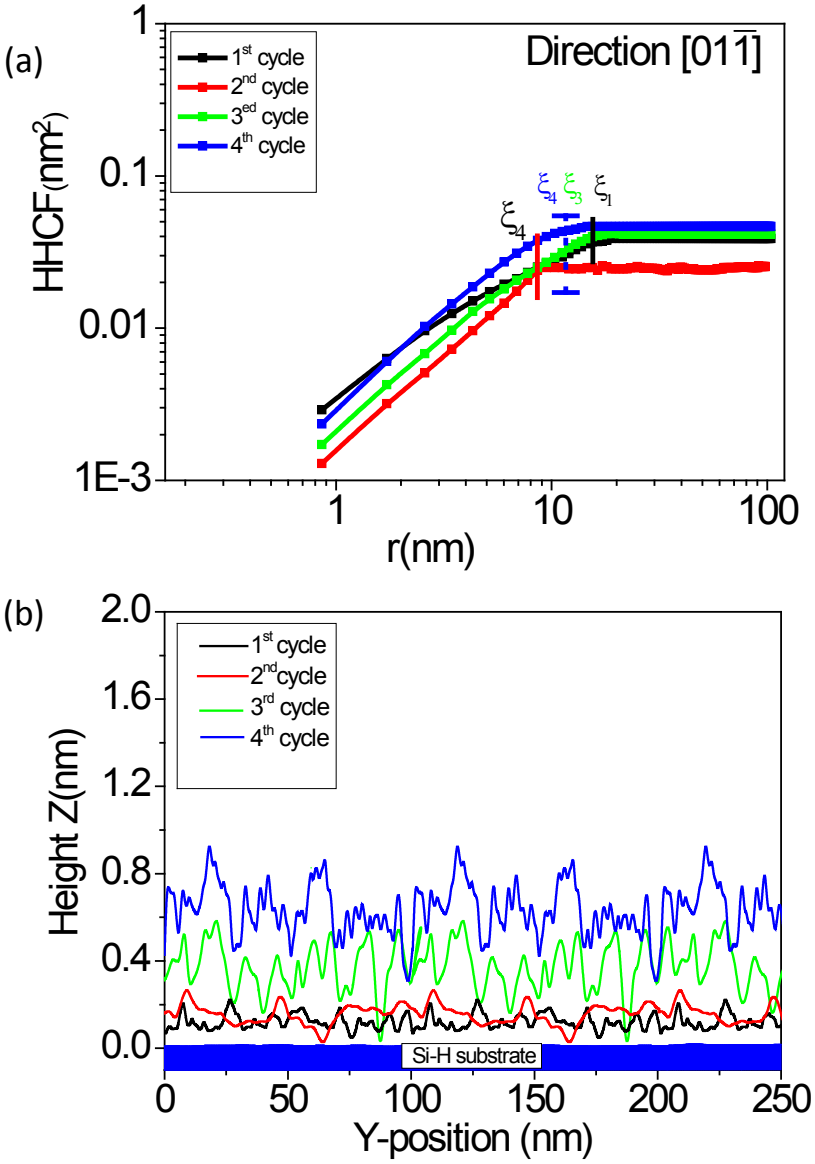

Figure 3.20: *(a) Log–log plots of the HHCF evolution during 1st- 4th, respectively. Black arrows indicate approximate positions where surface characteristics (Surface width w, lateral correlation length ζ and the roughness exponent α are acquired. (b) The profiles (separated in 2 graph) in the direction perpendicular to the steps* $[01\bar{1}]$.

***Table 3.3**: All the surface scaling component for different cycle at 280°C in both direction of Si(111)*

Scaling component	Direction	1st	2nd	3rd	4th
α	$[01\bar{1}]$	0,35	0,44	0,48	0,48
	$[\bar{2}11]$	0,48	0,55	0,6	0,61
w	$[01\bar{1}]$	0,14	0,12	0,2	0,28
	$[\bar{2}11]$	0,12	0,11	0,15	0,27
ζ	$[01\bar{1}]$	15.74	8.52	15.47	11.68
	$[\bar{2}11]$	17,32	11,05	17,57	18,5
m	$[01\bar{1}]$	0,009	0,005	0,011	0,017
	$[\bar{2}11]$	0,009	0,01	0,02	0,01

3.2. Al_2O_3 ALD HOPG/Ag-HOPG

3.2.1. Al_2O_3 ALD on HOPG

3.2.1.1. O1s/Al2p core level

The ALD of TMA and H_2O was characterized by x-ray photoelectron spectroscopy. For XPS Mg K alpha (1253.6 eV) X-ray source and spherical analyzer from spacelab is used.

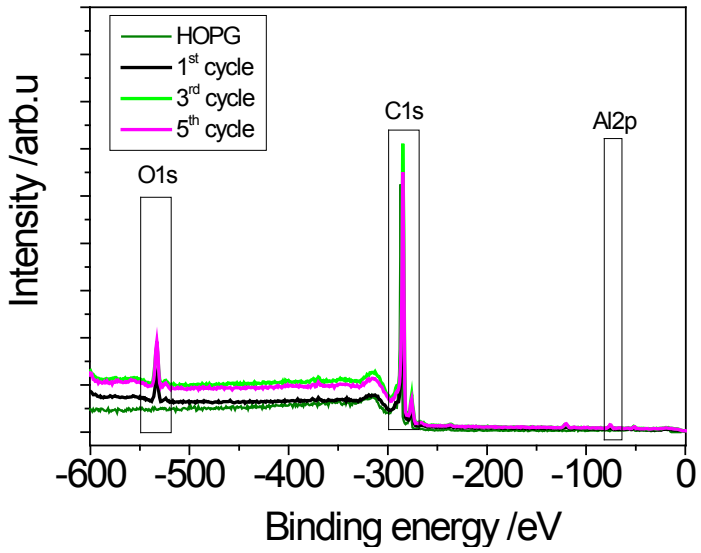

Figure 3.21: *The overview spectra of HOPG and TMA layers on HOPG.*

Figure 3.21, shows an overview of Al_2O_3 on the HOPG for the regions of oxygen, carbon and aluminum. Figure 3.22 (a) and (b) present the XPS spectra of O1s and Al2p for 1st, 3rd and 5th ALD cycles on HOPG surface.

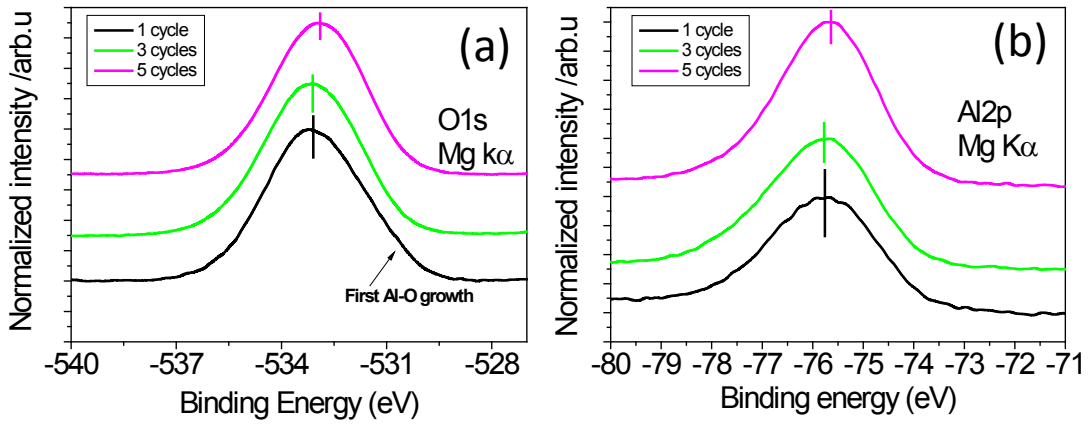

Figure 3.22: *(a) O1s XPS core level spectra of O1s and (b) Al2p Core level XPS of Al2p after 1st ,3rd and 5th ALD cycles. The spectra data are normalized to each peak maximum and shifted vertically.*

As a first observation, the peak positions from both O1s and Al2p core levels exhibit similar changes in binding energy with ALD cycle number increase (see Table 3.4.). After the first cycle the O1s and Al2p peaks are observed at 533.1 eV and 75.7 eV respectively, where the O1s line shows a shoulder at lower binding energy (~532 eV). Same peak position for both core level maintain fixed in the 3rd cycles. However a peak shift toward lower banding energy for both O1s and Al2p is observed in the 5th cycle. The shift in O1s and Al2p is 0.2eV. The core levels continue shifting to lower binding energy, where the O1s and Al2p are localized at 532.9 eV and 75.5 eV, respectively. Theses shifts of binding energy may be related to the nucleation properties of the ALD film. The Al2p core levels are rather symmetric and can be fitted by one single peak which we assign to Al–O [130-135]. In contrast, the O1s signals are rather broad.

***Table.3.4**. Summary of the data Peaks position, FWHM and O-Al/Al2p ratio for 1st, .3rd and 5th, of O1s and Al2p determined in this contribution for ALD layers deposition.*

	1st cycle	3rd cycle	5th cycle
O peak position(eV)	533.1	533.1	532.9
FWHM	3.6	2.7	2.6
Al peak position(eV)	75.7	75.7	75.5
FWHM	2.41	2.15	1.92

3.2.1.1. Growth morphology

The deposition of the TMA on the HOPG and Ag-HOPG is done in sequence on one cycle then three cycle and five cycles. The STM field magnifications are done in different scale. Where we the growth on large terraces and small terraces for every cycle described. The identification of the nucleation sites in the edge of the steps and on the large of terraces.

- **First cycle**

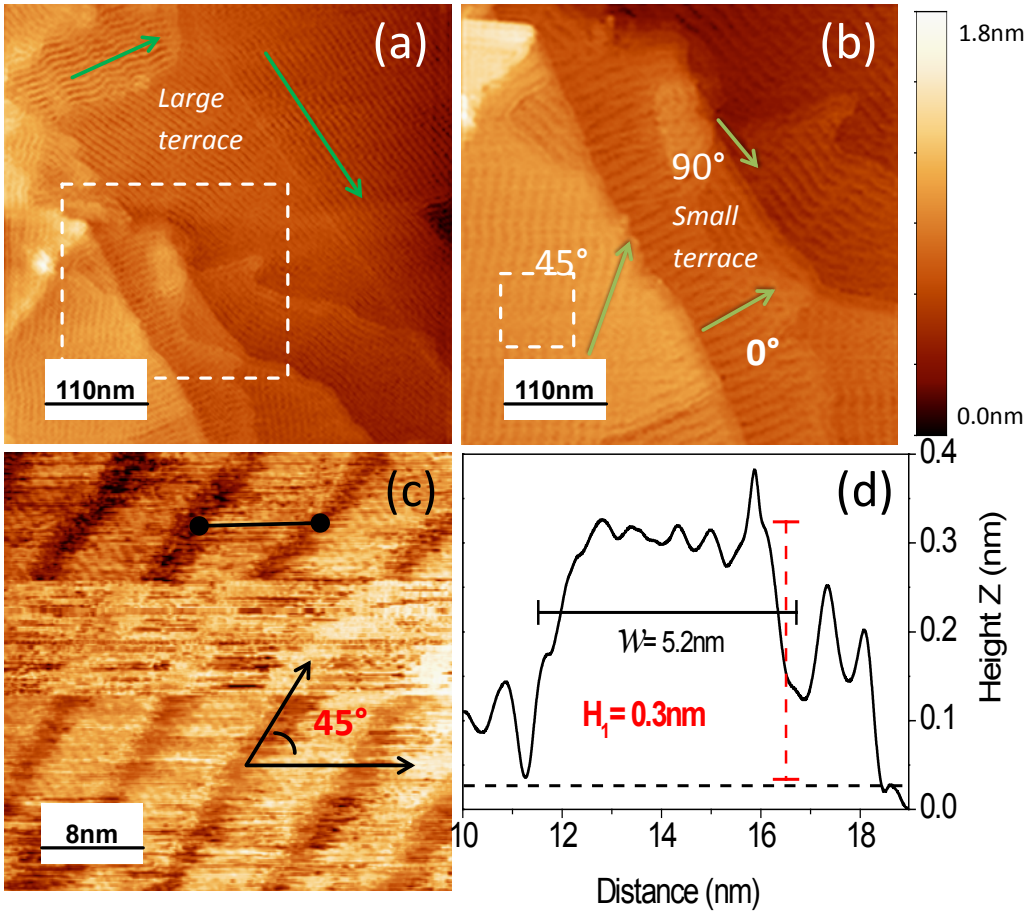

Figure 3.23: *Constant-current STM images of the growth in the 1st ALD cycle of TMA and H_2O revel the self-assemble of stripes over the steps and terraces.(a) (550nm × 550nm) of the growth at large field over large terraces of (> 300nm). (b) (285nmx258nm) magnification of the region limited by the dashed square (Small terrace), the green arrow shows the different orientation of the stripes regarding to the steps flow directions. These stripes are an arranged on molecules with higher cristalinty as its shown in (c), which is magnification of stripes with the angle of ~45°. (d)These stripes height is about 0.33nm and width of 6nm.*

In the first cycle the grown ALD materials has the same deposition arrangement on both large and small terraces. In first ALD cycle on HOPG substrate the Al_2O_3 was conformal deposited with homogeneous coverage ~ 90%. The features observed in this first cycle are nano-stripes with ~5.2nm width and 0.3nm of height. The alignment of nano-stripes on the HOPG substrate presented different directions regarding to the steps orientation. We distinguish three angles of the nano-wires alignments to the steps direction. First angle 0° where nano-wires are perpendicular to the edges of steps so

parallel to the direction of the steps flow, second angle is 90° with wires are parallel to the edge of the steps and perpendicular to the steps direction and we distinguish angle of 45° .

In Figure 3.23 (c) nano resolutions of the formed wires, which are molecules aligned in this structure. The interesting observation that no agglomeration happen on the steps edges which is non predicted in the case of substrate inhibited.

- **Third cycle**

Large Terraces

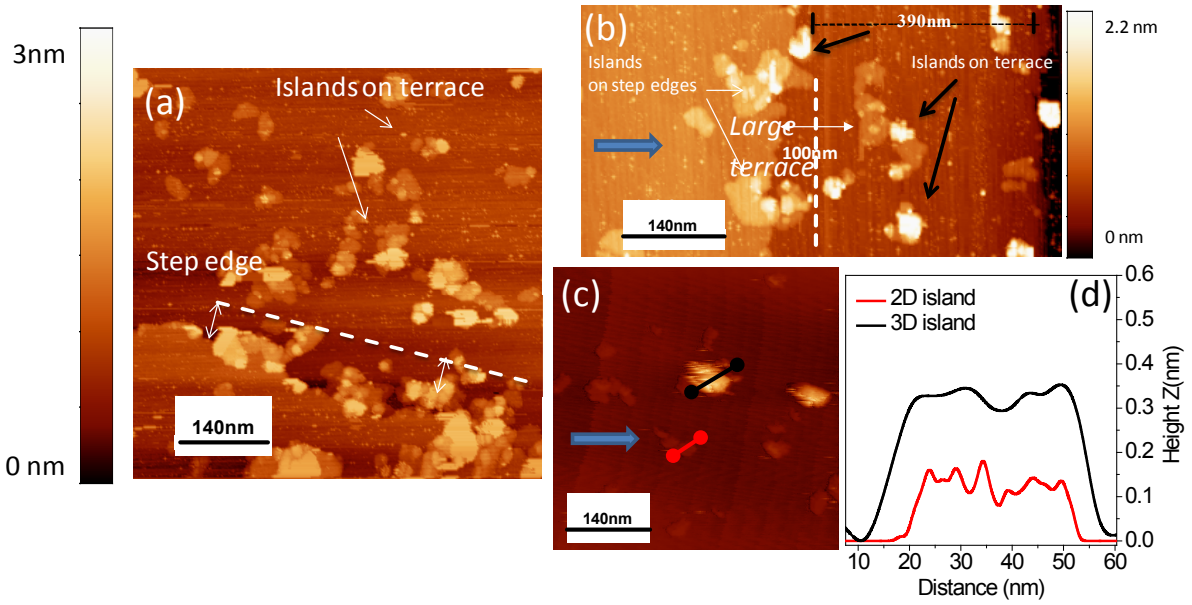

Figure 3.24: *Constant-current STM images(700nm ×700nm) of the nucleation occur in the 3rd cycle on the steps region (a)-(b) where the nucleation condensation happen near to the steps. Decoration of the steps by islands of 0.3-0.6nm heights. Nucleation on the terraces showed in (c) lead to formation of tow kind of island height with 2D structures of height in the range of 0.1nm however the 3D islands has important high where it is about 0.4nm (d)(profile).*

The transition between the 1st and 3rd cycle shows an important surface chemistry effect. While the precursor self-assembles in an arranged structure during the 1st cycle, the 3rd ALD cycle induces important nucleation with an RMS roughness of 0.7nm, resulting from 3D islands of 0.4-1.2nm height and ~40% surface coverage from the scanned zone. The nucleation sites are concentrated in two zones (Figure 3.24 (a), (b) and (c)): On the steps edges and in the area 100nm apart from the steps. Random nucleation takes place at least 100nm away from the step edges, resulting in 2D and 3D islands as

shown in Figure 3.24 (c) shows 3D islands (Black line) with a height of 0.35 nm and 2D islands (Red line) with height of 0.15nm.

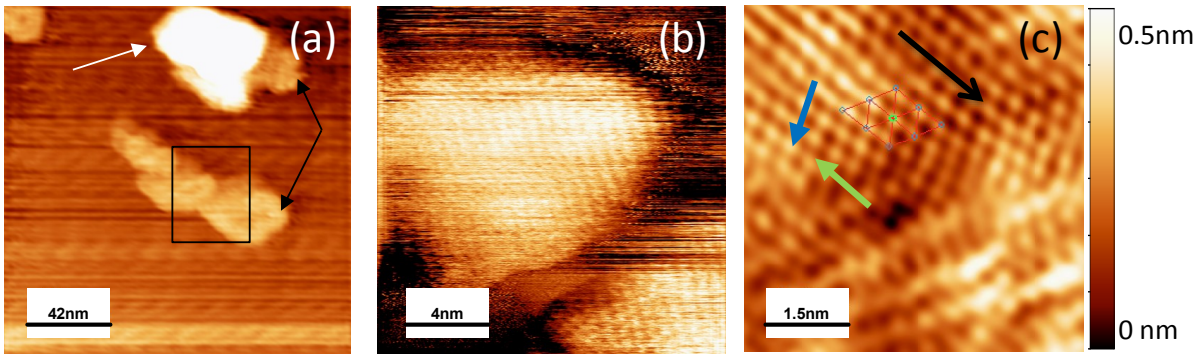

Figure 3.25: *Constant-current STM images in different scales showing island growth during the ALD of $Al(OH)_3$ on HOPG: (a) Field of view: 210nm × 210nm. Black and white arrows indicate islands. b) Field of view: 20nm × 20nm and c) Field of view: 7.5nm × 7.5nm. Here, the region indicated by the black square in panel (a) is scanned with nano-resolution. The direction of $Al(OH)_3$ is indicated by green and blue arrows in panel (c).*

The STM nano-resolution scan (Figure 3.25) show that the latter are indeed two dimensional structures generated from Al_2O_3 molecules arranged in a (5x5) lattice with a lateral distance L of ~ 0.5nm. The distance between the molecule and the first neighbor atom is about 0.1nm as it can be seen in the magnified picture (Figure 3.25 (c)).

Small Terraces

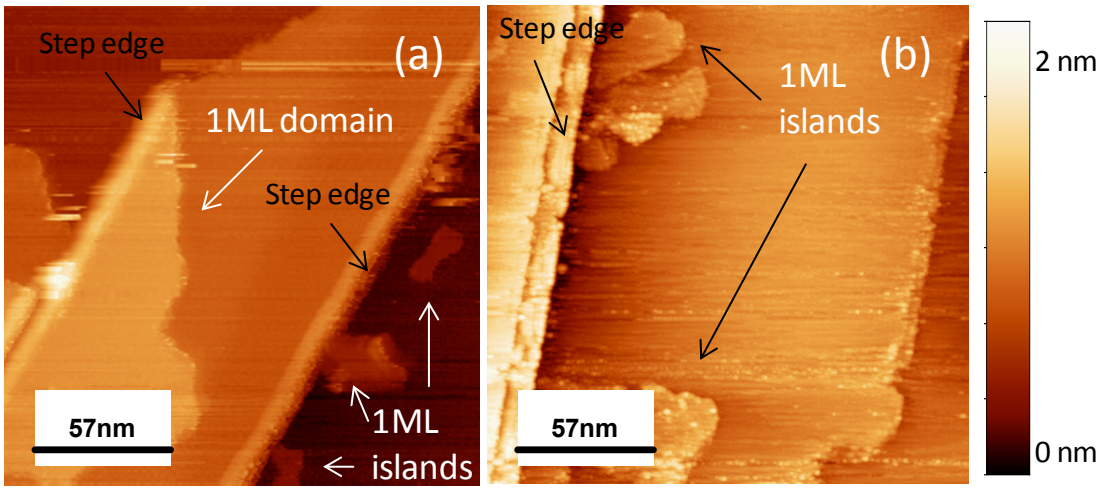

Figure 3.26: *STM images (285 × 285nm) for small terraces in two different spot showing island growth during the ALD of $Al(OH)_3$ on HOPG. 2D domain formed on the terraces in (a) of 1ML between two steps edges and (b) 2D structure formed on the bottom of the steps.*

The interesting part that in small terraces with widths (<300nm) the growth is more homogeneous in 2D structures. First this 2D (2ML) with height of 0.6nm, extended in some large domain near to the dimension of the terraces width (Figure 3.26 (a)). The growth start from the steps edges toward the bulk on the terraces. On the bottom of the terraces, a second nucleation sites the ALD reactant, 2D with lower height that is about 0.3nm (1ML). The islands are arranged in smaller homogeneous domain starting from the bottom of the steps and extend to the bulk of terraces ,i.e. are observed in the Figure 3.26 (a) and (b).

- **Fifth cycle**

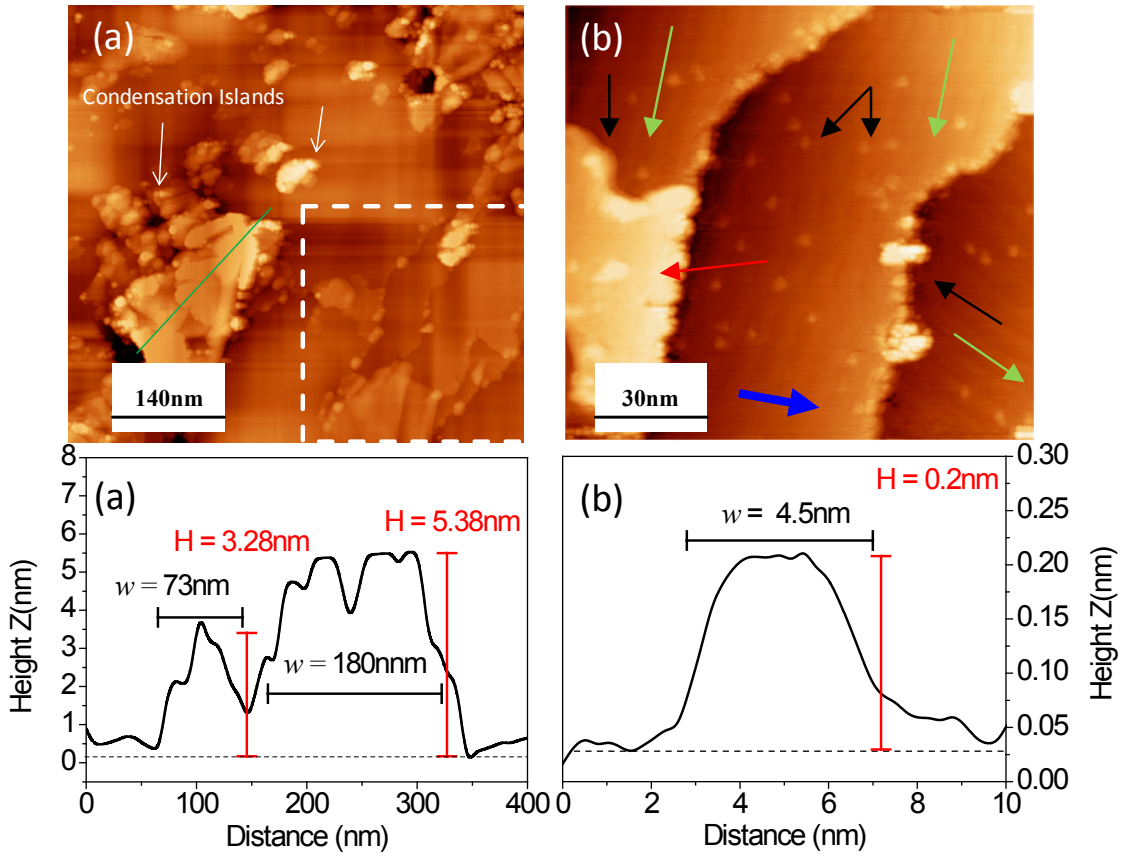

Figure 3.27: *Constant-current STM image (700nm × 700nm) field of large terraces (b) (150nmx150nm) of the small terraces and steps shows steps decoration but the formation of large domain of materials (red arrows) with formation of nano-island with the dimension of 0.1nm and ~4nm of width.*

The STM image of the ALD film/HOPG surface after the 5th ALD cycle (Figure 3.27) displays lower islands distribution (indicated by the black arrow) than after the 3th cycle and the surface coverage decreases to 18 %. However, the RMS roughness is 1.8nm. This is due to the height of those islands which becomes much larger, i.e. 3- 6nm. Therefore, those values indicate that the growth is no longer ALD model-like. The widths of different islands increase from 40nm in the 3th cycle to maximum of

120nm in 5th. The increases in the widths of islands are related to the diffusion over the surface of the coming precursors that nucleated in the existent one in the bulk of the large terraces. On the small steps in Figure 3.27, formation of nano islands with the dimension of 0.2nm is the new features appear in the fifth cycles. This dimension can be correlated to formation of ALD perfect nucleation. The surface coverage by those nano islands is about 10% of the surface. This growth per cycle is so pour regarding the number of ALD that lead to the formation of high materials condensation on larges terraces.

3.2.2. Al_2O_3 growth on Ag-HOPG

3.2.2.1. O1s/Al2p core level

The deposition of Ag on HOPG by PVD and TMA on Ag coated HOPG by ALD was characterized by x-ray photoelectron spectroscopy. For XPS Mg K alpha (1253.6 eV) X-ray source and spherical analyzer from spacelab is used.

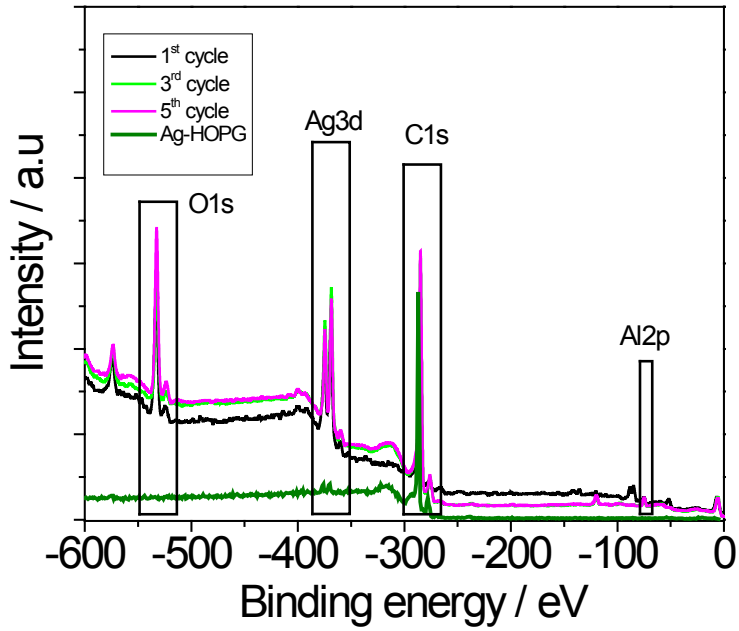

Figure 3.28: *The overview spectra of HOPG and TMA layers on Ag-HOPG.*

The scan of the surface Ag-HOPG is done at angle 90° to the substrate that why the intensity of the Ag-peack is very low, however the scan of the ALD cycles are more surface sensitive that's why an increase in the intensity of the Ag is observed. The After the deposition of Ag by PVD 1TMA layer is deposited on Ag/HOPG by ALD and the deposition is confirmed from the XPS spectra of 1TMA on Ag/HOPG spectra as shown in Figure 3.28. The peak at around -368.3 eV shows successful deposition of Ag on chemically inert surface of HOPG however after TMA deposition the signal of Al2p is very low in the overview spectra in Figure 3.28.With the increase of TMA ALD cycles the intensity of Al2p is visible but the Ag3d peak intensity is not attenuated as result of TMA deposition.

Moreover after the TMA deposition the O1s peak at around -532 eV. The dramatic increase in O1s peak intensity is as result of oxidation of TMA on Ag/HOPG**.**

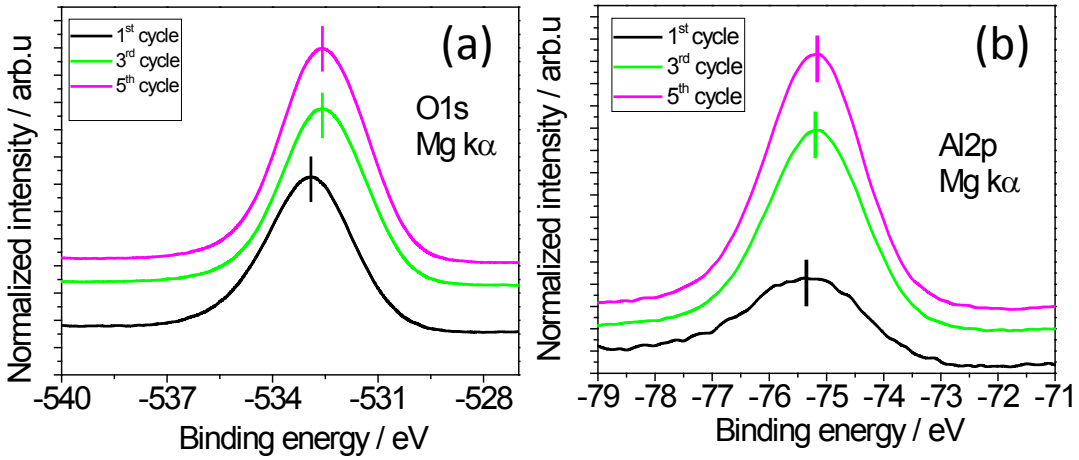

Figure 3.29: *(a) O1s XPS core level spectra after the1st, 3rd and 5th ALD cycles as indicated in the diagram. (b) Al2p Core level XPS of Al2p for 1st, 3rd and 5th cycles.*

In Figure 3.29, the detail spectra Al2p and O1s are shown for Ag-HOPG and 1, 3 and 5 TMA layer on Ag/HOPG. In Figure 3.29 (b) the intensity of Al2p increases with the increase in ALD layer. The increase in Al2p shows the increase in deposition of TMA layer but with certain pin holes. Moreover the O1s peak also confirm the increase in deposition of TMA layer as the TMA layers get oxidized when it comes with in contact of ambient air.

Table 3.5: *Summary of the data Peaks position, FWHM and O-Al/Al2p ratio for 1st, 3rd and 5th, of O1s and Al2p determined in this contribution for ALD layers deposition.*

	1st cycle	**3rd cycle**	**5th cycle**
O peak position (eV)	532.9	532.61	532.57
FWHM	2,98	2,81	2,86
Al peak position (eV)	75.7	75.8	75.7
FWHM	2,59	1,99	1,98

From the XPS analysis of HOPG and TMA layers on Ag/HOPG it can be conclude that the PVD deposition of Ag is possible on inert surface of HOPG. However the TMA growth is not conformal on Ag/HOPG surface. The growth of TMA could be on the defect site or the step of Ag/HOPG.

3.2.2.2. Surface morphology

- **Fist cycle**

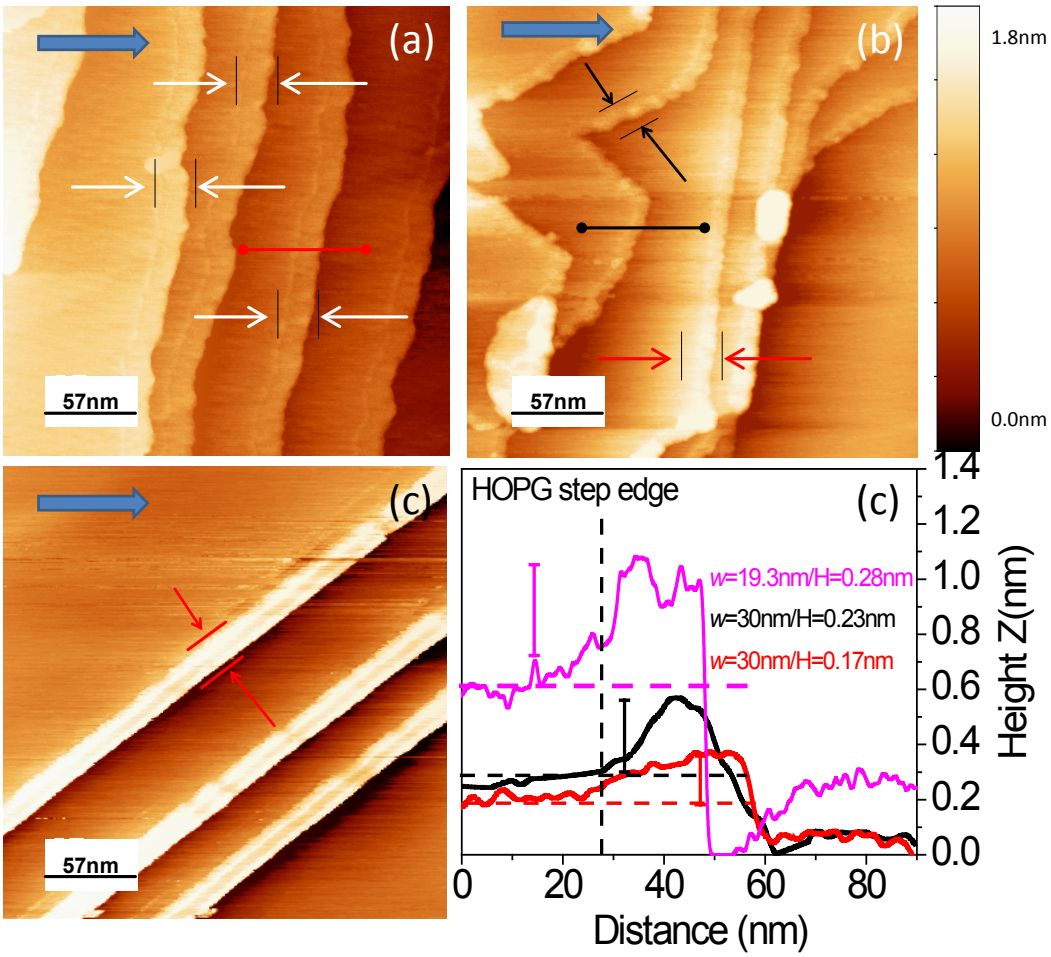

Figure 3.30: *Constant-current STM images (a), (b) and (c), (285nmx285nm) of different sport from the 1st cycle of the ALD on Ag-HOPG. The nucleation occurs on the steps edges with replication of the morphology of its geometry. The height the nucleation increase from a-b (the profile steps (d)) which are respectively 0.32nm, 0.56nm and 1.1nm. The width of the nucleation is also increasing with the height of nucleation respectively 10nm, 15nm and 28nm.*

The deposited Ag islands thermal evaporated on the steps edges of the HOPG occur where island of dimension important in height, e.g. 1nm, leading to preferential sites of nucleation's. The Figure 3.30 shows the features obtained by ALD on the steps edges. The arrival molecules on the surface diffuse over the surface where is attached to the Ag-island that are grown on the steps edges leading to

formation of wire parallel to the direction of the steps. This steps decoration has different height and some spot shows nucleation also of 3D on top of the steps (Figure 3.30(b)).

Figure 3.30 (a), the field of 285nm^2 of five adjacent steps and terraces, with height aspect ratio of duplication of the steps edges. This lead to translation of the surface in the direction of the growth from the initial substrate by ~10nm in the direction of the steps flow. The steps height is identical to the deposited materials with a small fraction of 0.1nm. Figure 3.30 (b) is a measurement of anther region on Ag-HOPG, where same deposition on the terraces edges is observed and the islands that are covered are shown (black and red arrows) and also an agglomeration of 3D islands and 2D with the height of 0.6nm and width changes with the nucleation regions. Nucleation again over the steps edges is occurring again as it shows in Figure 3.30 (c). Here, no agglomeration is seeing in the top edges of the steps however the grown wire over the steps is well defined with important height of 1.1nm and 28nm of width.

- **Third cycle and fifth cycle**

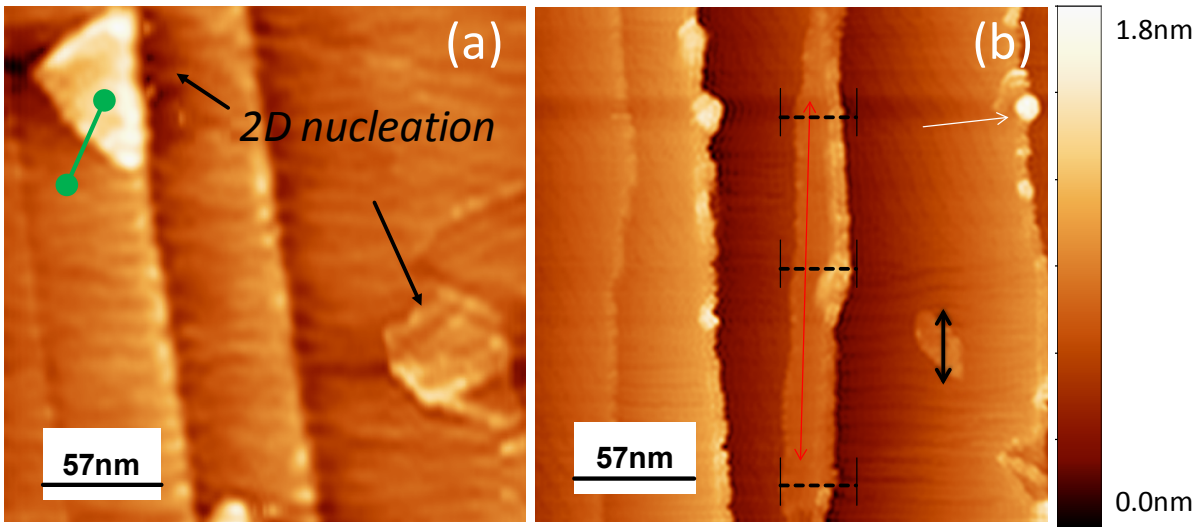

Figure 3.31: *Constant-current STM images (a) and (b) (285nmx285nm) of the 3rd and 5th ALD cycle, respectively. (a) Nucleation of triangular-2D structure starting from the edges and directed toward middle of terrace on the top edges (Green line). (b) The fifth ALD cycle, nucleation of 2D structures over the terraces edges (black arrow) with distance of 20nm.*

The transition between the 1st and 3rd cycle of the ALD(Figure 3.31 (a)) growth occur happen in 2D agglomeration on the top of the steps with height of 0.3nm. The condensation of materials is concentrated on the step region, especially on the top and the lower index of steps. Here we can

conclude that the growth is important in the defect sites as the basal plane of HOPG is inert to the reactions of ALD. The defects present an ALD nucleation reactive sites, it can be related to the energy in defect that are favorable to path reaction of Al_2O_3. The growth on the top edge where it stop by barrier effect and islands Ag decorating the steps edges. The molecules saturated in height of growth then they are arranged in the triangular feature. The STM image after the 5th cycle (Figure 3.31 (b)) indicated three kind of growth feature over the surface. First the growth of 2D structures (red line) on the steps region with height of 0.4nm and width of ~25nm. This structure grows along the step as an extending of the previous 2D islands growth observed already after the 3rd cycle. The precursor agglomerate near to the steps and the adsorption on the 2D structures leads to the formation of larger precursor domains. The steps also are decorated by formation of small islands on the steps edges with the height of 0.6nm. The nucleation are just localized on the steps, this can be related to the Ag islands already existed on the steps edges.

Chapter 4 Discussion

Based on the combination between the STM results and theoretical models, the effect of the surface morphology (orientation and steps presence) and chemistry (-H terminated, graphene) on the ALD nucleation's behavior are discussed in this chapter. This chapter contain two part, first one discuss the growth on the Si(111)-H (major part) and the second part is about the growth on HOPG and Ag-HOPG.

For the HfO_2 deposition on Si(111)-H, the application of the Purunen model (see chapter 1) , which relate the thickness increment per cycle (GPC) to the chemistry of the growth, on Si(111)-H at RT and 280ºC. As, the STM measured to growth on different nucleation sites (the steps and terraces) the possible reactions in this localized area are disused. ALD occur mainly tow type of chemisorptions on the surface, where the first one reside in ligand exchange between the ML_n and the interface group and dissociation or association mechanism. As Δh is determined from STM, ΔC_M is calculated then for different regions in every cycle of HfO_2 growth .As consequence , different possible reaction are presented and building surface thickness of the product materials grown.

To understand the growth model, an application of kinetic surface roughening of non equilibrium growth models was done. The universal values, results of theoretical of different growth equations characterized different dynamic of atoms/molecules on the surface in correlation with the properties of the film morphology. This kind of investigation was purely done on ALD in contrast to other deposition techniques as sputtering, CVD. Kolanek et al. applied this approach in the investigation of HfO_2 in-situ ALD cycles by cycles on Si-OH by AFM microscopy. The surface statistics obtained for Si(111)-H would be discussed, with the comparison to the Si-OH.

In the last part of this chapter, the discussion of the GPC of Al_2O_3 on HOPG and Ag-HOPG in relation with the terraces width and introducing a simple model to explain the effect of the widths and the barrier energy in the steps on the growth ALD behavior.

4.1. Puurunen model: HfO_2 on Si(111)-H

4.1.1. Model consideration

The model parameters $\Delta h, \Delta C_{Hf}$ and $\Delta C_{N(CH_3)_2}^{maxthr}$ are the key for investigation of which reaction mechanism of TDMAH and H_2O nucleation can occur on Si(111)-H terminated. As the ALD is characterized by self-limiting reactions, the fraction of materials grown on the substrate is not only saturated in height but also in the number of atoms attached to the substrates. The chemisorptions of the reactants on the surface has two main type that can occur, first a ligand exchange with the surface and the second association or dissociation where all part of the reactants are attached to the substrate Based on this model, the ratio $\Delta C_{N(CH_3)_2}/\Delta C_{Hf}$ is directly related to possible reaction of the Hf-$(N(CH_3)_2$ with surface species. The STM measurements prove that the height (Δh) of the nucleation varies in respect to the surfaces region. As consequence, the application of this model dictated to distinguish the reactions on the steps region and on the terraces (Figure 4.1).

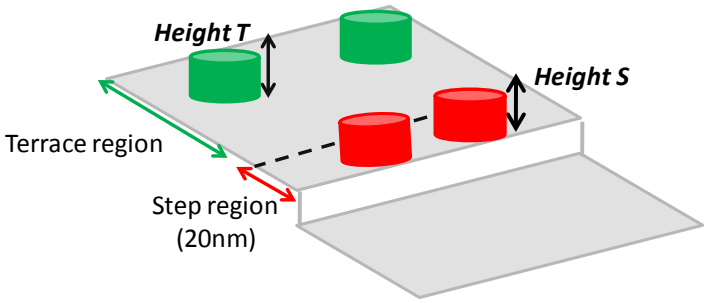

Figure 4.1: *Illustration of the tow region heights that are used in the application of the Puurunen model. The red color is an illustration of the materials grown on the steps region and the green one of the materials on the terraces region.*

The GPC is referred to $\Delta h(nm)$ as thickness increment from ALD reactions per cycle. This model correlated the mass balance of metal atom of the precursor (-Hf) reacted on the surface to Δh by the Equation (1.11)

$$\Delta h = \frac{M}{\rho N_A} \Delta C_{Hf}$$

The number ΔC_{Hf} (-Hf atoms) attached to the surface per unit surface area [nm^{-2}] of Si(111) surfaces are calculated then for each cycle are determined from every Δh *(nm)*. These values are presented in Table (4.1).

Table 4.1: *Different heights and number of Hf atoms attached for the Si-H at RT and 280°C for the steps region and terraces*

RT	ALD cycles	Experimental measurement Δh (nm)	Percentage of growth (%)	Model values ΔC_{Hf}	Percentage of growth (%)
Steps height	1	0.24	60.0%(0.6Ml)	3.84	64.0% (0.64Ml)
	2	-	-	-	-
	3	0.60	150%(1.5Ml)	9.6	160%(1.6Ml)
	4	0.85	212%(2.1Ml)	13.6	227%(2.1Ml)
Terraces features	1	0.48	133% (1.33Ml)	6.51	108% (1.08Ml)
	2	0.08	20.0%(0.2Ml)	1.28	21.0% (0.2Ml)
	3	1.20	300%(3.0Ml)	19.2	321%(3.0Ml)
	4	0.30	75.0%(0.75Ml)	4.8	80.0%(0.8Ml)

280°C	ALD cycles	Experimental measurement Δh (nm)	Percentage of growth (%)	Model values ΔC_{Hf}	Percentage of growth (%)
Steps height	1	0.14	35.0%(0.35Ml)	2.7	45.1%(0.45Ml)
	2	0.06	15.0%(0.15Ml)	1.62	27.0%(0.27Ml)
	3	0.07	17.5%(0.17Ml)	1.72	28.7%(0.28Ml)
	4	0.30	75.2%(0.75Ml)	4.4	73.5%(0.73Ml)
Terraces features	1	0.23	57.5%(0.57Ml)	3.78	63.2%(0.63Ml)
	2	0.08	15.6%(0.15Ml)	1.62	27.0%(0.15Ml)
	3	0.28	90.0%(0.9Ml)	5.41	90.4%(0.9Ml)
	4	-		-	

The average monolayer growth and average $\Delta h^{\overline{ml}}$ =0.36nm of number attached of -Hf atoms on the surface $\Delta C^{\overline{ml}}$ =5.98/nm^2, are respectively calculated from

$$\Delta h^{\overline{ml}} = \left(\frac{M}{\rho N_A}\right)^{\frac{1}{3}} \quad (4.1)$$

$$\Delta C^{\overline{ml}} = \left(\frac{\rho N_A}{M}\right)^{\frac{2}{3}} \quad (4.2)$$

For the growth at RT either in the steps and terraces regions, the values of growth percentage referred to the average of monolayer growth and –Hf attached to the substrate shows that the growth in the 1st and 2nd cycles are partial growth lower than one monolayer (ML) formation of HfO_2. The growth per cycle is about 60% and 64% ΔC_{Hf} of a monolayer. This percentage is increasing in the 3rd and 4th cycles, where more than one monolayer of deposited materials occurs. This increase is unlike ALD

growth process; because the formation of the layer is normally saturated to be constant with every cycle as lower than a complete layer.

In the case of the growth at 280°C, the growth per cycle is limited under one monolayer for every cycle. The height Δh and ΔC_{Hf} during the ALD-HfO_2 process have an important initial increase in the 1st cycle due to the deposition of the materials that is related directly to the number of reactive sites of the Si-H bonds and then decrease to lower values in the 3rd and 4th cycles, e.g. 27% and 28%. This behavior implies that the deposition is affected by the number of sites and also the fraction surface free for the deposition. The growth of HfO_2 from TDMAH and H_2O as precursors on the Si-H can be described by the reaction Equation (4.3):

$$Hf\,[N(CH_2)]_4 + Si\text{-}H \longrightarrow Si\text{-}HfO_X + n\ x\ H\,N(CH_2) \qquad (4.3)$$

The TDMAH reaction attaches -Hf $[N(CH_2)]_4$ through 0, 1 or 2 bonds to the surface. The H_2O remove the $N(CH_3)_2$ group from the surface as H-$N(CH_3)_2$, that are assumed to be purged with N_2, leaving behind a substrate with (-OH) groups. In our case, we deposited the TDMAH as first precursors, so this reaction happen in correlation with Si-H bonds, however for the 2nd, 3rd and 4th cycles (-OH) groups, normally, substitute the ligands and becoming the new reactive sites for the film growth. The ratio of number sites reacted to the numbers of all sites is denote $f = \frac{\Delta c_{si-H}}{C_{si-H}}$ (see model Purenen).

The parameters that define the possibility of the reaction occur is the coverage θ of fraction surface by the ligands. This value is directly connected to the radius of the ligand through Equation (1.8). Van der Waals radius for the $N(CH_3)_2$ (N→C= 0.146nm and C→H=0.11nm) ligand is about 0.256 then the radius is equal to 0.128nm (reference). Therefore the theoretical maximum number of ligand per nm^2 is $\Delta C^{maxthr}_{N(CH_3)_2} = 9.70\ nm^{-2}$ (see chapter 1). M= 354.4 $gmol^{-1}$ and density ρ = 9.6 x 10^{-21} gnm^{-3} of TDMAH in first cycle and the M=210.84 in the 2nd, 3rd and 4th cycles because it assumed that HfO_2 is formed.

4. 1. 2. Model application

1. 1. 2.1. Nucleation at RT

The model of the growth is based on coverage (θ) of ligands, which is a major factor to the verification of the possible numbers ligands exchanges or if there is no exchanges. In Table 4.2, the different coverage θ (ALD-RT and ALD-280°C) calculated for all possible surface- molecules reactions that can happen in ALD. The number of ligand after the reaction over the surface is related to the number of metal atoms by ratio $\frac{\Delta C_{N(CH_3)_2}}{\Delta C_{Hf}}$ = *n*-1 or *n*-2, where *n*=4 for TDMAH.

Table 4.2: *The determination of the ligand coverage θ from the ratio* $\frac{\Delta C_{N(CH_3)_2}}{\Delta C^{maxthr}_{N(CH_3)_2}}$ *for the fourt cycle ALD- HfO_2 at RT.*

		Values	1st cycle	2nd cycle	3rd cycle	4th cycle
STEPS	*n-1= 3*	$\Delta C_{N(CH_3)_2}$	11.52	11.52	28.8	40.8
		Θ	1.18	1.18	2.96	4.20
	n-2=2	$\Delta C_{N(CH_3)_2}$	7.68	7.68	19.2	27.2
		Θ	***0,79***	***0,79***	1.97	2.80
TERRACES	*n-1= 3*	$\Delta C_{N(CH_3)_2}$	11.52	6,48	58.8	14.4
		Θ	1.18	***0,66***	6.06	1.48
	n-2=2	$\Delta C_{N(CH_3)_2}$	7.68	4,32	38.4	9.6
		Θ	***0,79***	**0,44**	3.95	1.04

- ***Surface Reaction***

From the different values obtained from every possible reaction, the reasonable values of 0.79 in the 1st and 2nd cycle fit with the limit given by the PM which should be lower than the unit ($\theta \leq 1$). The values of $\Delta C_{N(CH_3)_2}$ at the steps region corresponding to θ = 0.79 surface coverage when the ratio $\Delta C_{N(CH_3)_2}/\Delta C_{Hf}$ =2 (two ligand exchanges) means that the total number of ligand that full the area surface of 1nm^2 is would be 7.68nm^{-2} attached to the 3.84 Hf atoms/nm^2 . The number of ligands is equal to the number of reactive sites of Si-H existent in 1nm^2, i.e. 7.82. So it can be concluded that the total Si-H sites are consumed thus *f* =1. For every TDMAH molecules deposited two ligand are released and two Si-H are consumed.

The founded values ΔC_{Hf} , $\Delta C_{N(CH_3)_2}$, θ and *f* can be associated to two possible type of reactions First a chemisorptions of two ligand of $N(CH_3)_2$ through subtraction of two H atoms leading to the formation of two molecules of -$HN(CH_3)_2$ purged from the surface. As consequence, a formation of Si-2Hf $N(CH_3)_2$-Si in the first half deposition of TDMAH as

$$Hf[N(CH_3)_2]_4 + 2\,Si-H \leftrightarrow Si-Hf[N(CH_3)_2]_2-Si + HN(CH_3)_2 \quad (4.4)$$

In this case, the exposure of the molecules Si-2Hf $N(CH_3)_2$-Si to H_2O can create an interface of $Hf(OH)_2$ if the two ligand $N(CH_3)_2$ reacted with the –H or $N(CH_3)_2$ -Hf-O-H only one ligand is

exchanged occur. From The STM measurement the height of the TDMAH initially deposited is about 0.29nm that is reduced with the deposition of H_2O to 0.24nm from this can be concluded that reaction between the water and Si-2Hf $N(CH_3)_2$-Si lead to the formation of HfO_2.
The second possible reaction between TDMAH and Si-H with the same parameters obtained can be a ligand exchanges that are accompanied with dissociation or association of the molecules in the surface. That mean the ligands can react with the Si-H be dissociation from the molecules Hf-$N(CH_3)_2$ leading to Si-$N(CH3)_2$. This kind of reaction was observed in many experimental and predicted by simulation of the TDMAH growth on Si-H terminated surfaces [136-137].

- ***Reaction saturation***

Two assumptions can be the origin of saturation of reaction, either the actives sites of nucleation or the steric hindrance effect where the grown molecules strongly interact, and Vander walls repulsion can prohibit the nearest molecules to grow on the free substrate. The values of the attached atoms ΔC_{Hf} calculated for the tow assumption are presented in the Table 4.3.

Table 4.3: *Saturation origin, comparison between the values obtained from steric saturation and from some reactive sites.*

Cycles	Ligand Exchange	ΔC_{Hf}: Saturation cause		ΔC_{Hf} (Experimental)
		Steric-hindrance	**Number of -SiH**	
1st	2-ligands	3.73	4.85	3.84
2nd	2-ligands	3.73	4.85	3.84

First, we assume that the origin is the steric hindrance, the number of free sites is fixed i.e. f =1. The molecules react over the surface by two ligand exchange by adsorption, so by the application of the equations of steric hindrance, if $\theta^{max} = 1$ then the values of attaching 3.84 metal - Hf ΔC_{Hf}=3.73 . This values is do not shows important difference from the number ΔC_{Hf} =3.84.obtained from the height calculation Equation (1.11).

The saturation origin is now related to the number of Si-H group. As results the number of metals atoms Hf 4.85 /nm^2. This value is higher than the values obtained for ΔC_{Hf}. The saturation caused by some reactive free sites (Si-H bond) can't be because the advantage of the certainty of Si(111)-H terminated plan that the reactive sites are determinate to be 7.82 atoms/nm^2. With the reaction on the

surface the number of reactive sites still free for adsorption, however, the interaction inter molecules lead to the small amount of some molecules HfO_2.

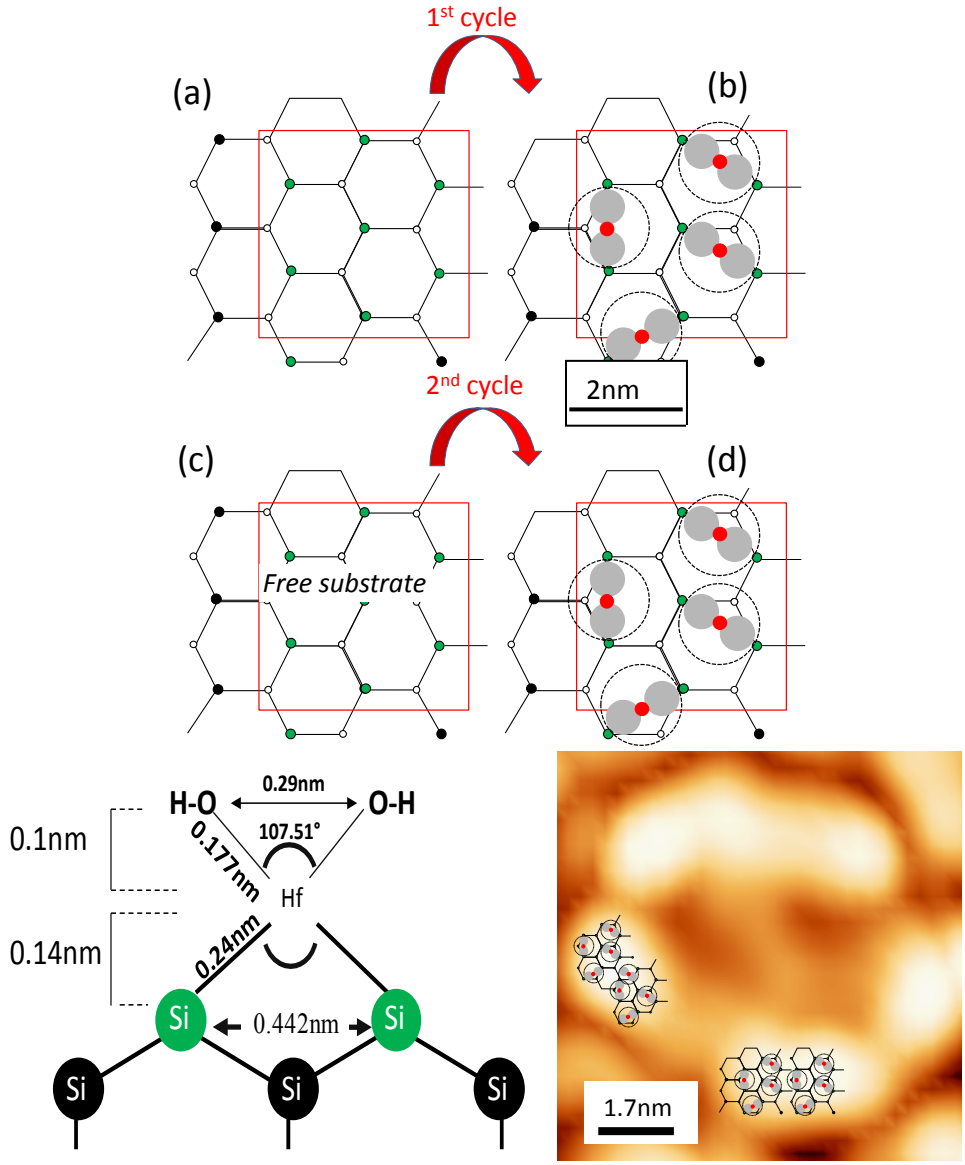

Figure 4.2: *The model of Puurunen of the ligand exchange reaction mechanism per unit area of [1nm^2] (red square). The number of –Hf are about 3.48/nm^2 (red circles) attached to the reactive sites Si-H (green circles). (a-b) 1st cycle of TDMAH adsorption reaction. (c-d) 2nd cycle on the free substrate reaction. (e) illustartion of the reaction with the bond lenghs dimension. (f) The print in of the model of reaction in the STM images from the frist TDMAH deposition.*

In the second cycle, the film is closed then the surface become with similar height in average with the decreasing of the RMS roughness. All the roughness parameters diverge to closed contentious film the growth in the second cycle is occur to be in the free substrate Here the thickness of the film is about

the same height of the first ALD islands. As results the growth happens in the first cycle is duplicated in the second cycles.

1. 1. 2. .2. Nucleation at 280°C

- ***Surface Reaction***

Table 4.4: *The determination o the ligand coverage θ from the ratio* $\frac{\Delta C_{N(CH_3)_2}}{\Delta C^{maxthr}_{N(CH_3)_2}}$ *for the fourt cycle ALD- HfO_2 at 280°C.*

		Values	1st cycle	2nd cycle	3rd cycle	4th cycle
STEPS	*n-1= 3*	$\Delta C_{N(CH_3)_2}$	8.1	4.86	4.05	13.2
		Θ	***0.83***	***0.50***	***0.41***	1.41
	n-2=2	$\Delta C_{N(CH_3)_2}$	5.4	3.24	2.7	9.6
		Θ	***0.55***	***0.33***	***0.27***	**0.95**
TERRACES	*n-1= 3*	$\Delta C_{N(CH_3)_2}$	11.34	4.86	16.23	-
		Θ	1.16	***0.50***	1.76	-
	n-2=2	$\Delta C_{N(CH_3)_2}$	7.56	3.24	19.44	-
		Θ	***0.77***	***0.33***	1.17	-

From the Table 4.4, coverage θ in 1 st, 2nd, 3rd and the 4th cycles on terrace and steps regions, i.e. expect the 4th cycle on terraces; fulfill the condition of chemisorptions reactions in Puurunen model ($\theta \leq 1$). As a first comparison with the growth at RT, all reactions are possible to occur on the surface in both regions on the steps and on the terraces. From the number of the atoms attached to the surface, it can be concluded that in the ALD window temperature the chemisorptions reactions are reactive for all cycles. To examine which reaction occur , the number of reactive sites is calculated and then referred to *f* from Purrenen model for ligand of 0.2nm which is at 280°C is define 0.2-0.4.

In the first cycle, the coverage in the steps region are θ_1=0.83 and θ_2=0.55 which mean one ligand exchanges or tow ligand exchanges can be results of the chemisorptions reaction of 2.7 -Hf atoms /nm^2. The values of coverage fulfill the criteria of the model as is it lower than the unit. The numbers of reactive sites possible for this reaction define by *f* is then equal to 0.34 and 0.68 respectively for 1 and 2 ligands exchanges with the surface (see Table 4.5). The ratio of 0.34 is in the same range of ratio of Si-H bond with the TDMAH and H_2O. As consequence, from both parameters θ and *f*, the reaction of one ligand exchange seems more adapted as reaction mechanism that occurs in the first cycle.

Table 4.5: *Relation between the coverage ligand values and the number of reactive sites for nucleation.*

Cycles	Ligand Exchange	Θ (coverage ligand)	*f* (number reacted SiH)
1st	1	0.83	0.34
	2	0.55	0.68
2nd	1	0.50	0.13
	2	0.33	0.27
3rd	1	0.41	0.14
	2	0.27	0.28
4th	2	0.95	0.56

In the second cycle, a decrease obtained in the number of -Hf atoms attached to the substrate to 1.6/nm^2. Accompanied by reduction of the the coverage θ. However the growth display a large number of reactive sites that are the Si-H still unreacted or the OH that are assumed to grow on -Hf(NCH_3). From 12 active sites, 4 -Hf from previous cycle and 8 OH, only 1.67 atoms are attached to the surfaces. STM measuring showed that complet coverge of surface occur with some apex of islands (see Figure 3.12 (e)). As consequence, it can be concluded that the growth occur in the lowest layers and on the top of ALD materials on -OH sites. The number of the reactive sites here for this growth is referred also to the number f=0.13 in the case of θ =0.50. Here also one ligand exchange also on this reaction of $Hf(NCH_3)_2$ with the surface. The 3rd cycle the number of Hf with 1.72 atoms near to the same values in the 2nd cycles. The growth in the second is then 0.07nm less than thickness of one cycle growth of HfO_2. The ratio between the number of reactive site and the ligand exchanges is reasonable more for the small ratio of reacted site to free one.

In the 4th cycle, the number of adsorbed atoms reaches 5.41/nm^2. This increase is a consequence of (-OH) group enriched the deposited materials from the exposure to H_2O. However the number of f for this case is out of the range for this temperature. This can is related to the oxidation of the surface with OH in the third cycle that mean the $Hf(NCH_3)_4$ reacted in the third cycle that lead to less than OH attached per molecules. This also is seen when we used to model for the origin of reaction saturation.

- ***Reaction saturation***

Table 4.6: *Saturation origin, comparison between the values obtained from steric saturation and number of reactive sites.*

Cycles	Ligand Exchange	ΔC_{Hf}: Saturation cause		ΔC_{Hf} (Exp)
		Steric-hindrance	Number of -SiH	
1st	1	2.57	7.8	2.67
	2	2.59	3.6	
2nd	1	1.56	13	1.67
	2	1.58	6.5	
3rd	1	1.35	7.8	1.72
	2	1.46	3.6	
4th	2	3.28	3.6	4.4

For determination of the steric hindrance origin, the calculation of the number of atoms attached to the substrate is dertemined by the equation of stric hindrance and number of reactives sites. The comparision of theoritical values of those recation saturation are then compared to the evaluted ΔC_{Hf} from the experimental values of the heights.In Table 4.6 it shwon that the numbers obtained from stric hindrance are equal to the experimental values for all the ALD cycle exppect the 4th cycles.

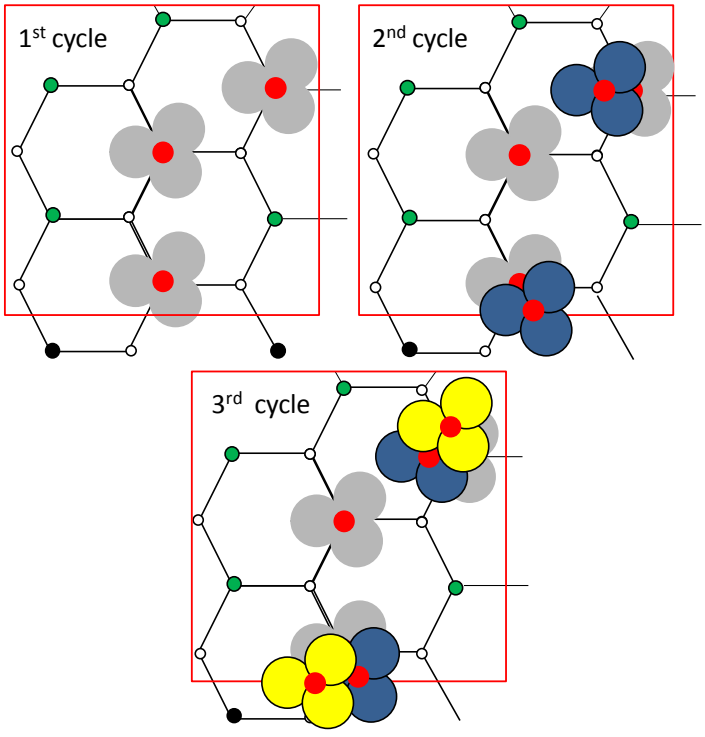

Figure 4.3: *The model of Puurunen of ligand exchange reactions mechanism per unit area of [1nm^2] ((a) red square). The number of –Hf are about 3.48/nm^2 (red circle) attached to the reactive sites Si-H (green circle).the number of Si per nm^{2}is 7.2 fit with the two ligand exchange with 3.84 of –Hf.*

- **Conclusion**

The application of the theoretical model developed by Puurunen on two ALD HfO_2 on the Si(111)-H terminated process (RT and 280°C) leads to determine to reaction occur from TDMAH/ H_2O precursors. It was found that depending on the temperature the parameters determined of the model such as the coverage rate and number of nucleation varies. The application that leads to define the growth reaction mechanism are highly coherent with the results obtained from STM observation.

For the RT 2 ligands exchanges only happen in the first cycle and the second cycles on the free substrate where the nucleation sites number and the steric hindrance effect both can be the origin of the saturation of reaction. In contrast the 3rd and th 4th cycle height don't belong to the height where the model can be applied. However at 280°C all cycles described a one ligand exchange with the surface and the steric hindrance is the origin of the saturation of reactions.The determinations of our growth with Puurunen model describe also values near to experimental found. Growth of TDMAH and H_2O on Si-H terminated results [120,123], describe the number of -Hf molecule per nm^2 assumed to be about 2.4 from HfO_2 film growth at 200-300ºC on the Si(100)-H terminated , however the reaction that occur on the surface can flow different path depending on the cites energy for chemisorptions. The surface roughness and morphology have important effect on the number of reaction not only the number of -OH groups in the interfaces. This would be discuses further (see section), where we compare to to growth on OH substrate.

4.2. ALD growth dynamic: Comparisons to experimental HfO_2 growth first 4 cycles on SiOH

To understand the growth feature, an application of kinetic surface roughening of no equilibrium growth models has been made. The universal values, origin from the theoretical resolution of different growth equation characterized different dynamic of atoms/molecules on the surface in correlation with the properties of the film morphology. The ALD ideal growth is expected to be layer by layer deposition where each atom/molecule can only sit on top of another atoms/molecules that overhangs and vacancies are not allowed. However, some other assumptions support the growth of islands by random deposition of deposition of materials. The mathematical model of the statistics surface component is one way to studies the model of the growth. This kind of investigation has been used by Kolanek et al, in the case of cycles by cycle's growth of HfO_2 on Si-OH/ in-situ ALD based on AFM measurements. In this part of the discussion, the surface statistics calculated from the height-height correlation function (HHCF) obtained for HfO_2 growth on Si(111)-H terminated would be compared with those obtained by et Kolanek al. The aim of this comparison is to reveal the effect of both surface chemistry and morphology on the film growth model.

First, the surface roughness parameters would be discuss as through the behavior of fluctuation of surfaces statistics and how is that related to the surface morphology. In the second part, the combination of different roughness exponent α, β, and $1/_Z$ are discussed in term of the universal values that are obtained for growth models..

4.2.1. Surfaces natures

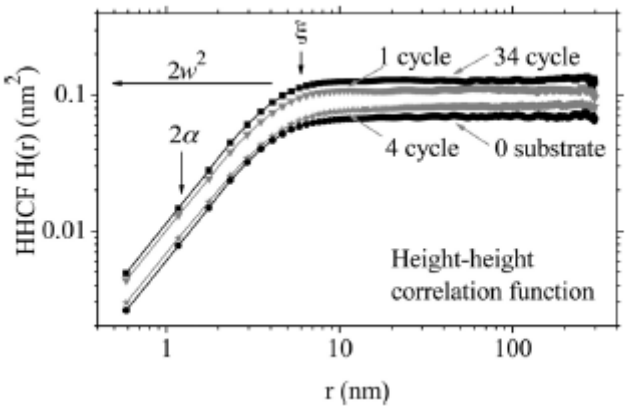

Figure 4.4: *Log–log plots of the HHCF evolution during ALD of SiOH substrate before ALD and after the 1st, 4th, and 34t^{h} cycles, respectively. Black arrows indicate approximate positions where surface characteristics (Surface width w, lateral correlation length ζ and the roughness exponent α) are acquired .*

The evolution of the H(r) for the Si-H at RT (1st and 2nd cycles), 280°C (The fourth cycles) and for the SiOH are similar growth, where both growths describe a self-affine surface. All the (HHCF) curves increase in with the position (r) as a linear line, then for $r \sim \zeta$ H(r) curve reach plateau and be constant for highest position (r) suggesting no spatial correlation of the surface features at larger length scales for distance above the lateral correlation length (ζ). The evolution behavior of the H(r) function fit with the H(r) evolution of the self-affine film growth surfaces.

In contrast with the film evolution of the Si-H at RT display characteristics growth of mounded surface in the 3rd and less in the 4th cycles in both surface directions. The height-height correlation function is similar to the self-affine surface. However, the difference in the behaviors arises at length scale r~ζ, where a peak is resulting and then at large scale r > ζ, the mounded surface is oscillating. This oscillation implies that the surface profile has quasi-periodic. A wavelength λ is a characteristic of the average distance between theses mounds. The origin of the mounded surface can be associated with many local effects related to the surface morphology, as the steps edges or local effect of shadowing (see chapter 1). In the case of Si-(111)-H at RT, the origin of the mounded surfaces in the 3rd and 4th cycles in the direction parallel to the steps is attrib to the shadowing effect. This effect

happens when taller surface features block the flux of molecules to reach the lower layer of the film. In relation, the STM measurement shows, 3rd half cycles (TDMAH pulses), an agglomeration of strips occur on the edge of the steps (first local growth) and spread in the direction of the steps flows $[\bar{2}11]$ over the terraces. The strips that are lined up in parallel created taller islands in the direction parallel to the steps $[01\bar{1}]$ (see Figure HHCF chapter 3). Therefore a shadowing effects lead to the non-uniform growth of film, and the surface display locally of growth in the region of the strips. The height increase in the 3rd cycle to reach 1.2nm, three times higher than the theoretical values 0.3nm. The average values between the mound λ calculated from H(r) for $r \gg \zeta$, are respectively 30nm and 10 nm for the 3rd and 4th cycles.

4.2.2. Surface statistics

4.2.2. 1. Roughness exponent α

As first finding, the ALD-RT of HfO_2 on Si(111)-H terminated showed a crossover that took place in the 2nd and 3rd cycle in both directions $[01\bar{1}]$ and $[\bar{2}11]$. The values are distinguished to local and global roughness. The presence of this crossover was discussed for many systems, where the values of local roughness exponent were related to the shape of islands/grain formed during the deposition of the materials.

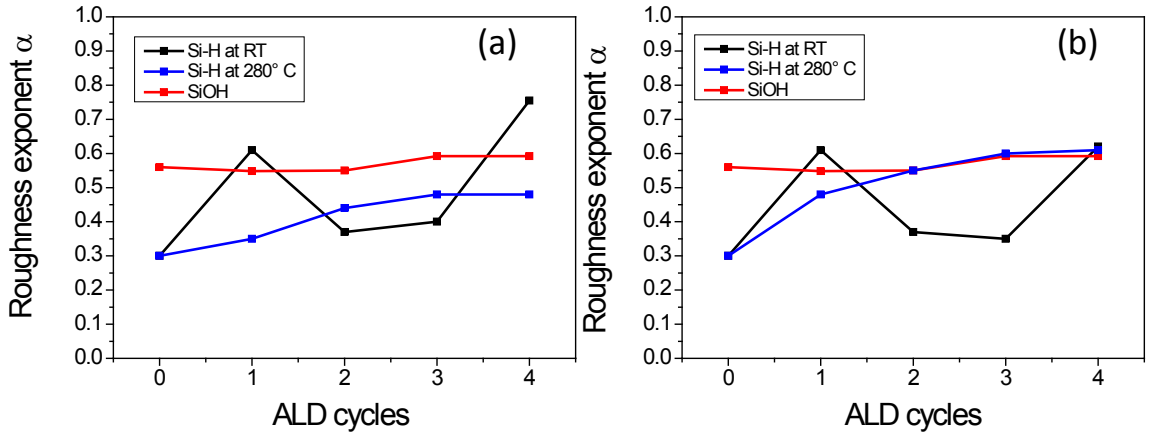

Figure 4.5: *The roughness exponent (α) evolution during ALD for Si-H at RT, Si-H at 280°C and SiOH. (a) The roughness exponent evolution in the direction parallel to the steps* $[01\bar{1}]$ *and (b) in the direction perpendicular to the steps* $[\bar{2}11]$.

First, the global roughness exponent curves, display a similar fluctuation for the ALD-RT and 280°C curves that are identical in both direction $[01\bar{1}]$ and $[\bar{2}11]$ with the number of cycles. This lead to the

conclusion that front roughness, define the height h(r) for r<< *ζ is* isotropic. The values of roughness exponent are not constant with the number of cycles. In comparison with the fluctuation of the α, the SiOH the values oscillated in the range of 0.54-0.59,quasi-constant roughness fluctuation with the scales. However for HfO_2 grown on Si(111)-H terminated at RT and 280°C varies with the number of cycles but in different evolution behavior, where α of RT oscillated between high and low values for each cycle, i.e. the limit α_{max}=0.8 and α_{min}=0.3. In contrast to the α at 280°C increase for cycle to cycles from α_{min} = 0.35 to α_{max} =0.61. Here the values are increasing with the number of cycles to reach in the 4th cycles near values to the Si-OH samples. Thus changing α value for grown film on the Si(111)-H during the growth indicates a change in the growth mechanism.

The local roughness for RT assigned to the crossovers of HHCF function obtained in the 2nd and 3rd cycles; Table 4.7 shows the values in both directions. For the second cycle, the roughness exponent values are equal to 0.8 in both directions, however in the 3rd cycle the local roughness exponent decrease from 0.9 to 0.74. T. J. Oliveira et al. [138-140], studies the relation between the shapes of the grain and the crossover values using modulation of HHCF evolution. They showed how to affect the grain shapes on the HHCF evolution with model growth. According to his calculation, the roughness exponent has values range of 0.85 -0.71 for grains shapes, semi-elliptical, conical and pyramidal.

Table 4.7**:** *Summarize of crossover of 2nd and 3rd cycle and the critical length associated to the crossovers.*

	Direction	α	Critical length r_c(nm)
2nd	$[01\bar{1}]$	0.8	1
	$[\bar{2}11]$	0.8	1
3rd	$[01\bar{1}]$	0.9	1
	$[\bar{2}11]$	0.74	2.3

According to our measurement the roughness exponent values fit with this range of values, as it's shown in Table 4.7. In another word the islands formed by ALD-RT, can be a mixtures of different shapes and geometry on the surface at RT. At the scale of 1nm of width, values fit with the numerically calculated values. O.Nilson [141], also calculated the growth in term of ALD for different shape basing on simulation. He showed how the ALD GPC is affected by the geometry of the formed islands in the case of islands morphology introduced numerical simulation of the ALD growth according to the formed shapes. Probably for the energetically reason of the surface at RT are the origin of the islands shapes and form.

Growth models classified by the roughness exponent values define tow growth process conservative and non-conservative. In conservative growth [142-143] the roughness exponent is defined to be α~ 0.67 [144]. The main relaxation mechanism is surface diffusion. Since desorption of molecules and formation of overhangs and voids are negligible, the density of the film is constant and high. This characterized the 1st cycle and the 4th cycle for the film at RT, where α =0.61 and α =0.62 respectively, e.g. α =0.75 in the $[01\bar{1}]$. For 280°C, the 3rd and 4th cycle also describe the values near to the conservative model where it is respectively α =0.60 and α =0.61.

For the 2nd and 3rd cycle for the film at RT α = 0.3-0.4, the model of growth is assumed to be non-conservative which mean that the relaxation mechanism is no dominated on the growth to compete and delete the local effect on the surface such the steps. In the second cycles, the film is grown is just the vacancies between the islands formed in the 1st cycles and for the 3rd cycle overhangs and voids are formed, i.e. stripes self-arranged. Which means that the growth happens in the vacancies in the film without important surface diffusion.

The flux of molecules purged on the surface for every cycle is affected by the materials that have been grown in the previous cycles. In the initial morphology, planar surface on the terraces leads to conservative growth from the random deposition of materials with relaxation.

The growth term of the initial morphology of the surface it can be concluded that with the initial surface where the substrate of SiOH had an initial surface curvature with the nucleated Si-OH group. The grown materials is then affected by this morphology that makes the roughness front more rounded shapes. Hhowever the growth on the Si-H is more shapes allowing peaks heights growth in the first cycle that with the deposition of the ALD the nearest scale of molecules interaction with the same height are extending leading to changes in the surface curvature.

From the roughness exponent the important conclusion about the front roughness that the growth of the film is far from equilibrium for the RT deposition. However, the film grown at 280°C on the Si(111)-H display a constant regime of non-conservative growth because the chemisorptions mechanism of molecules by the temperature effect compete with the diffusion of the molecules over the surfaces .

4.2.2. 2. Surface width (w)

The surface width is a commune statistic parameters of the profile height used to describe the roughness of the surface, it is defined as the square root of the mean height values in different position x of the height profile .

$$w = \sqrt{\langle [h(x)]^2 \rangle}$$

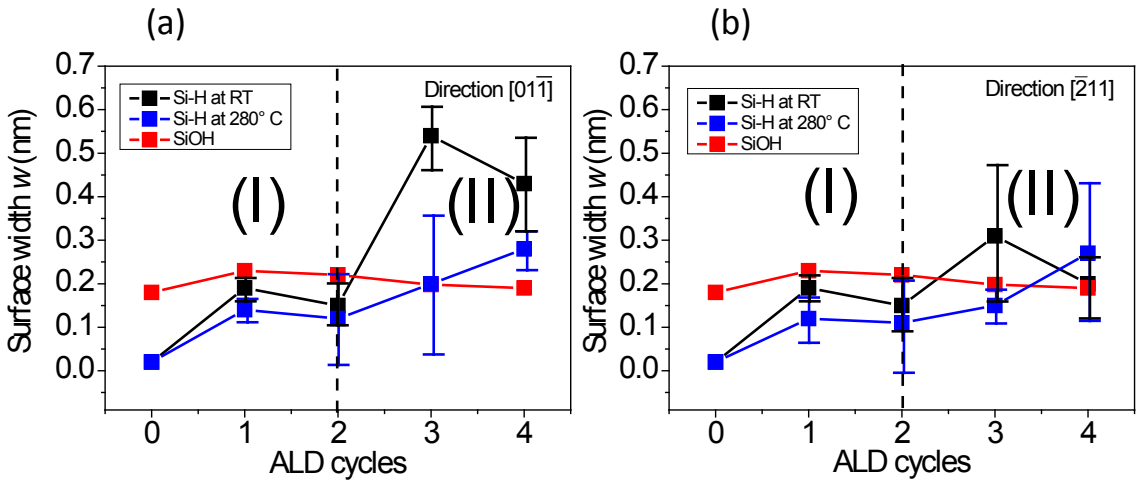

Figure 4.6: *Surface width evolution during ALD for Si-H at RT, Si-H at 280°C and SiOH. (a) The surface width evolution in the direction parallel to the steps* $[01\bar{1}]$ *and (b) in the direction perpendicular to the steps* $[\bar{2}11]$ *.First regime (I) shows a peak in 1st cycle and reduces in the 2nd cycle. The second regime (II) for RT peak in the 3rd cycle and decrease in the 4th cycles in contrast for the 280°C its increase linear for the direction parallel and shows a peak in the perpendicular direction.*

The behavior of the surface width evolution is similar to the roughness as calculated in the results section. Close relation between the values of the RMS roughness and the surface width is approving the validity of the HHCF analyses. Where in both direction w oscillated in tow peaks with a period of 2 cycles. This similarity between the RMS roughness and surface width w evolution was observed for Si-OH surfaces in the first, fourth cycles. However, in the case of Si-OH, an increase of surface width in the first cycle then decrease continuously till the 4th cycles, i.e. lowest values in fourth cycle 0.19nm. The author analyzed these behaviors as a complete layer formation of the film. The complete growth is related to the number sites of nucleation of -OH group where it is assumed to be 100% covering the surface and then consumed during the four ALD cycles. From another hand, The reactions on the surface are not related to a number of sites nucleation for Si-H. As it was discussed in the previous section, the self-limiting reaction is caused by steric hindrance and is not limited to the number of nucleation sites for the most case of the ALD growth. To compare both surface evolution width on Si-OH and Si-H a recourse to the stationary behavior that can be determined from the ratio $\frac{w_{n+1}}{w_n}$ that describe the growth in the vertical direction of the materials nucleation during the ALD deposition (see Table 4.8)

***Table 4.8*:** *Surface width evolution ration for every cycle for Si(111)-H and SiOH.*

	0-1		**1-2**		**2-3**		**3-4**	
	$[01\bar{1}]$	$[\bar{2}11]$	$[01\bar{1}]$	$[\bar{2}11]$	$[01\bar{1}]$	$[\bar{2}11]$	$[01\bar{1}]$	$[\bar{2}11]$
ALD-RT	9.5	9.5	0.8	0.8	3.6	2.06	0.8	0.65
ALD-280°C	7	6	0.85	0.91	1.66	1.36	1.4	1.8
SiOH	1.27		0.95		0.9		0.95	

The ALD growth assumed to be layer-by-layer or islands agglomeration lead to overlap; this mean that the growth can occur on the free substrate to created layer or on the existent materials that deposited with the previous cycles. The ratio of the surface width from cycle to cycle can be related to the mode growth of its layer by layer so it should be stationary where the growth on high is constant with the cycle. However, for the random islands growth, the ratio is not stationary but strong fluctuation happen between the height of every cycle means that the growth on the materials deposited can occur more than grown on free substrate. Both growth regime, have a different fluctuation of surface width.

Now, the evolution of the surface width ratio during the ALD deposition $\frac{w_{n+1}}{w_n}$, show that the growth in the first cycle is non-stationary for the ALD film on Si(111) , where the width ratio in both direction for both temperature is $\frac{w_1}{w_0} \gg 1$ (see Table 4.8) this means that the growth on the planar surface created highly rough surface regarding to the initial flat Si(111), no duplication of the surface morphology in the terraces regions. This peak of roughness is logical seeing as a consequence of the amorphous materials deposition in the 1st cycle. The selective growth of materials which is basically a result of self-termination reaction over the surface induces this roughness where partial growth was obtained with coverage of fraction of the surface. In comparison with the Si-OH, the deposition was not stationary as well, where the surface width increased from 0.186nm to 0.23nm however the variation in the case of Si-H stepped surface implies higher changes in the roughness in other word higher growth on the vertical position. That mean the materials agglomeration has larger number of nucleation then agglomeration of materials grown on SiOH. This can be consequences of initial roughness . In the case of Si-OH with an initial roughness of 0.186 from islands of Si-OH leading to less nucleation sites that are in the perpendicular direction to the flux of molecules coming. The islands apex are the first one reacted with the TDMAH and H_2O reaching the surface. As results this fraction of substrate is saturated with precursors, then with the rest of cycle the molecules defuse more in the between of islands leading to decrease of the roughness and then the surface widths.

However, in the case of a Si-stepped surface, the plan (111) has an initials roughness of 0.02nm, ideal flat surface, presented an equal probability of nucleation. The initial growth peak of roughness in the first cycle results from ALD i.e. surface coverage 71% for RT and 54 % for 280ºC. In the second cycle, the roughness and surface width decrease to the lowest values in this 4 ALD cycles. In the resulting vacancies from the partial growth are filled up with the materials inducing a reduction of the surface width where the growth is homogeneous and closed layer results after the complete 2nd cycle for both sample Si-H terminated at RT and 280ºC (STM measurement shows this behavior). The ratio of *w* in both samples is near to ~one which means a stationary growth here in transition between the first cycle and 2nd cycle, where the same amount of materials grow in the 1st and 2nd cycles. What this decreasing in the width *w* is assigned to the Layer-By-Layer (LBL) growth characterized by the oscillation of the surface width. This oscillation is seen again for the 3rd and 4th cycles, where agglomeration make higher the roughness (3rd cycle) and then decrease again in the fourth cycle which feet with the ratio of *w*.

4.2.2. 3. Lateral correlation length

The lateral correlation length (ζ) defines the scale of correlated nearest neighbor- heights. Indiscreet process as the ALD, the fluctuation of (ζ) is assigned to the behavior of the molecules growth in the lateral direction in every cycle. The theoretical model of ALD describes the growth in lateral dimension as an increase of the radius of islands r by (Δr) constant with the numbers of cycles predicting a coalescence after n numbers of cycles to formed one layer. However, this description is idealistic car it assume that the growth in lateral position is constant and overcome the growth in the vertical position which lead to overlaps of islands in homogeneous complete layers.

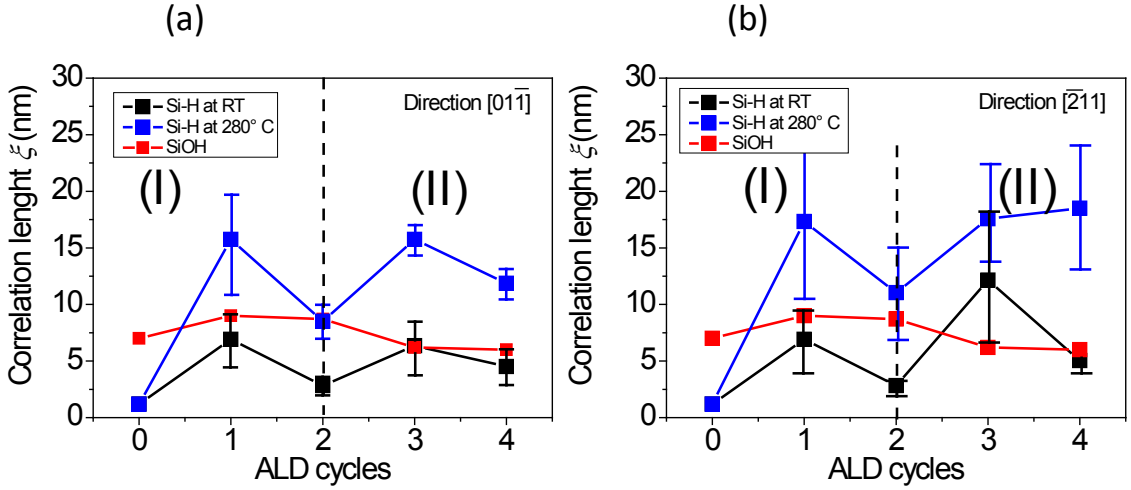

Figure 4.7: *Lateral correlation length (ζ) evolution during ALD for Si-H at RT, Si-H at 280°C and SiOH. (a) Direction parallel to the steps* [01$\bar{1}$] *and (b) in the direction perpendicular to the steps* [$\bar{2}$11].

The simple model of the correlation length evolution describes the growth process in the lateral direction in (1+1) dimension induce the locality of the film growth in the lateral direction. The film can show self-affine surface if the lateral correlation is still invariant during the growth. The deposited materials interact in the range of the length scale ζ leading to the correlation between heights at this distance. However, if molecules diffusion length $D_L < \zeta$, the surface morphology dominating is the wild formation of column height as the model of Grass. This model also predicted that if the diffusion of surface is important, then the surface morphology can be smoother.

- **Film at RT**

The Si-H at RT shows complicated behavior depending on the direction of the surface. From the Figure 4.7, the evolution of the lateral correlation in the first two cycle is similar in both direction however in the 3rd and 4th a dependence on direction result in different values of ζ.

In the first two cycles, the value shows a peak in the 1st cycle and then decrease to a lower value of ζ=0.2nm in the 2nd cycles. The STM results show that islands with similar heights are assembled in a surface fraction with the same morphology, i.e. nano-islands on the steps region and islands assemble on the terraces. The dimension lateral dimension of the nano-islands is in the range of 4-6nm on both region is nearby the lateral correlation length in the first cycles where it is 5.7nm. Then, ζ decrease during the 2nd, where a closed film was obtained. This decrease means that the scale of nearest neighbor height is reduced. As consequence, the growth here in the 2nd cycle would be dominated by front roughness. The first coming precursors chemisorbed and grew on the free substrate area, i.e 71% coverage in first cycle. The full coverage of the surface reduced the mobility of the molecules origin from streic hindrance effect (demonstrated in part 1 of this chapter) which can lead to lower diffusion of the molecules after the growth and leads to grass mode. The moment roughness, Skewness (R_{sk}) and Kurtosis (R_{ku}) are respectively 3.20 and 19.51 which are identify values of surface dominated by height peak.

For 3rd and 4th cycles, ζ is quasi-constant in the direction $[01\bar{1}]$ on 3rd and 4th cycle, the relatively small values of the correlation length implies domination of front roughness on the surface. In contrast in the perpendicular direction, the lateral lengths increase in the 3rd cycle to 12.11nm and decrease with the 4th cycle. Here the direction effect the lateral correlation growth where the coming molecules are more distributed in the direction perpendicular to the steps $[\bar{2}11]$ that means the preferential nucleation for the precursor, in this case, is in the perpendicular direction. This behaviour is coherent with the effect of shadowing results from tall features' confirmed by the HHCF calculation and STM images. The growth velocity of ALD-film, is more important in the vertical direction than in the lateral direction this is because of the short length of molecules that are trapped in the formed strips

because of the shadowing effect. So the coming molecules grow on the top of the formed strips. This result just reflects the end of process, however here the dynamic can be containing tow part. First important diffusion of first molecules coming diffused toward the steps where they agglomerate and then condense, the second part the flux on coming molecules continue on growing there as the diffusion is not possible.

- **Film at 280ºC**

For Si-H at 280ºC, in the direction parallel to the steps the lateral correlation, increase in linear why to reach constant values after the second cycles. That mean, the growth in the second two cycles is important in the lateral direction with constant steps of ~10nm/cycles. These results can be associated to the STM measurement that shows important pin-hole on the film that generated diffusion-limited-aggregations (DLA). The DLA occurs once the molecules are in the range of strong interaction. The large lateral correlation lengths of growing materials found experimentally are due to longer range particle interactions beyond the nearest neighbor interactions. The same behavior is seen in the perpendicular direction, with an exception for the second cycles where the values of ζ decrease to 11.15nm. This decrease in the 3rd cycles can result from non-isotropic distribution of the interactions between molecules in the two directions.

The temperature effect here is clear in the extending of scale length of the nearest neighbor molecules interaction of the deposited HfO_2. The effect of tempearture reside in two effect: Increasing the diffusion lengh pinhole results as consequence. The second effect is the increase of the reactivity not only for the chemispsortion but with the molecules that react a goup of molecules that are alredy bonding with the surface.

The illustration in Figure 4.8 shows the different between the growths of different surfaces. Regarding the results obtained for Si-OH, where the lateral correlation shows a peak only in the first cycle with 9.2 nm and then reduced to 6 nm in the 4th cycle, the author relies on this behavior as an indication of the closure of the first HfO_2 layer. The similar surface width and correlation length after the 4th cycle indicate that the HfO_2 surface is a replica of the starting SiOH substrate as is expected from ideal ALD process, where conformal grow this obtained. The initial roughness of both substrate Si(111) and Si-OH display two morphology different where the Si-OH morphology can be responsible on the reduction of the surface diffusion then the chemisorptions is stronger. In contrast, the planar Si(111)-H obey to competition between the chemisorptions activated with ALD window temperature and the free diffusion of molecules unreacted on surface.

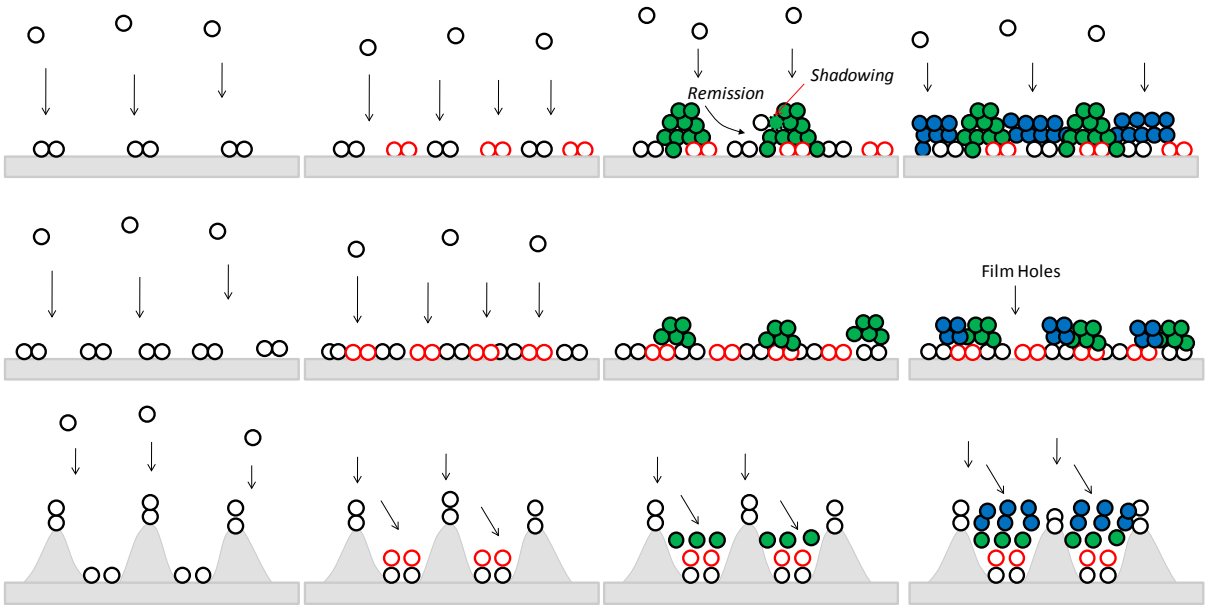

Figure 4.8: *Illustration of the film growth in relation with the w and ζ .(a) and (b) the growth on Si(111)-H at RT and 280°C and (c) of SiOH. The illustration shows that the evolution of the width and lateral scale depend on the initial roughness and the locality of the growth.*

4.2.3. Dynamics exponent

The dynamic part of the growth can be determined, from the evolution of surface width and lateral correlation (ζ) as the power of thickness *t*, i.e. $w \sim t^{\beta}$ and $\zeta \sim t^{1/z}$, where β are 1/z are the dynamic exponent of the growth (see chapter 1). β are 1/z are respectively the slope of the surface width and the lateral correlation.

Two kind of process can occur, the local mode where the rate of the growth depends on the local properties of the surface so only on the local interaction between the molecules in local regions. The second model of growth is the non-local growth if the rate of deposition is not affected by the surface morphology properties, however, the grown film its self can lead to non-local effects, such as the shadowing effect or important surface diffusion (see chapter 1). The universal values of β are defined in the interval of [0,1] for different techniques of deposition such as CVD, sputtering, and MBE. For local growth, β values mostly exist in the interval $[0, 0.25]$, for these small values of β the dynamic of the growth is leading to the smoothing effect of the surfaces. As consequence $w \sim t^{\beta}$ characters a decrease of the height of profile in front of increasing of thickness. However for $\beta \in [\,0.25, 1]$, the

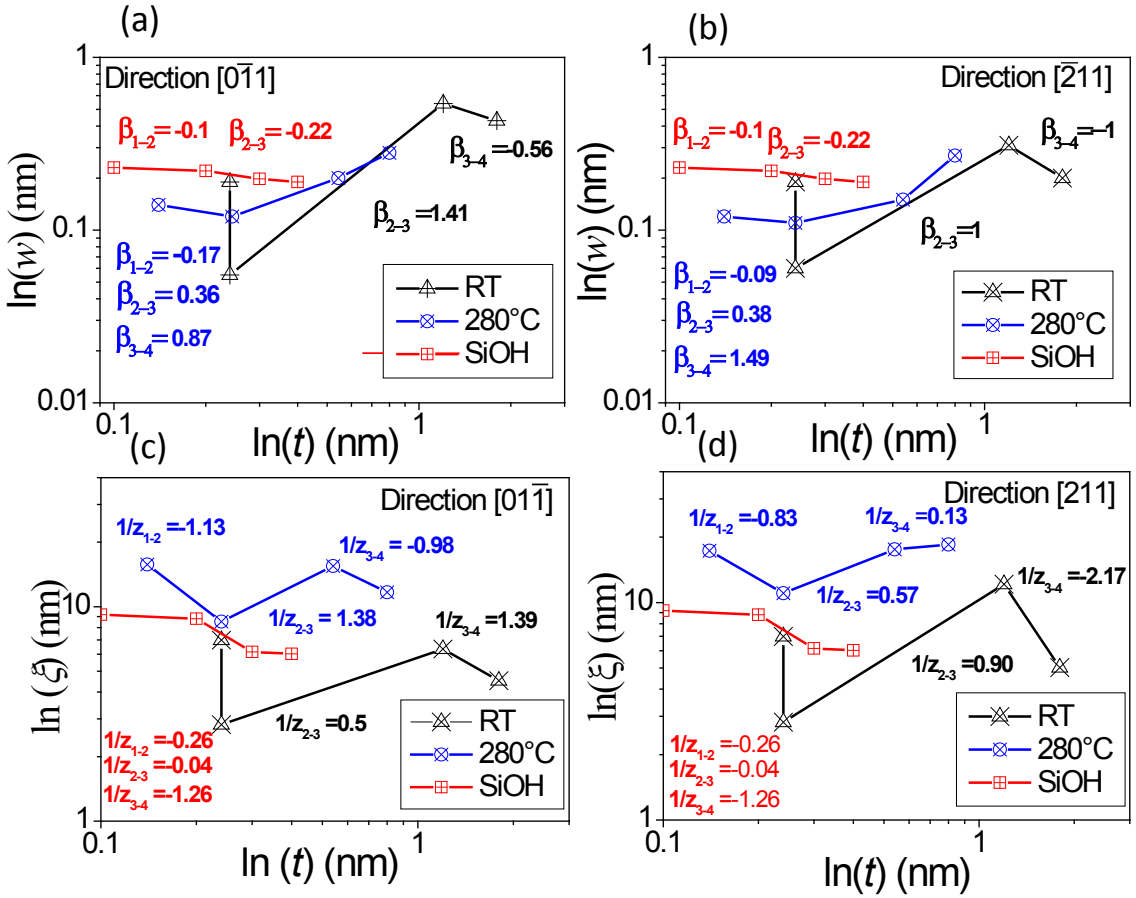

Figure 4.9. *(a) and (b) plot log-log of Surface width (Ln(w)) evolution during ALD in function of film thickness(Ln(t)) respectively for Si-H at R(black line)T, at 280°C (blue line) and SOH (red line). (a) The direction parallel to the steps* [$01\bar{1}$] *and (b) in the direction perpendicular to the steps* [$\bar{2}11$]. *(c) and (d) plot log-log of of Lateral correlation length (Ln(w)) evolution during ALD in function of film thickness for Si-H at RT, at 280°C and SiOH. (c) in the direction parallel to the steps* [$01\bar{1}$] *and (d) in the direction perpendicular to the steps* [$\bar{2}11$].

surface is rougher with an increase of the *w* with the thickness, e.g. β=1, so *w* ~ t, the dynamic of the growth on the height is then lead to non-local growth [145-150].

Fluctuation of roughness dynamic exponent β obtained for each cycle of ALD films for SiOH and Si-H in both directions are shown in Figure (4.9). β is the slope of the curves versus the cycle number listed in Table (4.9).

Table 4.9**:** *Roughness exponent β for the film growth dynamic for every cycle on Si(111)-H and SiOH*

	0-1		**1-2**		**2-3**		**3-4**	
	$[01\bar{1}]$	$[\bar{2}11]$	$[01\bar{1}]$	$[\bar{2}11]$	$[01\bar{1}]$	$[\bar{2}11]$	$[01\bar{1}]$	$[\bar{2}11]$
ALD-RT	1.1	1.1	0.32	0.32	1	1.4	0.56	1
ALD-280°C	0.57	0.57	0.17	0.09	0.36	0.38	0.87	1.49
Si-OH	0.44		-0.10		-0.22		-0.01	

SiOH and Si-H at 280°C, display a fluctuation of the value β between local model and non-local model of growth, in contrasts the values of ALD-RT are all located in the range of non-local growth. This reveals that the dynamic behavior is complicated and characterized by discrete growth that occurs different dynamic for every cycle for all ALD-HfO_2 films. This non-continuity of β values with the number of cycles is referred to the discrete characteristic of ALD growth dynamic.

The 1st cycles for SiOH and Si(111)-H have the values β for non-local growth. In this cycle, the non-stationary growth means that the *w* obtained from materials growth are not affected by the properties of the surface, no steps effect that can change the growth behavior, i.e. no steps decoration. So it can be concluded that the growth in a vertical direction related to the molecules deposited on the surfaces without respect to the initial substrate crystallinity or chemistry.

In the second cycle, the surface *w* decrease and stationary evolution occur with the closest of the first layer of ALD-film growth. The growth in this cycle on SiOH and Si-H at 280ºC are local growth model that means the molecules are coming on the surface preferred grown in preferential sites that are depending on the amorphous materials deposited. The partially grown materials in the first cycle change the interface morphology and chemistry by created new energetic surface and the self-termination reaction probably prohibited the growth of materials on the existent materials. This local effect leads to an effect on the surface widths evolution.

In the 3rd cycle, RT film displays an interesting behavior, where STM results show condensed materials agglomeration of molecules in strips in the perpendicular direction of the steps. The HHCF evolution for this film results as a mounded surface which by definition origin of the local effect. Then normally β should be in the range of the local model. But it has been shown that in the 3rd half deposition where only TDMAH has deposited already the stripes was formed this growth lead to a non-local effect by the growth of taller feature of TDMAH that results in shadowing effect for the flux of molecules defused on the surface during the deposition of materials. Therefore the first coming

molecules were condensed in that nucleation's sites but generated a non-local -effect of showing leading with the time of deposition (1.5s) to contentious agglomeration just in that region. The question here can be why they just agglomerated in the region near to the steps? The answer can be related to the previous section, where it was demonstrated by Puurunen model, that the growth in steps region could be attributed to ALD growth then the fraction of surface resulting from the first two cycle is more ideal for contentious growth as it has an interfacial ALD of 0.24nm. Also about the activation energy for the chemisorptions is weak and as it's predicted by ALD in the temperature out of ALD-window materials dense and physisorbed on the surfaces.

The ALD at 280ºC has the same behaviors of β fluctuation in this cycle. The growth is not -local means that the dynamic of the film is not affected by the surface morphology. The role here of the temperature is to make the higher distribution of the molecules, so the competition between the chemisorptions and diffusion lead to non-effect of substrate morphology.

In the 4th cycle the values of Si-H decrease for lowest values, however, the dependence of the dynamic on the surface direction is obtained in this cycle. Non local mode in the direction $[01\bar{1}]$, and local for $[\bar{2}11]$. The competition between the shadowing effect and the random deposition took place in the fourth cycle and lead to higher effect of the showing in the parallel direction. That's why for ALD-RT STM deliver a growth of more strips in the 4th half cycle of TDMAH and then with the oxidation the distribution of strips become more closed in the direction parallel to the steps . In the case of ALD-280ºC STM also shows the formation of important holes in the film are more arranged in the terraces this effect generated a local effect of the growth. In the steps direction, the local mode takes over with means that in this direction no effect of the steps. Those result also fit with the HHCF. For SiOH, the first values are not about the same average, and this is a result of the initial surface morphology, where the surface width initial is 0.18nm higher the film thickness for the first cycle deposition which is 0.1nm, so β is negative.

4.2.4. Growth models

From HHCF calculation it was obvious that ALD film growth on Si(111)-H manifested complicated dynamic growth behavior. The evolution behavior of the film investigated troughs $w \sim t^{\beta}$ and $\zeta \sim t^{1/Z}$ and m as a function of w and ζ describe the film morphology of ALD growth. It was also shown that the growth roughness depends on local properties of the surface, e.g. steps edges. Roughness scaling parameters belonged to the solid-solid approximation growth for dimension d=1+1 of self-affine and mounded surface are the results of the non-equilibrium growth that is related to local effects (steps), or the locality effect on the growth generated by the relaxation mechanism.

The solid-solid model of growth is based on the equation belongs to the class of contentious growth. The stochastic equation describe this kind of growth is known as Langevin- Equation. These models are often able to predict values for the exponents α, β, and z, defining universality classes.

$$\frac{\partial h(r)}{\partial t} = \Phi(r) + \eta(r)$$

η is the noise in the system, and Φ is a function of the height profile which reflects the growth process. The evolution of the profile with time defines the dynamic growth residue on the behavior of Φ(r). This function is the key to the dynamic growth and contains information about the non-local, and local effect, all the models of growth, discussed this function in relation to the non-local effect of the growth. The combination of all the roughness scaling parameters leads to distinguish the dynamic equation of the surface growth. Here we discuss cycle-by-cycle the model of growth (relative equation) and the relative model that can attribute to each cycle from the exponent α,β, and 1/z.

Some experimental suggested that that roughness exponent can be overestimated especially in the beginning of the growth of any process. As a consequence, the model below attributed to the different values obtained in our measurement would be discussed in analogy with the STM results

4.2.4.1. HfO_2 at RT

The combination of all roughness exponents (see Table 4.10) of the HfO_2 film growth cycle unveils a discontinuity of the dynamics behaviors from cycle to cycle. According to discreet ALD process, every cycle can be treated. The values in the two directions of roughness exponent are almost equal. The model that can describe this saturation in height is the random deposition, where it consists of saturation amount of materials which is the case of ALD. However the height should be similar and do not fluctuated through the film. So if there is a diffusion of molecules over the substrate from a random deposition model a term of noise should be added to the growth dynamic. All these combinations are fulfilling for all the cycles growth of HfO_2 at RT.

4.10: *Different values of the scaling dynamic and roughness of the ALD-film formed during the ALD cycles on Si-H at RT.*

Scaling exponent	0-1	1-2	2-3	3-4
α	0.61 / 0.61	0.37 / 0.37	0.4 / 0.35	0.75 / 0.62
β	0.73 / 0.73	0.32/0.31	1.41 / 1	0.56/ 1
1/z	0.8/0.8	0.22/0.22	0.5/1.39	0.9 / 2.17
Growth model	Random deposition	Mullins Diffusion	KPZ	-
α	**0.5**	**0.5**	**0.5**	**0.5**
β	**0.5**	**0. 5**	**0.33**	**0.5**
1/Z	**0.5**	**0.25**	**0.66**	**0.25**

- **First cycle**

The self-limiting of the growth discussed with Purruenen model shows that the GPC in the region near to the steps has the height that fit with the growth of HfO_2 in contrast GPC in the terraces is higher. The difference in height by region can be resulting from diffusion of molecules to agglomerate on the terraces. Now the roughness exponent values in this 1st cycle the nearest universal values are a solution of Edwards - Wilkinson (ED) equation of growth [78]. Where the film grows from the random deposition of materials but include the diffusion of molecules reaching the surface that can lead changes in the height of the nearest neighborhood by relaxation effect. This is why in this first cycle for the ALD on Si-H at RT height in the steps region differs from the height on the terraces. In the steps region, relaxation as chemisorptions can be resulting from the self-limiting process lead to nano-islands of HfO_2-ALD growth with 0.24nm in vertical direction and 4nm in the lateral direction. In the terraces region, the free diffusion of molecules over the surface can be the taller height and lead to a condensation of materials. The local slope m also calculated from the first cycles has very low values which are related to the geometry of the nearest correlated heights.

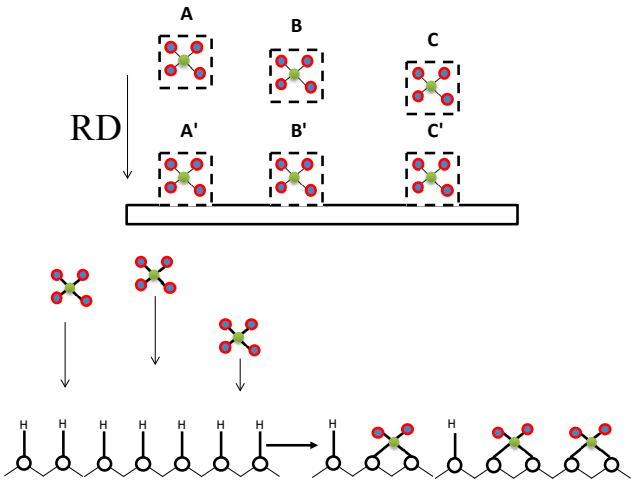

Figure 4.10: *Illustration of the random deposition model of growth where each molecule is deposited in a random place on the surface, occupying the position immediately above the surface at the site by chemisorptions reactions.*

- **Second cycle**

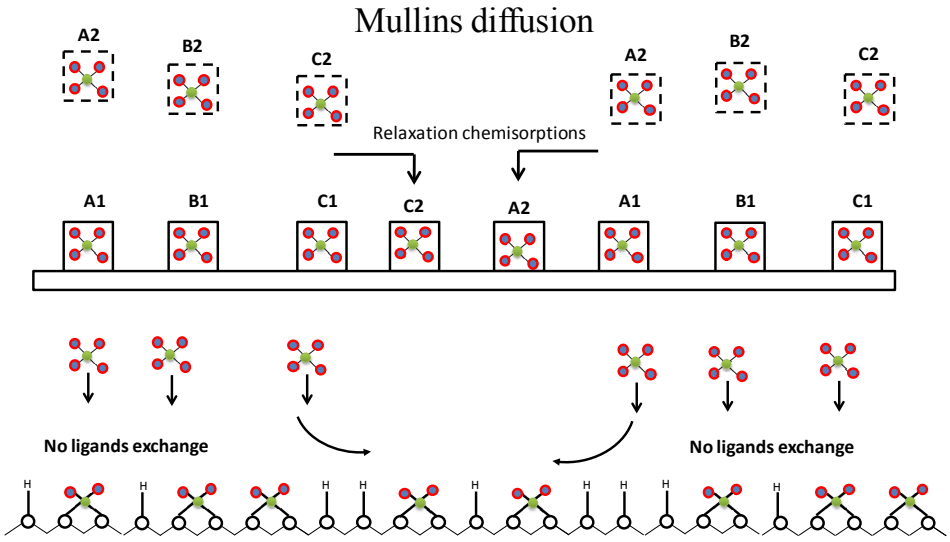

Figure 4.11: *Illustration of the growth model in the 2nd cycle. Random deposition on direct sites, do not lead to chemisorptions, so the flux of molecules converges to reduce the difference in height over the surfaces. With relaxation effect, the substrate free from the first cycle reacted with the molecules to grow complete layer in the 2nd cycle.*

The growth model is illustrated in the Figure (4.11) of the dynamic growth of molecules in the 2nd cycle. In the second cycle, the layer is closed where all parameters of the roughness decrease to short

scales, global roughness, surface width, lateral correlation. So that the reaction over the surface and the dynamic of the flux of molecules coming on the surface behavior in the direction of smoothing the surface. This effect off smoothing is directly driven from the install morphology in the first cycle. One good reason for this behavior can be the surface energy that can be changed after the deposition of the first partial layer then the global surface energies converge to be reduced within the second cycles. A dynamic model that can describe this growth would be a resolution of Mullins Diffusion Equation [151-152]. This model consist of surface diffusion with conservation of a total number of molecules on the surface this dynamic lead to increasing the height h(x) in an x position that has initial lower vertical height [153-154].

$$\frac{\partial h(x)}{\partial T} = -k\nabla^4 h + \eta \tag{4.5}$$

- **Third cycle**

In the third cycle roughness, exponent α has a near values to the second cycle with means that the noise growth is keeping important for the film grown, however, values from β and Z changes dramatically which are related to related to competition between the growth in lateral and vertical position. This competition is the origin of nonlinear growth resides in an important surface diffusions stopped in the region of steps leading to mounded surface as it was determined from HHCF. STM results shows the growth of important nucleation features in the 3rd cycle of islands arranged in stripes. This kind of growth is theoretically predicted for inhibited-surfaces, where the precursors diffuse to the defect of surface where it nucleated.

The dynamic exponent for this cycle doesn't fit exactly with universal values for the growth equation. However the values of β is higher than 1 in this case. That means important diffusion happen of the molecules over the surface leading to the h(x) at the different region. Some numerical approach in the investigation of the relation between β and the sticking coefficient S_0 , that for higher β the sticking coefficient increases. Accordingly the molecules can't stick on the surface so it diffuse as it was observed in the STM measuring. The non-sticking can be cause by the surface saturation of the reaction or sufficient energy for the reaction activation.

by the of The model of growth that can be concluded from the roughness values is the nonlinear differential Equation of Lai-Das Sarma [155], where the equation of the growth is

$$\frac{\partial h(x)}{\partial T} = -k\nabla^4 h + \frac{\lambda}{2}\nabla^2|\nabla h|^2 + \eta \tag{4.6}$$

The term $\frac{\lambda}{2}\nabla^2|\nabla h|^2$ is associated to effect of mounded surface structure the distance between two lateral correlations. It seems that the molecules coming on the surface immigrated in the direction of the steps flows, as it was discussed with Puurunen model this stripes formed do not fulfill the ALD criteria then a physisorption is mostly the reaction that happen over the surface. mean an immigration happened of the molecules initially site on the surface but with the coming flux of molecules as this model was described in the section, the growth obey to fourth-order conserved growth nonlinearities by the term $-k\nabla^4 h$ .This means that the dynamic of molecules on the surface are the value of β is presenting an anomalous in the scaling, where the universal values is β= 0.25

The ballistic deposition is the simplest model that presents porosity. This model also includes correlation between more distant neighbors; the particles are deposited randomly on the surface and are correlated with any site that presents the first contact with the interface. That condition enables the formation of voids, or porosity, inducing a porous structure in the film during its formation because the interface can also grow tangentially to the surface of the initial substrate. The roughness evolves, after an initial time t_x, to saturation, and in this model, the growth exponents are α ≈0:50 and β ≈0:33 for the one-dimensional condition, $d = 1$. The parameter d represents the dimension of the surface. The stochastic differential equation which represents the growth of the film for the BM is the equation developed by Kardar, Parisi, and Zhang (KPZ) [156].

In the Figure 4.12, the model of the growth in relation with the KPZ equation and the STM observation that display the growth of tall stripes in the 3rd cycles that lead to an important increase in the local slope which is a prove of high surface diffusion as m~$\sqrt{T}$.

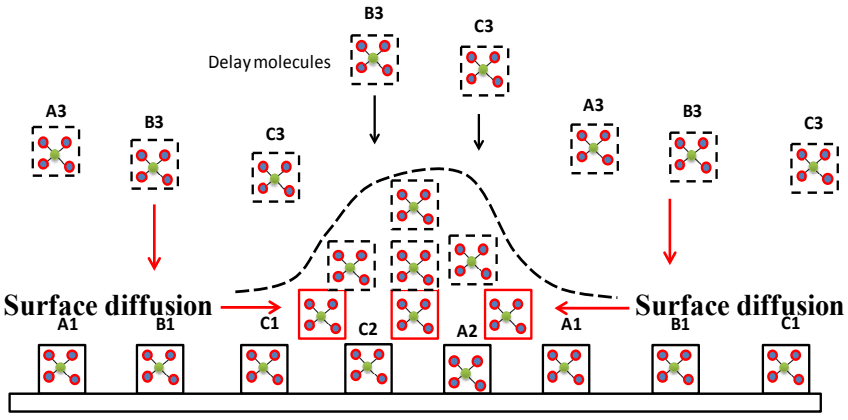

Figure 4.12: *Illustration of the surface diffusion in the 3rd cycles from the coming molecules that do not react and absorbed on the surface, so surface diffusion is dominating the surface. The local slope increases in this cycle to high values with implies the important surface*

width and lateral correlation happened from important feature created. The term $\frac{\lambda}{2}\nabla^2|\nabla h|^2$ *of KPZ model is non linear term of the condensation of the materials on tall feature, non- equilibrium model.*

- **Fourth cycle**

The fourth cycle display the same behavior as the second cycle where the molecules growth mostly in the vaccines on the surface leading to smoothing effect, that why the roughness exponent α

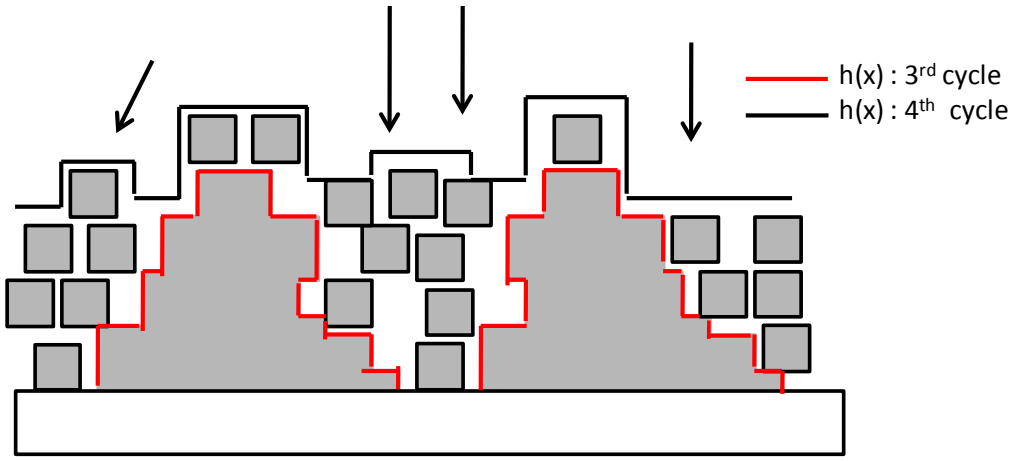

Figure 4.13*: Illustration of Mullins diffusion model for the 4th cycle. The flux of molecules coming on the surface diffuses and grows in the film vacancies to changes the height to be correlated at a lower scale.*

The dynamic of the film growth, as in the second cycles, increase to reduce the uncorrelated heights over the surface. The growth of strips and tall features in the 3rd cycles changes the morphology in dramatical ways. So that the coming flux of molecules is reduced in mobility and diffuse in the lower energy sites that are basically in the bottom of the strips. So the growth on the height is reduced, and the film width decreases versus the thickness of the film, β=0.26 in the direction perpendicular to the steps and so the surface is smoother in this direction , however the dynamic exponent in the parallel direction is β=0.6 which mean that the growth is more affecting the reduction of height in the perpendicular direction to the steps..

4.2.4.2. HfO_2 at 280ºC

Table 4.11: *Different values of the scaling dynamic roughness of the ALD-film formed during the ALD cycles on Si-H at 280°C.*

Scaling parameter	0-1	1-2	2-3	3-4
α	0.35/ 0.48	0.44/ 0.55	0.4 / 0.6	0.48/ 0.61
β	0.57/ 0.57	0.17/ 0.09	0.36/ 0.38	0.87/ 1.49
1/z	0.27/ 0.24	1.13/ 0.83	1.38/0.57	0.9/ 0.13
Growth model	Random deposition	Random deposition + Mullins Diffusion	Random deposition	Random deposition
α	0.5	0.5	0.5	0.5
β	0.5	0.25	0.5	0.5
1/z	0.5	0.5	0.5	0.5

The different values obtained for the growth of HfO_2 on the Si(111)-H are associated to the growth model from the equations describing the random deposition and the Mullins diffusion. The comparison with this model are based not only on the exact values but also on the STM measurement of the films.

- **First cycle**

In the first cycle the roughness increase in relation to the materials deposited on the surface accompanied by partial layer growth leading to the formation of islands with height 0.1-0.14nm. The nucleation is random where no arranged structure of islands-assemble is observed with STM measurement. With the very small local slope that varies as m~$\sqrt{t}$, mean no important diffusion of the molecules reaching the surfaces. The exact value of the RD model are α=0.5 and β= 0.25.

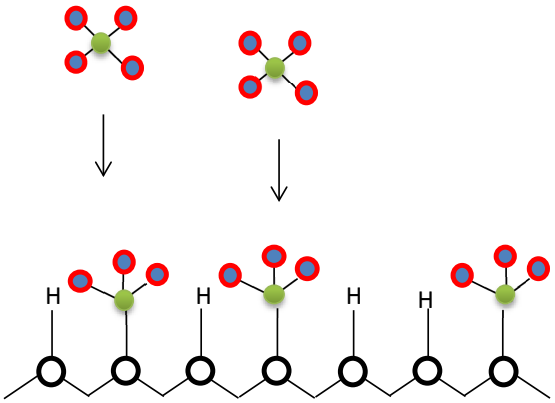

Figure 4.15: *Illustration of the random deposition model of growth where each molecule is deposited in a random place on the surface, occupying the position immediately above the surface at the site by chemisorptions reactions.*

That exponent varies in both direction but in the same range of values can be related to the same dynamic growth. As we showed in the previous section, the growth is local and then regarding the values obtained the equation that can be assumed that there is a competition of growth dynamic. As a relatively a fluctuation of the roughness exponent values completion between the two direction Edwards-Wilkinson equation (EW):

$$\frac{\partial h(x)}{\partial T} = -k\nabla^2 h + \eta \tag{4.6}$$

where the Laplacian term in the EW equation is referred to as the surface relaxation term, because the effect of the Laplacian is to smooth the surface profile while keeping the mean height unchanged.

- **Second cycle**

Mullins Diffusion Equation This model consist of surface diffusion with conservation of a total number of molecules on the surface this dynamic lead to increasing the height h(x) in an x position that has initial lower vertical height. The equation is: $\frac{\partial h(x)}{\partial T} = -k\nabla^4 h + \eta$

Macroscopic current of particles on the surface, represented by the vector **j**(**x**, t). Because diffusion conserves the total number of particles on the surface, **j**(**x**, t) must satisfy the continuity relation

$$\frac{\partial h(x)}{\partial T} = -\nabla \mathrm{J(x)} = -k\nabla^4 h + \eta$$

The surface current **j**(**x**) is related to the gradient of the chemical potential, $\nabla j(x) \propto -\boldsymbol{\nabla\mu}(x)$, because the surface current will flow from areas of higher potential to areas of lower potential. Also, the chemical potential μ(**x**, t) is related to the number of bonds that must be broken by an atom to diffuse.

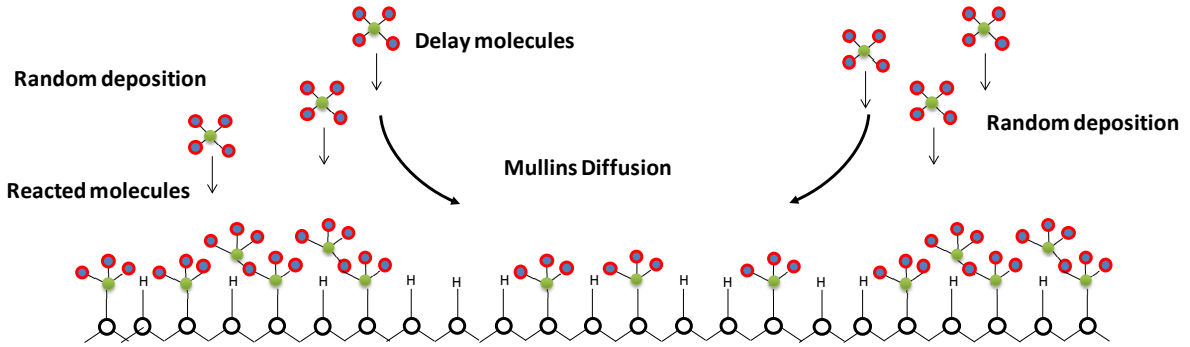

Figure 4.16: *Illustration of the growth model in the 2nd cycle. Random deposition on direct sites, do not lead to chemisorptions, so the flux of molecules converges to reduce the difference in height over the surfaces. With relaxation effect, the substrate free from the first cycle reacted with the molecules to grow complete layer in the 2nd cycle.*

- **Third and fourth cycle**

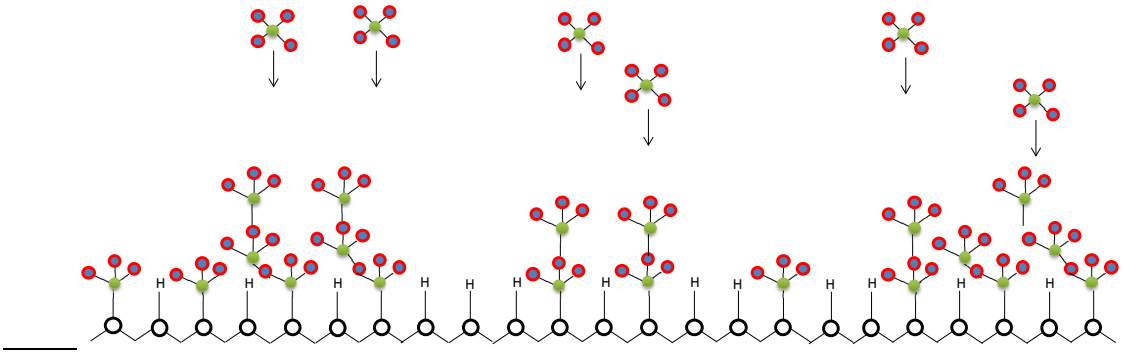

Figure 4.17: *Random deposition model by deposited molecules on reactive sites that are limited by the steric hindrance effect. This random deposition leads to the rough surface.*

In the 3rd and 4th cycle the growth is can be model as growth random deposition , the surface width and the roughness increases in those two cycle and are higher than the second cycle which is assumed as closed film layer. Like this the flux of molecules coming on the surface are randomly deposited but with saturation of height. The bonds are assumed to be one ligand-exchanged in every cycle (3rd and 4th).

- **Conclusion**

The height-height correlation function (HHCF) display an evolution of self-affine surface isotropic in the first and second cycle. The surface statistics ζ and *w* are described a stationary evolution of the film dimension (in height and lateral directions) during the deposition, which is an important result proving that the growth in the first two cycle obeys to the same dynamic independent on the temperature. The values obtained of the dynamic scaling exponent β and 1/z for the first two cycle are

near to the universal values of Mullins Diffusion model where the molecules current reaching the surface diffuse with the conservation of the total number of molecules by the equilibration between the high potential sites and lower potential sites. Since Si(111) stepped surface to present a homogeneous potential on the terraces but also, molecules filled and cover the surface in a homogenous way. After the close of the film layer in the second cycle, the nucleation is not occurring anymore for the growth at RT leading to high surface diffusion. In contrast the growth at 280°C have the same dynamic of random deposition growth. The temperature then leads to activation of the chemisorptions reaction and at lower temperature the molecules do not chemisorbed and diffuse toward the steps. The comparison of our finding to the growth on Si-OH, proved that with the presence of OH group the dynamic of the film is random deposition growth because the molecules reaching the surface reacted with the OH group through direct chemisorption so no diffusion occurs.

4.3. Al_2O_3 on HOPG and Ag-HOPG

Graphene is an ideal inhibited- surface for ALD growth. The graphene surface inertia hinders the conformal nucleation of the precursors, inducing a rough, non-uniform, and non-conformal film growth. Here we examined the growth of the Al_2O_3 on the HOPG surface as an ideal inhabited substrate for ALD. The theoretical assumptions about the ALD growth on an inhibited substrate predict the diffusion of the precursors in the absence of chemisorptions adsorption. The precursors then nucleated on the defects in islands. With the deposition of materials, the growth occurs on the previous materials sites grown on defects and then toward the different direction of the surface with the deposition of ALD in every cycle.

From the results, the terrace widths show an effect on the ALD film growth behavior. The GPC varies from large terraces to small ones. Here the type of HOPG and Ag-HOPG inhibited-surfaces would be discussed, i.e. growth type 1 or 2, for large and small terraces. The stepped surface is known for barrier on the edges of the steps. Also, a model explaining the growth behavior in correlation with the terraces width and steps barrier effect would be introduced.

4.3.1. Nucleation on HOPG and Ag-HOPG

As it was mentioned before, the cleaving of the HOPG surface created inert steps with different widths of the terraces. The definition of large terraces and small terraces are referred to the diffusion length of precursors. The ALD process consists of the first pulse of TMA and then H_2O, so first precursors TMA reaching the surface diffuses on the surface and nucleated. The H_2O coming up react on the same sites of TMA nucleation, assuming that the H_2O do not react in other sites other then

TMA ones. A.D. Gates and L.Robins [155] described that the atom/molecules deposition on steeped surfaces depend on the terraces width by the relation

$I = R \times W$

Where (I) is the island's number, (R) the arrival rate of deposited atoms at the surface and (W) the width of the terraces. For ALD the amount of materials deposited is fixed by the pulsing time of the precurors .Therefore the rate (R) is fixed for different terraces, so like that the relation between the numbers of islands formed is affected only by the width of the terraces. The formation of the islands depends on the terraces width by $W \propto 2 \times \lambda$, where λ is the diffusion length of the molecules.

At RT, Al has adsorption energy (Ea) on HOPG of 0.8 eV and diffusion energy (Ed) of 0.02 eV, respectively, determined by Ganz and by Moullet [156]. This energy difference leads to a diffusion length of 170 ± 80nm. We define large terraces (LT) for W > 340± 160nm ($2 \times \lambda$) and small terraces with W < 340nm± 160nm. The different statistics of film nucleated are summarized for large and small terraces.

Table 4.12: *Summary of the different statistics of the TMA and H_2O ALD-RT on HOPG.*

	Cycles	***Cluster height*** **(nm)**	***Cluster size*** **(nm^2)**	***Nano-stripes*** **width (nm)**	***Nano-stripes*** **Height (nm)**	***RMS Roughness*** ***(nm)***
HOPG-Large terraces	*1st cycle*	*1*	*5*	*5.2*	*0.3*	*0.25*
	3rd cycle	*0.4-1.2*	*30-50*	*-*	*-*	*0.7*
	5th cycle	*3-6*	*70-180*	*-*	*-*	*0.8*
HOPG-Small terraces	*1st cycle*	*-*	*-*	*5.2*	*0.3*	*0.25*
	3rd cycle	*0.3-0.6*	*10-40*	*-*	*-*	*0.3*
	5th cycle	*0.2*	*4.5*	*-*	*-*	*0.2*

Table 4.13: *Summary of the different statistics of the TMA and H_2O ALD-RT on Ag-HOPG.*

Sample	***Cycles***	***Cluster height*** **(nm)**	***Cluster size*** **(nm^2)**	***Stripes-edge*** **width (nm)**	***Stripes*-edge** **height (nm)**	***RMS Roughness*** **(nm)**
Ag-HOPG	*1st cycle*	*-*	*-*	*10-30*	*0.1*	*-*
	3rd cycle	*0.3*	*20-50*	*-*	*-*	*0.2*

	5th cycle	*0.4-0.6*	*25*	-	-	*0.23*

4.2.1. 1. Growth-per-cycle (GPC): Inhibited substrate types

The growths of the film depend on the surface morphology. The terraces widths, steps and Ag-clusters on steps are parameters of the surface morphology. An important dependence of ALD selectivity is observed where the ALD nucleation parameters changes with the changes of surfaces parameters. The GPC parameters of ALD film can define the substrate type from HOPG to Ag-HOPG.

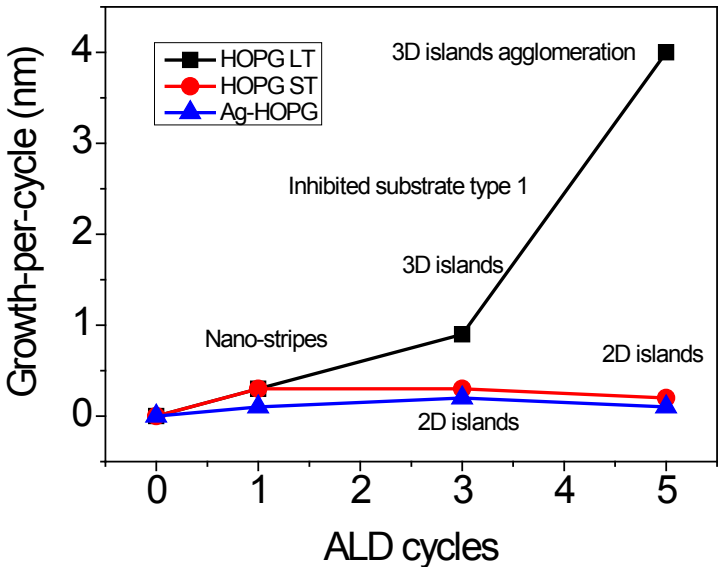

Figure 4.18: *The growth per cycle for Al_2O_3 on HOPG large and small terraces and Ag-HOPG. The growth on small terraces HOPG and Ag-HOPG behavior as inhibited substrate type 1 and the growth on large HOPG terraces is inhibited type 2.*

In Figure 4.18, the curves of the GPC evolution with the numbers of cycles is calculated for large and small terraces of HOPG and also for Ag-HOPG. The determination of the growth per cycle for large terraces is increasing with the number of cycles. It started with 0.3nm which is about 1ML height of Al_2O_3 in the 1st cycle where the GPC in the three systems is similar. However the nucleation feature changes dramatically from HOPG to Ag-HOPG. On HOPG, the Al_2O_3 was conformally deposited with homogeneous coverage of ~ 90% of the observed surface area. The grown films observed in this first cycle are nano stripes with 6nm width and ~0.35nm of height. This morphology of the deposited film is not identical to the case of inhibited substrate where in such case the precursor should diffuse

toward the defect leading to islands formation. However, in these cases, no islands formed on the steps and also this structure is a pattern in the same way over the terraces large and small ones.

On large terraces in the 3rd cycle, the growth heights reach 1.2nm results from formation of 3D islands, i.e. GPC is 0.85nm. This high is important regarding the theoretical height of Al_2O_3 for 3 cycles which is about 0.36nm, i.e. 3 ALD cycles. Almost 3 ML are formed in 3D islands.However, the surface coverage by the film decreased. The density of nucleation is important in the steps region and over the terraces. The nucleation sites are concentrated in two zones: On steps edges (bottom and top) and in the area of 100nm distance apart from the steps (see Figure 3.27). In the 5th cycle higher islands formed again, however, the density of islands become lower and the coverage of the surface lower islands distribution reach < 18 % of the observed surface. The RMS roughness is 1.8nm due to the height of those islands which becomes much larger (3nm- 5nm). Therefore, those values indicate that the growth is no longer ALD model-like. The widths of islands increases from 40nm to 120nm this is a result of diffusion of molecules through the surface without any reaction and stopped on the formed islands.
The GPC is increasing with the deposition of materials tell the 5th cycle, where it reached ~4nm. This value of GPC was observed for other ALD system of inhibited surface type 2 where the growth increases in the initial regime of the growth with the number of cycle to reach then a maximum in the transition regime. The dimension of the formed islands is increasing in the width and the height so with the deposition the materials growth on the surface by 3ML and 10ML respectively in the 3rd and 5th cycles where high diffusions leads to higher nucleation. That means the islands can overlap at some number of ALD cycles but the problem is the film is not possible to control as the ALD ideal growth can be.

The growth on small terraces of HOPG and Ag-HOPG the GPC has another curve shape. Starting from 0.35nm in the 1st cycle for HOPG then decreases for 3rd and 5th cyles. The islands formed are 2D on the bottom and top of the terraces (see Figure) in the 3rd cycle. Again in the 5th cycle, the growth per cycle is decreasing to 0.2nm where nano-islands are formed in the terraces with less than 10% of surface coverage. The reduction of the GPC is non important regarding the ratio of the materials deposited. This GPC can be considered as constant for 3rd and 5th cycles, which means that the growth in the initial stage of ALD increases in the first cycle because of the surface diffusion to the steppes and then with the ALD cycle the materials diffuse and grow in the existent materials but with constant amount. The growth on the small terraces can be associated to the inhibited ALD growth surface type 1.

The growth of the Ag-HOPG substrate is typical a growth on inhibited substrate type 1. The materials deposited diffuse in the first cycle to nucleate on the steps edges, i.e. Ag islands. No nucleation is

observed in other part of the terraces which makes the growth conformal just on the edges of the steps. The steps are then decorated with the precursors and fill the vacancies between the Ag islands. Within the the 3rd cycles, molecules diffuse to the steps edges but reacted with the materials deposited.

4.3. 2. Steps barrier and terraces width effect on the ALD

In the previous paragraph it was shown that the growth per cycle differs with the widths of terraces and the steps region. Recently, Aleix et al. [157] calculated the energy barrier of the HOPG steps in terms of current on the steps, where a 10 times higher current on the steps in comparison to the current on the terraces was found. Thus, high barriers at short distances can have important effective gradients which can lead to lower material deposition rate and 2D structure and nano-islands features.

- **Al_2O_3 on HOPG**

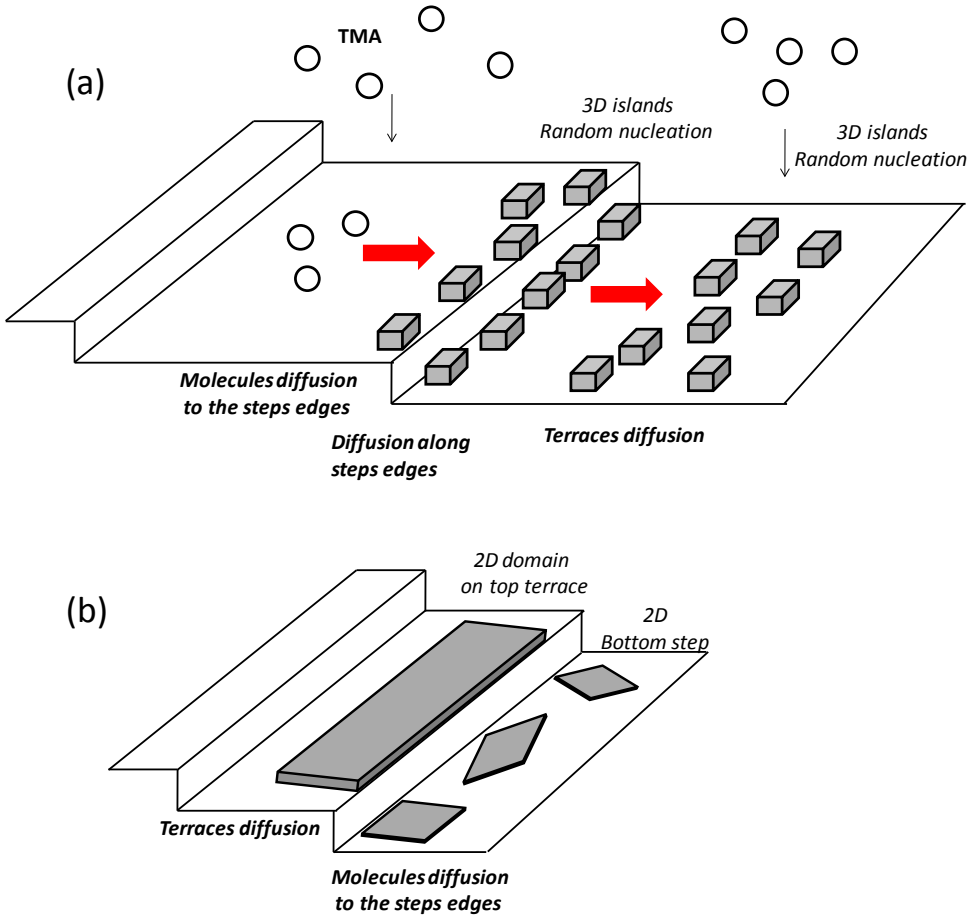

Figure 4.19: *Illustration of the growth on large terraces and small terraces. (a) On large terraces the nucleation occurs on the steps edges randomly and nucleated also in distance from the steps on the bulk of the terraces. (b) On small terraces the growth on the top terraces occur in 2D domain starting from the steps toward the bulk of terrace and the growth on bottom of the terraces of 2D structures.*

- **Al_2O_3 on HOPG**

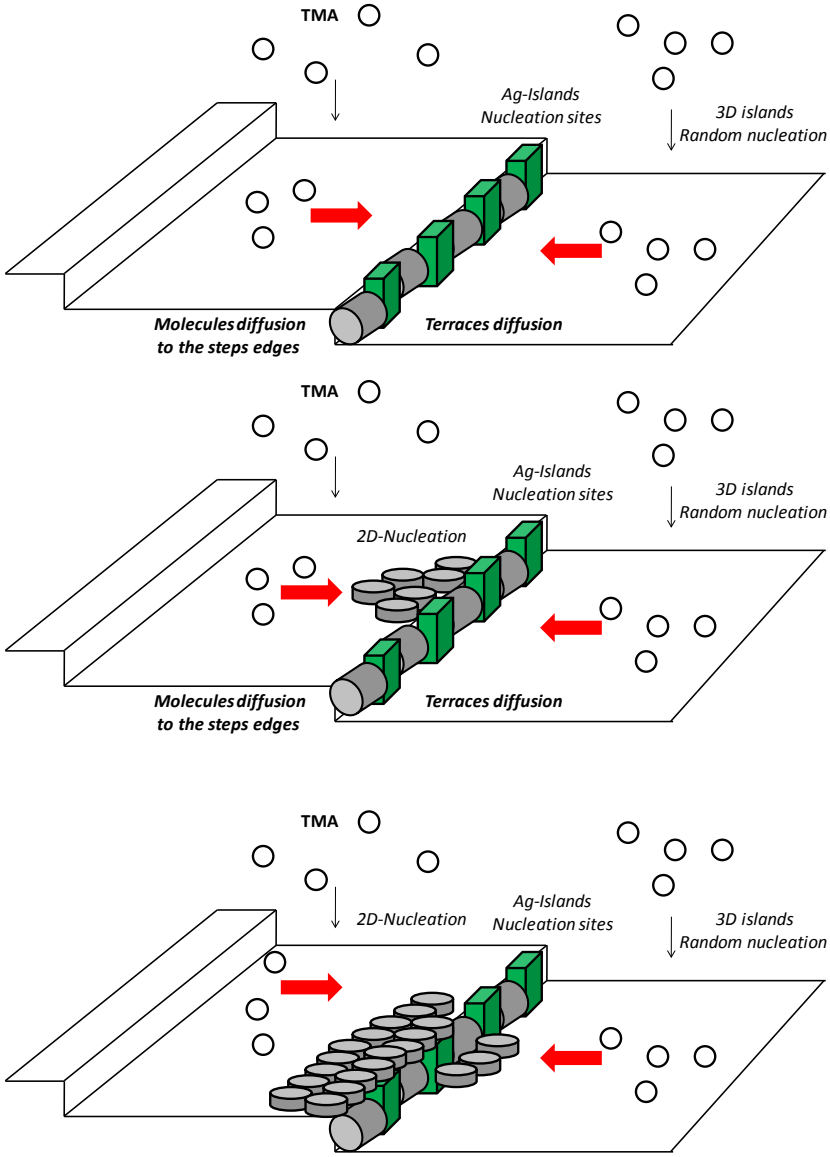

Figure 4.20. *The effect of the barrier on the edges of the steps on the nucleation process. The TMA reaching the surface diffuse toward the edges of the steps and nucleate on the edge with high aspect ratio to the steps. Then the coming molecules reacted along the top edge in 2D structures.*

This behavior of the growth can be caused by the presence of the steps barrier once the molecules reach the surface they diffuse in a different direction. The Al growth on HOPG at RT has values of Ea and Ed of 0.8eV and 0.02eV, respectively, The corresponding diffusion length is 170 ± 80nm

Therefore TMA precursor molecules arriving the surface in the step area (≤ 170 ± 80nm apart the steps) diffuse towards the step edges, where broken dangling bonds C-C serve as nucleation sites [158]. Al-O species decorate the steps from top and bottom. Because of this phenomenon, more precursor molecules can reach the step edges, resulting in enhanced nucleation growth near them and thus explaining this morphology in terms of energetic barrier [159-160]. The precursor diffuses on the surface towards the steps and its diffusion is stopped by the corresponding repulsive barrier, leading to agglomeration on the top of the steps. At the bottom of the steps, the precursor is repulsed near to the edge leading to the nucleation in the bottom. However, there is also another nucleation sites for a distance far from the steps edges (>100nm). Random nucleation takes place at least 100nm away from the step edges, resulting in 2D and 3D islands as shown in Figure 3.27 and 3.28 shows 3D islands with a height of 1nm and 2D islands with a height of 0.2-0.5nm. On the small terraces a formation of the 2D domain that is near to the width of the terraces with a complete coverage of the terraces. This behavior is like the assumption of the growth from the defect toward the bulk of terraces. In this case, the width of the terraces is lower than the diffusion length of Al precursors. On bottom also 2D structure are formed with different structure arrangement.

The Schwoebel-Ehrlich barrier is localized on the steps edge can cause a particular emotion of molecules by attraction or repulses of the molecules from the steps edges. Villain showed that a Schwoebel-Ehrlich barrier creates an effective gradient, leading to unstable growth and the creation of roughness in the film. This is can be the reason of the unstable ALD growth on the large terraces. The question still why we don't observe the same behavior on small terraces, for Schwoebel-Ehrlich barriers it's not clear if the distance between two barriers affects the homogeneity of the growth. In Figure 4.21, we give an intuitive explanation of the difference between the barrier in large and in small steps.

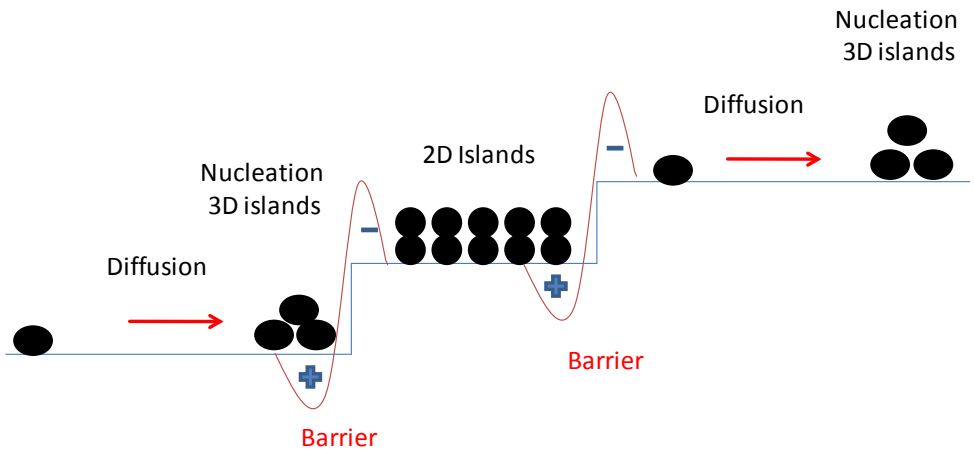

Figure 4.21: *The illustration of the behavior of precursor diffusion with Schwoebel-Ehrlich barriers.*

If diffusing atoms are strongly repelled by the lower step, this can stabilize a stepped surface. The steps B and D collect most of the atoms landing on the broad terraces and therefore go faster than A. Therefore the narrow terrace grows at the expense of the broad ones, and a flat surface is stabilized. this empirical approach fit with the result especially in Figure 4.21 where we can see clearly that the growth in the same region has a high agglomeration in the large terrace while in the small terrace showed in Figure is homogeneous. We can conclude that the ALD nucleation is not just depending on the chemisorptions but also on the surface morphology. Stepped surface, even with poor species for nucleation as the HOPG surface, can lead to ALD growth if the width of terraces is in not $\geq 2\lambda$. The diffusion length is known for the precursors but we can control it also by controlling the temperature of deposition.

Chapter 5: Conclusion

In this thesis it has been demonstrated that the approach of studying the ALD growth process based on the combination of experimental data delivered by STM and statistic models is powerful to investigate the growth modes and reaction mechanisms of ALD on stepped surfaces in the initial stage of growth. The deep investigation of the different film parameters lead to the correlation of the surface morphology (e.g. steps) and chemistry (reactive cites) to the behavior of the deposited molecules' nucleation and reveals the most realistic growth model for the ALD on the stepped surfaces.

An in-situ ALD STM system was used to investigate the growth process of ALD layers applying thermal ALD technique. Tow metal oxide ALD processes have been studied, the first one is HfO_2 on stepped Si(111)-H grown at RT and 280°C. The second system includes the growth of Al_2O_3 on HOPG and Ag-HOPG (Ag steps decoration) at RT. The microscopy of the film features in the initial ALD cycles was done in that way to distinguish the preferential sites of precursor's adsorption on the terraces and on the steps. For every deposition step, the imaging of an overview and of the heights of the steps allows to follow the changes of the film morphology. Nano-resolution imaging of the formed islands, delivers distinct data of their height, width and geometry. Those data are systematically analyzed through the determination of the islands dimensions, surface roughness and surface coverage rates for the each ALD cycle. The surface roughness evolution presents an important parameter to define the film morphology as a direct consequence of the nucleation behavior and the surface termination.

The most important finding is that the growth behavior in the first two ALD cycles of HfO_2 on Si(111)-H terminated is similar independent on the substrate temperature. The first cycle shows an important roughness increase as a result of partial film growth where the materials converge reach ~ 54-71% of the surface. This behavior of partial growth was predicted theoretically and observed for

some ALD-systems, e.g. HfO_2 on Si-OH . No steps decoration was observed, leading to the conclusion of repulsion behavior which avoids any agglomeration of precursor molecules on the Si-H dangling bonds of the step. The islands heights increase with the distance to steps edges, where near to the steps the islands height is two times lower than the heights of islands far from the steps. In the 2nd cycle a full coverage of the surface, with the same film height as in the first cycle and homogeneous islands distribution is observed. This data extracted from STM are then analyzed using the Puurunen model. The adsorptions reactions mechanisms determined by this model, are depending on the distance to the steps and also on the substrate temperatures for the first two cycles. In addition, the steric hindrance effect of precursors was found to be the origin of the reaction saturation. Here, the numbers of reaction sites do not affect the growth. This means that the nucleation does not depend on the surface reactive sites. The height-height correlation function calculated for the first two cycles has an evolution of a self-affine surface. The scaling components ζ and w are fluctuating with the roughness of the surfaces (in height and lateral directions) during the deposition. This fact is an important result proving that the growth in the first two cycles obeys the same dynamics. The values obtained for the dynamic scaling exponents β and $1/Z$ within the first two ALD cycles are near to the universal values of random deposition and Mullins diffusion model. In this model the molecules reach the surface and diffuse with the conservation of the total number of molecules by the equilibration between the high potential sites and lower potential sites. In the 3rd and 4th ALD cycle the growth depends on the substrate temperature. At 280°C, the growth continues with the duplication of the same behavior as in the 1st and 2nd cycles. The Puurunen model application shows that the number of nucleated precursor molecules increases with the number of ALD cycles; this is related to the activation temperature of the surface reaction. A partial growth which fulfills the random deposition model (where the surface statistics has a HHCF of a self-affine surface) with diffusion occurs in the 4th cycles leading to pin holes in the film. At RT, the 3rd cycle displays growth behavior changes with high condensation of materials formed on the edges of steps and grown toward the middle of the terraces. The materials condensed in patterned way in self-assembled stripes with ~1.3nm of height and an inter-stripe distance of 20-40nm. This condensation is predicted by the Puurunen model for the first ALD cycles where no ligand exchanges can be determined in this case. Those stripes are about 5 times higher than the ideal HfO_2 thickness after 3 complete ALD cycles (i.e. 0.1nm/cycle). The application of the HHCF leads to the conclusion of a mounded surface behavior evolution which is the origin of local surface effects such as the steps and the self-arranged structure over the terraces. This growth behavior and the resolved surface statistics components fulfill the criteria of the non equilibrium growth model of Kardar, Parisi, and Zhang (KPZ). The surface diffusion of the molecules to the step edges and their agglomeration is like the expected theoretical ALD growth on inhibited surfaces. For the 4th cycles Mullins diffusion is occurring once more leading to the reduction of the surface roughness again.

The comparison of the ALD growth of TDMAH and H_2O on stepped surface Si(111)-H terminated to the growth of the same precursors on the planar Si-OH surface shows the effect of the initial surface roughness and termination, where the analysis of the HHFC delivers random deposition as the main dynamics within the growth on Si-OH without local effects of the surface on the kind of molecule's adsorption.

The HOPG substrate represents an ideal inhibited-surface for the ALD growth. Once molecules are reaching the surface, they are diffusing toward the steps where high agglomeration happens but no nucleation at the carbon dangling bonds takes place. This can be related to the effect of the barrier of the steps. However, in the 5^{th} cycle the growth of nano-islands on the middle of terraces is observed. The observation of random distribution of islands on 2D and 3D structures can be explained that the growth happens only on the already existing deposited material but no generation of new nucleation sites occurs.

The growth on the Ag-HOPG surface is completely different to the one on the pure HOPG. Here the islands grow in the first cycles on the edges of the steps with high-aspect ratio. The arriving/precursors diffuse to the edges of the steps but lead to the formation of a continued partial layer which grows from the steps edges towards the terraces. Hence, the presence of the Ag-island on the steps edges changes the effect of the steps on the nucleation of the Al_2O_3 film.

In conclusion, this thesis is based on the use of STM and the application of mathematical models for the detailed description of the ALD nucleation on stepped surfaces. A complete picture of the morphological growth and the understanding of the influence of different surface properties on the precursors-surface interaction were in the main focus of this work. Some limitations are considered, e.g. The over-estimation of the scaling component values which was also reported in other studies and low statistics numbers of experimental points that can be an outlook for other experimental from this kind with different parameters of the ALD growth, e.g temperature. This knowledge about the ALD growth on stepped surface can be extended to be used for more complex surfaces such as polycrystalline surfaces which are potential substrates for many important applications.

Reference

1. T. Suntola and J.Antson. 4,058,430 U.S. November 15 (1977).
2. *Atomic layer deposition of metal and nitride thin films: Current research efforts and applications for semiconductor device processing*. H. J. Kim. Vac. Sci. Technol. B, 21, 2231 (2003).
3. *Applications of atomic layer deposition to nanofabrication and emerging nanodevices.* Kim, H.; Lee, H. B. R.; Maeng, W. J. *Thin Solid Films*, *517*, 2563 (2009).
4. *Synthesis and Surface Engineering of Complex Nanostructures by Atomic Layer Deposition*.Knez, M.; Niesch, K.; Niinisto, L. *Adv. Mater.19*, 3425 (2007)
5. *Advanced electronic and optoelectronic materials by Atomic Layer Deposition: An overview with special emphasis on recent progress in processing of high-k dielectrics and other oxide materials* L. Niinisto, J. Paivasaari, J. Niinisto. M. Putkonen, M. Nieminen. *Phys. Status Solidi A*. *201*, 1443 (2004)
6. *Atomic layer epitaxy—a valuable toolfor nanotechnology?*.*M.*Ritala, M. Leskela. *Nanotechnology*, *10*, 19 (1999)
7. *A Kinetic Model for Step Coverage by Atomic Layer Deposition in Narrow Holes or Trenches*. Roy G.Gordan, H. Dennis, K. Esther , Sh. Joseph . Chem.Vap. Deposition. 9, No 2, (2003)
8. *Microstructural evolution of ZrO_2–HfO_2 nanolaminate structures grown by atomic layer deposition.* H. Kim, P.C. McIntyre, K.C. Saraswat. J. Mater. Res. 19 (2) 643(2004).
9. Z.A. Sechrist, F.H. Fabreguette, O. Heintz, T.M. Phung, D.C. Johnson, S.M. George, Chem. Mater. 17 (13) 3475 (2005).
10. *Optimization and Structural Characterization of W/Al_2O_3 Nanolaminates Grown Using Atomic Layer Deposition Techniques.* F.H. Fabreguette, R.A. Wind, S.M. George, Appl. Phys. Lett. 88 (1) (2006).
11. *Thin film atomic layer deposition equipment for semiconductor processing*. O.Sneh, R.B.Clark-Phelps, A.R. Londergan, J. Winkler, T.E, Seidel. *Thin Solid Films*, *402*, 248 (2002).
12. *Atomic layer deposition of metal and nitride thin films: Current research efforts and applications for semiconductor device processing*. H. Kim J. Vac. Sci. Technol. B 21 (2003)
14. *ZnO−Al_2O_3 and ZnO−TiO_2 Core−Shell Nanowire Dye-Sensitized Solar Cells.* M. Law, L.E. Greene, A. Radenovic, T. Kuykendall, J. Liphardt, P. Yang. J. Phys. Chem. B 110 (45) 22652 (2006).
15. *Destruction of Deinococcus geothermalis biofilm by photocatalytic ALD and sol-gel TiO_2 surfaces*. M. Raulio, V. Pore, S. Areva, M. Ritala, M. Leskel, M. Lindn, J.B. Rosenholm, K. Lounatmaa, M. Salkinoja-Salonen. J. Ind. Microbiol. Biotech. 33 (4) 261(2006).
17. *Atomic Layer Deposition Chemistry: Recent Developments and Future Challenges*. M. Leskel and M. Ritala. Angew.Chem.Int.Ed. ,42, 5548 –5554 (2003).
18. *HfO_2 and Al_2O_3 gate dielectrics on GaAs grown by atomic layer deposition*.M. M. Frank, G. D. Wilk, D. Starodub, T. Gustafsson. Appl. Phys. Lett. 86 152904 (2005).
19. *GaAs interfacial self-cleaning by atomic layer deposition.* C. L. Hinkle, A. M. Sonnet, M. Vogel, S. McDonnell, G. J. Hughes, M. Milojevic, B. Lee, F. S.Aguirre-Tostado, K. J. Choi, H. C. Kim, J. Kim, R. M. Wallace. Appl. Phys. Lett. 92 071901 (2008).
20. *Surface chemistry and Fermi level movement during the self-cleaning of GaAs by trimethyl-aluminum*. M. Tallarida, C. Adelmann, A. Delabie, S. Van Elshocht, M. Caymax, D. Schmeißer. Appl. Phys. Lett. 99, 042906 (2011).

21. *Role of interfacial reaction in Atomic Layer Deposition of TiO_2 thin films using $Ti(OiPr)_2(tmhd)_2$ on Ru or RuO_2 substrates*. S. W. Lee, J. H. Han, S. K. Kim, S. Han, W. Lee, C. S. Hwang: " Chem. Mater. 23, 976 (2011).
22. *Recent progress in atomic layer epitaxy of III–V compounds*. S. M. Bedair, B.T, McDermott,Y.Ide, N.H. Karam, H. Hashemi. J. Cryst. Growth 93, 182 (1988).
23. *Atomic Layer Epitaxy of II-VI compound semiconductor, in Festkörper problem*. H. Sitter and W. Faschinger. Advances in Solid State Physics. 30, 219 (Vieweg, Braunschweig) (1990).
24. *Atomic Layer Epitaxy* M. Leskelä and L. Niinistö, edited by T. Suntolaand, M. Simpson Blackie and Son. London. 1990, pp. 1–39
25. M. Leskelä, Acta Polytech. Scand., Chem. Technol. Ser. 195, 67 (1990)
26. *Very High Speed Integrated Circuits: Heterostructure* H. Watanabe, T. Mizutani, and A. Usui, Semiconductors and Semimetals. Vol. 30, edited by T. Ikoma Academic, San Diego, pp. 152 (1990).
27. *Electrochemical atomic layer epitaxy (ECALE).*B. W. Gregory and J. L. Stickney. J. Electroanal. Chem. Interfacial Electrochem. 300, 543 (1991)
28. *Atomic layer epitaxy of III–V compounds using metalorganic and hydride sources*. M. Ozeki, Mater. Sci. Rep. **8**, 97 1992.
29. T. Suntola, in *Handbook of Crystal Growth*, edited by D. T. J. Hurle Elsevier, Amsterdam, Vol. 3, pp. 601–663 (1994).
30. *Nucleation and growth during tungsten atomic layer deposition on SiO_2 surfaces.* J. W. Elam, C. E. Nelson, R. K. Grubbs, and S. M. George, Thin Solid Films 386, 41 (2001).
31. *Low-temperature growth of GaAs and AlAs-GaAs quantum-well layers by modified molecular beam epitaxy*. Y. Horikoshi, M. Kawashima, and H. Yamaguchi, Jpn. J. Appl. Phys., Part 2 **25**, L 868 (1986).
32. *Island growth in the atomic layer deposition of zirconium oxide and aluminum oxide on hydrogen-terminated silicon: Growth mode modeling and transmission electron microscopy*. R. L. Puurunen et al., J. Appl. Phys. 96, 4878 (2004).
33. Island growth as a growth mode in atomic layer deposition: A phenomenological model. R. L. Puurunen and W. Vandervorst, J. Appl. Phys. 96, 7686 (2004).
34. *Surfaces and Interfaces of Solids*. H. Lüth, 2nd ed. (Springer, Berlin, 1993)
35. *Synthesis and characterization of nanosized titanium oxide films on the (0001) α-Al_2O_3 surface*. N. V. Dolgushev, A. A. Malkov, A. A. Malygin, S. A. Suvorov, A. V. Shchukarev, A. V. Beljaev, and V. A. Bykov, Thin Solid Films 293, 91 (1997)
36. L. I. Chernaya, P. E. Matkovskii, V. M. Rudakov, Yu. M. Shul'ga, I. V. Markov, V. I. Tomilo, and Z. G. Busheva, Zh. Obshch. Khim. **62**, 28 (1992) . J. Gen. Chem. USSR 62, 21 (1992)
37. *A study of ZnTe films grown on glass substrates using an atomic layer evaporation method.* M. Ahonen, M. Pessa, and T. Suntola, Thin Solid Films 65, 301 (1980)
38. *Atomic layer deposition of Al_2O_3 and SiO_2 on BN particles using sequential surface reactions*. D. Ferguson, A. W. Weimer, and S. M. George, Appl. Surf. Sci. 162/163, 280 (2000)
39. *Island growth in the atomic layer deposition of zirconium oxide and aluminum oxide on hydrogen-terminated silicon: Growth mode modeling and transmission electron microscopy*. Riikka L. Puurunena , W. Vandervorst ,W. F. A. Besling O. Richard, H. Bender, Th.Conard, Ch. Zhao, A Delabie, M. Caymax, S.D. Gendt, M.H. M.M. Viitanen, M.Ridder, H. H. Brongersma ,Y. Tamminga, T. Dao, T. Win, M. Verheijen, M. K. M. Tuominenb, J. Appl. Phys. 96, 4878 (2004)
40. *Growth mechanism and continuity of atomic layer deposited TiN films on thermal SiO_2*. A. Satta, J. Schuhmacher, C. M. Whelan, W. Vandervorst, S. H. Brongersma, G. P. Beyer, and K. Maex A.

Vantomme M. M. Viitanen and H. H. Brongersma W. F. A. Besling, J. Appl. Phys. 92, 7641 (2002)
41. *Nucleation and Surface Roughness in Self-Limiting Monolayer Epitaxy of GaAs*. K. Kono, T. Kurabayashi, J. Nishizawa, and M. Esashi, Jpn. J. Appl. Phys., Part 1 **39**, 5737 (2000)
42. *Transmission electron microscopic study of AlAs/Si heterostructures grown by atomic layer epitaxy*. O. Ueda, K. Kitahara, N. Ohtsuka, A. Hobbs, and M. Ozeki, J. Cryst.Growth ,115, 133 (1991)
43. *Growth of Aluminum Nitride on Porous Alumina and Silica through Separate Saturated Gas−Solid Reactions of Trimethylaluminum and Ammonia*. R. L. Puurunen, A. Root, P. Sarv, M. M. Viitanen, H. H. Brongersma, M. Lindblad, and A. O. I. Krause, Chem. Mater. 14, 720 (2002).
44. *Growth of Iron Oxide on Yttria-Stabilized Zirconia by Atomic Layer Deposition*. M. Ridder, P. C. van de Ven, R. G. van Welzenis, and H. H. Brongersma, S.Helfensteyn, C. Creemers , P.V.Voort, M.Baltes, M.Mathieu, and E. F. Vansant. J. Phys. Chem. B **106**, 13146 (2002).
45. *Growth Per Cycle in Atomic Layer Deposition: A Theoretical Model*. R.L. Puurunen, Chem. Vap. Deposition, 9, No5 (2003)
46. *In situ study of the atomic layer deposition of HfO_2 on Si*. K. Kolanek, M. Tallaridaa, M. Michling, and Dieter Schmeisser. J. Vac. Sci. Technol. A 30 (1), (2012).
47. *Spectroscopic and electrochemical study of TiO_2/Si photocathode*. C. Das PhD theses 2015.
48. *Surface chemistry of atomic layer deposition: A case study for the trimethylaluminum/water process*. Riikka L. Puurunen. J. Appl. Phys. 97, 121301 (2005).
49. *Growth of ZnO/Al_2O_3 Alloy Films Using Atomic Layer Deposition Techniques. J. W. Elam and S. M. George*. *Chem. Mater*, 15 (4), pp 1020–1028 (2003).
50. *Atomic Layer Epitaxy Growth of Titanium Dioxide Thin Films from Titanium Ethoxide* .M. Ritala, M. Leskelä, and E. Rauhala, Chem. Mater. **6**, 556 (1994)
51. *Titanium Isopropoxide as a Precursor in Atomic Layer Epitaxy of Titanium Dioxide Thin Films*.M. Ritala, M. Leskelä, L. Niinistö, and P. Haussalo, Chem. Mater. **5**,1174 (1993)
52. S. A. Morozov, A. A. Malkov, and A. A. Malygin, Zh. Prikl. Khim. S.-Peterburg **76**, 9 (2003) Russ. J. Appl. Chem. **76**, 7 (2003)
53. *Monolayer thickness in atomic layer deposition*. M. Ylilammi, Thin Solid Films **279**, 124 (1996)
54. *Thickness profiles of thin films caused by secondary reactions in flow-type atomic layer deposition reactors*. H. Siimon and J. Aarik, J. Phys. D **30**, 1725 (1997)
55. *Growth per Cycle in Atomic Layer Deposition: Real Application Examples of a Theoretical Model*. Riikka L. Puurunen. Chem. Vap. Deposition, 9, No.6 (2003)
56. *Surface Studies by Scanning Tunneling Microscopy*. G. Binnig, H. Rohrer, Ch. Gerber, H. Weibel, Phys. Rev. Lett. **49**, 57 (1982)
57. *Scanning Tunneling Microscopy and Related Methods*, R.J.Behm, N. Garcia, and H. Rohrer eds. NATO ASI Series, Series E: Applied Sciences – vol.184
58. *Tunnelling from a many-particle point of view*. J. Bardeen, Phys. Rev. Lett. 6, 57 (1961).
59. *Theory and Application for the Scanning Tunneling Microscope*. J. Tersoff and D.R. Hamann, Phys. Rev. Lett, 50, 1998 (1983).
60. *Theory of the scanning tunneling microscope*. J. Tersoff and D.R. Hamann, Phys. Rev. B 31, 805 (1985).
61. *Spektroskopie der Röntgenstrahlen* . Siegbahn, M. Berlin : Springer, (1931)
62. *Calculations of electron inelastic mean free paths V Data for 14 organic compounds over the 50-2000 eV range.* S. Tanuma, C.J. Powell, D.R. Penn, Surf. Interface Anal., Vol. 21, p. 165 (1994).
63. *Atomic subshell photoionization cross sections and asymmetry parameters: $1 \leqslant Z \leqslant 103$.* J. Yeh, I. Lindau., Atomic Data and Nuclear Data Tables, Vol. 32, p. 1. (1985)

64. *Scanning Tunneling Microscopy Observation of Self-Affine Fractal Roughness in Ion-Bombarded Film Surfaces*. J. Krim, I. Heyvaert, C. V. Haesendonck, and Y. Bruynseraede. Phy. Rev.Lett. 70, (1993).
65. *Scaling of rough surfaces: effects of surface diffusion.* F. Family. J. Phys. A: Math. Gen., 441-44619 (1986).
66. *Surface Roughness Scaling of Plasma Polymer Films*. G.W. Collins, S.A. Letts, E.M. Fearon, R.L. McEachern, and T.P. Bernat Phy. Rev.Lett,73 (1994)
67. *Scaling of the active zone in the Eden process on percolation networks and the ballistic deposition model.* F. Family and T. Vicsek .J. Phys. A: Math. Gen. 18 (19C5)
68. *Scaling of Surface Roughness in Obliquely Sputtered Chromium Films*. D. LE BELLAC, G. A. NIKLASSON and C. G. GRANQVIS. Europhys. Lett., 32 (2), pp. 155-159 (1995)
69. X-ray reflectivity and scanning-tunneling-microscopy study of surface roughness scaling of molybdenum films**.** J. Wang, G. Li, P. Yang, M. Cui, Xi. Jiang, B. Dong **and** H. Liu. **Europhys**. Lett, 42 (3), pp. 283-288 (1998).
70. *Anomalous dynamic scaling on the ion-sputtered Si(111)surface*. H.-N. Yang, G.-C. Wang, and T.-M. Lu. PHYSICAL REVIEW B, 50 (1994)
71. *Fractals, Scaling, and Growth Far from Equilibrium* .P. Meakin .Cambridge University Press, (1998)
72. *Fractal Concepts in Surface Growth*. A.-L. Barab´asi and H. E. Stanley. Cambridge University Press, (1995).
73. *X-ray reflectivity and adsorption isotherm study of fractal scaling in vapor-deposited films*.R. Chiarello, V. Panella, J. Krim, C. Thompson: Phys. Rev. Lett. 67, 3408 (1991)
74. *Evolution of Thin Film Morphology*. Matthew Pelliccione, Toh-Ming Lu. Springer series in materials science 108
75. *Characterization of Amorphous and Crystalline Rough Surface: Principles and Applications*. Y.-P. Zhao, G.-C. Wang, T.-M. Lu .Academic Press, New York (2001)
76. *Self-affine fractals and fractal dimension* .B.B. Mandelbrot.. Physica Scripta 32, 257 (1985)
77. *X-ray and neutron scattering from rough surfaces*. S.K. Sinha, E.B. Sirota, S. Garoff, H.B. Stanley.Phys. Rev. B 38, 2297 (1988).
78. *The surface statistics of a granular aggregate* .S.F. Edwards, D.R. Wilkinson. Proc. R. Soc. London Ser. A **381**, 17 (1982)
79. *Dynamic scaling of growing interfaces* .M. Kardar, G. Parisi, Y.C. Zhang:. Phys. Rev. Lett. **56**, 889 (1986)
80. Groove instabilities in surface growth with diffusion. J.G. Amar, P.-M. Lam, F. Family:. Phys. Rev. E **47**, 3242 (1993)
81. *A new universality class for kinetic growth: One-dimensional molecular-beam epitaxy* .S. Das Sarma, P. Tamborenea:. Phys. Rev. Lett. **66**, 325 (1991)
82. *Growth with surface diffusion* . D.E. Wolf, J. Villain. Europhys. Lett. 13, 389 (1990)
83. *Kinetic roughening in polymer film growth by vapor deposition* .Y.-P. Zhao, J.B. Fortin, G. Bonvallet, G.-C. Wang, T.-M. Lu. Phys. Rev. Lett. **85**, 3229 (2000)
84. *Kinetic growth with surface relaxation: Continuum versus atomistic models* .Z.W. Lai, S. Das Sarma. Phys. Rev. Lett. 66, 2348 (1991)
85. *Numerical analysis of the noisy Kuramoto-Sivashinsky equation in 2+1 dimensions* . J.T. Drotar, Y.-P. Zhao, T.-M. Lu, G.-C. Wang:. Phys. Rev. E 59, 177 (1999)
86. *Characterization of Amorphous and Crystalline Rough Surface: Principles and Applications*.Y.-P. Zhao, G.-C. Wang, T.-M. Lu. Academic Press, New York (2001).

87. *Topographic evolution during deposition of plasma-deposited hydrogenated silicon on glass.* George T. Dalakos. G.T. Dalakos, J.P. Plawsky, P.D. Persans:. Phys. Rev. B 72, 205305 (2005)
88. *Surface roughening in low pressure chemical vapor deposition*. J.T. Drotar, Y.-P. Zhao, T.-M. Lu, G.-C. Wang. Phys. Rev. B 64, 125411 (2001)
89. *Tailoring the surface morphology of amorphous thin films by appropriately chosen deposition conditions*.S.G. Mayr, K. Samwer:. J. Appl. Phys. 91, 2779 (2002)
90. *Temperature dependence of the surface roughness evolution during hydrogenated amorphous silicon film growth*. A.H.M. Smets, W.M.M. Kessels, M.C.M. van de Sanden:. Appl. Phys. Lett. 82, 865 (2003)
91. *Dynamical scaling of sputter-roughened surfaces in 2+1 dimensions*.E.S. Tok, S.W. Ong, H.C. Kang:. Phys. Rev. E 70, 011604 (2004).
92. *Kinetic roughening of vicinal Si(001).* P.E. Hegeman, H.J.W. Zandvliet, G.A.M. Kip, A. van Silfhout:. Surf. Sci. 311, L655 (1994)
93. *Stable and unstable growth in molecular beam epitaxy* . M.D. Johnson, C. Orme, A.W. Hunt, D. Graff, J. Sudijono, L.M. Sander, B.G. Orr:. Phys. Rev. Lett. 72, 116 (1994)
94. *Slope selection and coarsening in molecular beam epitaxy*. M. Siegert, M. Plischke: Phys. Rev. Lett. 73, 1517 (1994)
95. *Coarsening of unstable surface features during Fe(001) homoepitaxy* .J.A. Stroscio, D.T. Pierce, M.D. Stiles, A. Zangwill, L.M. Sander:. Phys. Rev. Lett. 75, 4246 (1995)
96. *Morphology transition and layer-by layer growth of Rh(111).* F. Tsui, J. Wellman, C. Uher, R. Clarke:. Phys. Rev. Lett. 76, 3164 (1996)
97. *Handbook of Theoretical and Computational Nanotechnology*. M. Rieth, W. Schommers .American Scientific, California p 256 (2006)
98. *Evolution of mound morphology in reversible homoepitaxy on Cu(100)*.J.-K. Zuo, J.F. Wendelken: . Phys. Rev. Lett. 78, 2791 (1997)
99. *Morphology transition during low-pressure chemical vapor deposition.* Y.-P. Zhao, J.T. Drotar, G.-C. Wang, T.-M. Lu: Phys. Rev. Lett. 87, 136102 (2001).
100. *WSXM: A software for scanning probe microscopy and a tool for nanotechnology* I. Horcas and R. Fernández J. M. Gómez-Rodríguez J. Colchero J. Gómez-Herrero A. M. Baro. Rev. Sci. Instrum. 78, 013705(2007)
101. *In situ ALD experiments with synchrotron radiation photoelectron spectroscopy*. Massimo Tallarida. Semiconductor Science and Technology · June (2012)
102. *On the electrochemical etching of tips for scanning tunneling microscopy* .J. P. Ibe, P. P. Bey Jr., S. L. Brandow, R. A. Brizzolara, N. A. Burnham, D. P. DiLella, K. P. Lee, C. R. K. Marrian, and R. J. Colton. J. Vac. Sci. Technol. A, 8(4):3570, 1990
103. *Low-Temperature Al_2O_3 Atomic Layer Deposition*. M. D. Groner, F. H. Fabreguette, J. W. Elam, and S. M. George. Chem. Mater., Vol. 16, No. 4, (2004)
104. *Growth of ZnO/Al_2O_3 Alloy Films Using Atomic Layer Deposition Techniques*. J. W. Elam and S. M. George. Chem. Mater.,15,1020-1028 (2003)
105. *Thin film atomic layer deposition equipment for semiconductor processing.* Ofer Sneh, , Robert B Clark-Phelps, Ana R Londergan, Jereld Winkler, Thomas E Seidel. Thin Solid Films 402,248–261(2002).
106. *Energy-band parameters of atomic-layer-deposition Al_2O_3/ InGaAs heterostructure*. M. L. Huang, Y. C. Chang, C. H. Chang, and T. D. Lin. Appl.Phys. Lett, 89, 012903 (2006).
107. *Surface chemistry of Al_2O_3 deposition using $Al(CH_3)_3$ and H_2O in a binary reaction sequence.* Dillon, A. C.; Ott, A. W.; Way, J. D.; George, S. M.Surf. Sci. (1995) ,322, 230

108. *Al_3O_3 thin film growth on Si(100) using binary reaction sequence chemistry.* Ott, A. W.; Klaus, J. W.; Johnson, J. M.; George, S. M. Thin Solid Films (1997) ,292, 13
109. *Perfectly Conformal TiN and Al_2O_3 Films Deposited by Atomic Layer Deposition*.Ritala, M.; Leskela, M.; Dekker: J. P.; Mutsaers, C.; Soininen, P. J.; Skarp, J. Chem. Vap. Dep.(1999),5,7.
110. *Surface Chemistry for Atomic Layer Growth.* S. M. George, A. W. Ott, J. W. Klaus. J. Phys. Chem., 100, 13121 (1996)
111. Ott, A. W.; Klaus, J. W.; Johnson, J. M.; George, S. M. *Thin Solid Films*, *292*, 135 (1997)
112. Dillon, A. C.; Ott, A. W.; Way, J. D.; George, S. M. *Surf. Sci.*, *322*, 230 (1995)
113. *Quantum chemical study of the mechanism of aluminum oxide atomic layer deposition*. Widjaja, Y.; Musgrave, C. B. Appl. Phys. Lett., 80, 3304 (2002)
114. *High-κ gate dielectrics: Current status and materials properties considerations*. G. D. Wilk, R. M. Wallace, and J. M. Anthony, J. Appl. Phys.,89, 5243 (2001).
115. Mass production worthy HfO/sub 2/-Al/sub 2/O/sub 3/ laminate capacitor technology using Hf liquid precursor for sub-100 nm DRAMs. J. H. Lee,Tech. Dig. - Int. Electron Devices Meet , 9.1(2002)
116. *ALD of Hafnium Oxide Thin Films from Tetrakis(ethylmethylamino)hafnium and Ozone*. X. Liu , S. Ramanathan, A. Longdergan, A. Srivastava, E.Lee, T.E. Seidel, J.T. Barton, D. Pang and R. G. Gordon.
117. *Atomic Layer Deposition of Hafnium Dioxide Film from Hafinuim Tetrakis(ethylmethylamide) and water.* K. Kukli, M. Ritala, T. Sajavaara, J. Keinonen, and M. Leskela, Chem. Vap. Deposition, 8, 5, 199 (2002)
118. *Atomic Layer Deposition of Hafnium and Zirconium Oxides Using Metal Amide Precursors*. D. M. Hausmann, E. Kim, J. Becker, and R. G. Gordon,Chem. Mater.,14, 4350 (2002)
119. *Nucleation of HfO_2 atomic layer deposition films on chemical oxide and H-terminated Si*. Justin C. Hackley and Theodosia Gougous. J.Appl.Phys. 102, 034101 (2007)
120. *Properties of atomic layer deposited HfO_2 thin films*. Justin C. Hackley, Theodosia Gougousi. Thin Solid Films 517 6576–6583(2009)
121. *Nucleation Studies of HfO_2 Thin Films Produced by Atomic Layer Deposition*. Justin C. Hackley, J.Derek Demaree and Theodosia Gougousi. MRS Proceedings, 2007 - Cambridge Univ Press
122. *Selectivity of metal oxide atomic layer deposition on hydrogen terminated and oxidized Si(001)-(2×1) surface*. Roberto C. Longo, Stephen McDonnell, D. Dick, R. M. Wallace, and Yves J. Chabal James H. G. Owen, Josh B. Ballard, and John N. Randall Kyeongjae Cho. J. Vac. Sci. Technol. B 32(3), (2014)
123. *In-Situ Infrared Spectroscopy and Density Functional Theory Modeling of Hafnium Alkylamine Adsorption on Si−OH and Si−H Surfaces*. M. Jason Kelly,Joseph H. Han,Charles B. Musgrave, and Gregory N. Parsons. Chem. Mater,17,5305-5314 (2005),
124. *Ideal hydrogen termination of the Si (111) surface*. G. S. Higashi, Y. J. Chabal, G. W. Trucks, and K. Raghavachari, Appl. Phys. Lett, 12, 656 (1990)
125. *Kinetic model of the chemical etching of Si(111) surfaces by buffered HF solutions.* P. Jakob, Y. J. Chabal, K. Raghavachari, R. S. Becker, and A. J.Becker, Surf. Sci. 275, 407 (1992)
126. *Etching mechanism and atomic structure of H-Si(111) surfaces prepared in NH_4F.* P. Allongue, V. Kieling, and H. Gerischer. Electrochim. Acta 40, 1353 (1995).
127. Etch-pit initiation by dissolved oxygen on terraces of H-Si(111). C.P. Wade, C.E.D. Chidsey, Appl. Phys. Lett. 71,1679 (1997)
128. *Multiscale Modeling of the Atomic Layer Deposition of HfO_2 Thin Film Grown on Silicon: How to Deal with a Kinetic Monte Carlo Procedure*. A. Dkhissi, A. Este`ve, C. Mastail, S. Olivier, G. Mazaleyrat, L. Jeloaica, and M. Djafari Rouhani, J. Chem. Theory Comput. 4, 1915 (2008).

129. *Surface Roughness Analysis and Measurement Techniques*. Bharat Bhushan .The Ohio State University. CRC Press LCC (2001).
130. *Status and prospects of Al2O3-based surface passivation schemes for silicon solar cells.* G. Dingemans, W. M. M Kessels, J. Vac. Sci. Technol, A ,30,040802 (2012),.
131. *Metal Oxide Thin Films Deposited from Metal Organic Precursors in Supercritical CO_2 Solutions.* T.Gougousi, D. Barua, E. D .Young, G. N . Parsons, Chem. Mater., 17, 5093–5100.(2005)
132. *Angle-resolved x-ray photoelectron spectroscopy of ultrathin Al_2O_3 films grown by atomic layer deposition*. O. Renault, L. G. Gosset, D. Rouchon, and A. Ermolieff, J. Vac. Sci.Technol. A 20 1867 (2002).
134. *Conformal Al_2 O_3 dielectric layer deposited by atomic layer deposition for graphenebased Nanoelectronics.* B. Lee, S.Y. Park, H.C.Kim, K. C. Eric , M. Vogel, M. J. Kim, Ro. M. Wallace, J. Kim., Appl. Phys.Lett,92, 203102 (2008).
135. *Atomic subshell photoionization cross sections and asymmetry parameters: $1 \leqslant Z \leqslant 103$*.J. J. Yeh, I. Lindau, Data Nucl. Data Tables 32 1–155(1985),.
136. *Toward Selective Ultra-High-Vacuum Atomic Layer Deposition of Metal Oxides on Si(100)*. D. Dick, J. B. Ballard,R. C. Longo ,J. N. Randall, K. Cho, and Y. J. Chabal. J. Phys. Chem. C, 120, 24213−24223 (2016)
137. *Selectivity of Metal Oxide Atomic Layer Deposition on Hydrogen Terminated and Oxidized Si(001)-(2x1) Surface*. R. C. Longo, S. McDonnell, D. Dick, R. M. Wallace, Y. J. Chabal and K. Cho. J. Vac. Sci. Technol. B 32(3), (2014).
138. *Effects of grains' features in surface roughness scaling*. T. J. Oliveiraa and F. D. A. Aarao Reisb. Journal of applied physics (2007).
139. *Finite-size effects in roughness distribution scaling.* T. J. Oliveiraa and F. D. A. Aarao Reisb Physical Review E, (2007)
140. *Roughness exponents and grain shapes*. T. J. Oliveiraa and F. D. A. Aarao Reisb. Physical Review E, (2011).
141. *Analytical model for island growth in atomic layer deposition using geometrical principles*. O. Nilsen, C. E. Mohn, A. Kjekshus, and H. Fjellvåg. J. Appl. Phys. 102, 024906 (2007)
142. *Kinetic Growth with Surface Relaxation: Continuum versus Atomistic Models*.Z.-W. Lai and S. Das Sarma PHYSICAL REVIEW LETTERS 6 MAY 1991. 136. D. E. Wolf and J. Villain, Europhys. Lett. **13**, 389 (1990).
143. *Growth with Surface Diffusion*. D. E. Wolf and J. Villain, Europhys. Lett. **13**, 389 (1990).
144. *Dynamic scaling of the growth process of GaN thin films deposited on sapphire substrates by HVPE*. D. Lu, R. Zhang, H. Yu, X. Xiu, X. Li, S. Gu, B. Shen, Y. Shi, and Y.Zheng, Phys. Lett. A 327, 78 (2004).
145. *Dynamics of surface evolution in semiconductor thin films grown from a chemical bath*. I. Gupta and B. C. Mohanty . Scientific Reports. (2016).
146. *Thin-film growth dynamics with shadowing and re-emission effects.* Tansel Karabacak. Journal of Nanophotonics. Vol. 5, (2011)
147. *Network behavior in thin-film growth dynamics*.T. Karabacak, H. Guclu, and M. Yuksel, Phys. Rev. B 79, 195418 (2009).
148. *Physical self-assembly and the nucleation of 3D nanostructures by oblique angle deposition*. T. Karabacak, G.-C. Wang, and T.-M. Lu, J. Vac. Sci. Technol. A 22, 1778–1784 (2004).
149. *Growth front roughening in amorphous silicon films by sputtering* .T. Karabacak, Y.-P. Zhao, G.-C. Wang, and T.-M. Lu,, Phys. Rev. B 64, 085323 (2001).

150. *Scaling during shadowing growth of isolated nano-columns* T. Karabacak, J. P. Singh, Y.-P. Zhao, G.-C. Wang, and T.-M. Lu, "," Phys. Rev. B 68, 125408 (2003).
151. *Theory of thermal grooving* .W.W. Mullins. J. Appl. Phys. 28, 333 (1957)
152.*Groove instabilities in surface growth with diffusion*. J.G. Amar, P.-M. Lam, F. Family.Phys. Rev. E 47, 3242 (1993)
153. *Instability of kinetic roughening in sputter-deposition growth of Pt on glass*. J.H. Jeffries, J.-K. Zuo, M.M. Craig. Phys. Rev. Lett. 76, 4931 (1996).
154. *When Interface Gets Rough*. T.-M. Lu, H.-N. Yang, G.-C. Wang. Mat. Res.Soc. Symp. Proc. 367, 283 (1995).
155. *Scale invariance and dynamical correlations in growth models of molecular beam epitaxy.* S. Das Sarma, C. J. Lanczycki, R. Kotlyar, and S.V. Ghaisast. PHYSICAL REVIEW E,53 (1996).
156. *Dynamic scaling of growing interfaces*. M. Kardar, G. Parisi, Y.C. Zhang:. Phys.Rev. Lett. 56, 889 (1986).
155. *Nucleation on cleavage steps Comparison of experiment and theory*..A.D. Gates, J.L. Robins. Heterogenious Surface Science 188-204(1982),.
156. *Ab-initio molecular dynamics study of the interaction of aluminium clusters on a graphite surface* .I. Moullet.. Surface Science 697-702. (1995)
157. *Nanoscale Electrochemistry of sp^2 Carbon Materials: From Graphite and Graphene to Carbon Nanotubes.* P.R. Unwin, A.G. Güell, and G. Zhang. Acc. Chem. Res., 49, 2041−2048(2016)
158. Step Motion on Crystal Surfaces. R. L. Schwoebel, E. J. Shipsey.. J. Appl. Phys. (37) 3682. (1966)
159. *Atomic View of Surface Self Diffusion: Tungsten on Tungsten*. G. Ehrlich, F. G. Hudda.. J. Chem. Phys. (44) 1039(1966).

Abbreviation of phrases

STM	Scanning tunnelling microscopy
ALD	Atomic layer deposition
CVD	Chemical vapor deposition
XPS	X-ray photoelectron spectroscopy
GPC	Growth per cycle
TDMAH	Tetrakis dimethylamino Hafnium
TMA	Tri-methyl-aluminium
HHCF	Height-height correlation function
HOPG	Highly oriented pyrolytic graphite
RMS	Root-mean-square
LBL	Layer by layer

Conference and Meeting Contributions:

Oral presentation

DPG Spring Meeting, Regensburg (Germany), March 06-11, 2016

" HfO_2 grow by ALD on Si(111)-H terminated stepped surface"

Z. Rouissi, M. Tallarida, D. Schmeißer,

" ALD growth of Al_2O_3 on Stepped Surface of HOPG and Ag-HOPG".

Z. Rouissi, M. Tallarida, D. Schmeißer.

11th Interregional Workshop on Advanced Nanomaterials, Cottbus (Germany), November, 18-19, 2015

" ALD growth of Al_2O_3 on HOPG and Ag-HOPG -a STM study".

Z.Rouissi, D. Schmeißer.

EMRS Fall Meeting, Warsawa (Poland), Sept 15-18, 2015

"Atomic layer deposition of HfO_2 on stepped Si(111) surfaces studied by scanning tunnelling microscopy".

Z. Rouissi, M. Tallarida, D. Schmeißer.

Poster presentation

DPG Spring Meeting, Berlin (Berlin) March, 15-20, 2015.

"Study of atomic layer deposition with scanning tunneling microscopy"
Z. Rouissi, M. Tallarida, D. Schmeißer. Poster A Verhandlungen der DPG (VI) 50, 3/2015 (2015) 401, ISSN 0420-0195.

" Comparison of charge neutrality level of $Cu/CuO/HfO_2$ and $Si/SiO_2/HfO_2$"
Z. Rouissi, S. Brizzi, S. Alberton Corrêa, M. Tallarida, D. Schmeißer. Poster A Verhandlungen der DPG (VI) 50, 3/2015 (2015) 208, ISSN 0420-0195

Publication (not related to the thesis)

Room-Temperature Atomic Layer Deposition of Al_2O_3: Impact on Efficiency, Stability and Surface Properties in Perovskite Solar Cells. Malgorzata Kot, Chittaranjan Das, Zhiping Wang, Karsten Henkel, Zied Rouissi, Konrad Wojciechowski, Henry J. Snaith, and Dieter Schmeisser. ChemSusChem, 9, 1 – 7 (2016)

Acknowledgement

I would like to express my keen gratitude to Prof. Dr. Dieter Schmeißer for providing me an opportunity to work on my PhD thesis with him. It was his advice and discussion on different scientific issue that led my work to reach at thesis level.

I am thankful to Dr. Karsten Hankel who help in things range from science to academics as well as he extended his help in personal level. He was main instrumental in corrected my thesis at a final level.

I would like to thank Guido Beuckert for his help in setting of experimental setups and help to operate different instruments.

I am thankful to my peer group colleagues Malgorzata Kot, Jörg Haeberle, Simone Brizzi, Matthias Städter, Klaus Müller, Ioanna Poulumpa, Fabian Rachow, Johannes Israel and Carola Schwiertz for their help in my experiments and valuable suggestions.

I am thankful to the DFG to provide me financial assistance during my research work.